MAX-PLANCK-INSTITUT FÜR CHEMIE

JOHANNES GUTENBERG UNIVERSITÄT MAINZ

Trends of atmospheric radicals, trace gases and their residence time

Dissertation
zur Erlangung des Grades
„Doktor der Naturwissenschaften“
im Promotionsfach Chemie

am Fachbereich Chemie, Pharmazie, Geographie und Geowissenschaften
der Johannes Gutenberg-Universität Mainz

Mengze Li

geb. in Jilin, V.R.China

Mainz, 2020

Tag der mündlichen Prüfung:17.12.2020

Declaration

I hereby declare that I wrote the dissertation submitted without any unauthorized external assistance and used only sources acknowledged in the work. All textual passages which are appropriated verbatim or paraphrased from published and unpublished texts as well as all information obtained from oral sources are duly indicated and listed in accordance with bibliographical rules. In carrying out this research, I complied with the rules of standard scientific practice as formulated in the statutes of Johannes-Gutenberg-Universität Mainz to ensure standard scientific practice.

Mainz, Mengze Li

Summary

Atmospheric trace gases have considerable impact on air quality, climate, and human health. Greenhouse gases (GHGs), such as carbon dioxide (CO_2), methane (CH_4), nitrous oxide (N_2O), and sulfur hexafluoride (SF_6), have long atmospheric lifetimes and contribute to global warming. Non-methane hydrocarbons (NMHCs) have shorter lifetimes and impact tropospheric ozone and aerosol formation, both of which also affect the Earth´s radiative balance. Anthropogenic emissions are the main sources of these atmospheric trace gases. Oxidation with atmospheric radicals (mostly with hydroxyl radicals) and uptake by vegetation are their major sinks. Long-term measurements of trace gases provide insights into changes of the sources and sinks. Such measurements of several important gases have been made at the ground sites around the globe for decades, whereas stratospheric data for the same species are very rare or only available for the few gases that can be measured by satellites. The IAGOS-CARIBIC project provides long-term (more than ten years) global measurements of important GHGs and NMHCs in the upper-troposphere lower-stratosphere (UTLS) region. In this PhD project, by using the CARIBIC data set, several key questions in atmospheric science are addressed. These are summarized as follows:

(1) What are the concentrations of OH and Cl radicals in the UTLS region and do they change with time? With airborne and ground based measurements of CH_4, SF_6, and CH_3Cl, OH radical concentrations in the troposphere and stratosphere during 2008-2015 were estimated to be 10.9×10^5 ($\sigma = 9.6 \times 10^5$), and 1.1×10^5 ($\sigma = 0.8 \times 10^5$) molecules cm^{-3}, respectively. Cl radical concentration in the lower stratosphere was derived to be 1.1×10^4 ($\sigma = 0.6 \times 10^4$) molecules cm^{-3}. The main altitude for tropospheric CH_4 oxidation was derived to be 4.5 ~ 10.5

km. The year 2013 showed highest stratospheric OH and lowest Cl concentrations.

(2) How does the residence time of CO_2 vary across the globe? By using the variability-residence time relationship, global tropospheric and stratospheric CO_2 residence times were estimated to be 28.4±18.2, and 458.6±115.1 (mean ± one standard deviation), respectively, during 2006-2015. CO_2 has shorter residence time in the Northern Hemisphere compared to the Southern Hemisphere, due to larger uptake by vegetation.

(3) How is the stratospheric ethane trend? A general decreasing trend of stratospheric ethane during 2006-2016 is observed, with two peaks in 2010 and 2013, which may be caused by more samplings over North America and Asia where ethane emissions are reported to be increasing due to oil and gas emissions. Results from model simulations at the same sampling location showed that the model underestimated stratospheric ethane concentrations about 10% (median). The model, which is based on the best current emission inventory estimates does capture some similar trends as the observations, such as the decrease during 2006-2009, peaks in 2010 and 2013, but the absolute ethane growth rates are much lower in the model simulations than in the measurements.

Zusammenfassung

Atmosphärische Spurengase haben beträchtliche Auswirkungen auf die Luftqualität, das Klima und die menschliche Gesundheit. Treibhausgase (THGs) wie Kohlendioxid (CO_2), Methan (CH_4), Distickstoffoxid (N_2O) und Schwefelhexafluorid (SF_6) haben lange Lebensdauer in der Atmosphäre und tragen zu der globalen Erwärmung bei. Nicht-Methan-Kohlenwasserstoffe (NMHCs) haben eine kürzere Lebensdauer und wirken sich auf die Bildung von Ozon und Aerosolen in der Troposphäre aus, die beide auch das Strahlungsgleichgewicht der Erde beeinflussen. Die Hauptquelle für diese atmosphärischen Spurengase sind anthropogene Emissionen. Die Oxidation mit atmosphärischen Radikalen (meist mit Hydroxylradikalen) und die Aufnahme durch die Vegetation sind ihre wichtigsten Senken. Durch die Langzeitmessungen von Spurengasen lassen sich Erkenntnisse über die Veränderung von Quellen und Senken gewinnen. Solche Messungen meherer wichtiger Gase werden an den globalen Bodenstationen jahrzehntelang durchgeführt, während stratosphärische Daten für dieselbe Art sehr wenig sind oder nur begrenzte Mengen von Gasen mit Satelliten gemessen werden können. Im Rahmen des Projekts IAGOS-CARIBIC werden langfristige (mehr als zehn Jahre) globale Messungen wichtiger THGs und NMHCs im Bereich der oberen Troposphäre und der unteren Stratosphäre (UTLS) durchgeführt. In diesem Dissertationsprojekt werden unter Verwendung des CARIBIC-Datensatzes einige Schlüsselfragen der Atmosphärenforschung behandelt, die sich wie folgt zusammenfassen lassen:

(1) Wie hoch sind die Konzentrationen an OH- und Cl-Radikalen in der UTLS-Region und ändern sie sich mit der Zeit? Mit Messungen von CH_4, SF_6 und CH_3Cl in der Luft und am Boden wurden die Konzentrationen von OH-Radikalen in der Troposphäre und Stratosphäre in den Jahren 2008-2015 auf

$10{,}9 \times 10^5$ ($\sigma = 9{,}6 \times 10^5$) bzw. $1{,}1 \times 10^5$ ($\sigma = 0{,}8 \times 10^5$) Moleküle cm^{-3} geschätzt. Die Konzentration von Cl-Radikalen in der unteren Stratosphäre wurde ermittelt als $1{,}1 \times 10^4$ ($\sigma = 0{,}6 \times 10^4$) Moleküle cm^{-3}. Die Höhenangabe für die troposphärische CH_4-Oxidation wurde auf 4,5 ~ 10,5 km hergeleitet. Das Jahr 2013 zeigte die höchsten stratosphärischen OH- und niedrigsten Cl-Konzentrationen.

(2) Wie variiert die Verweilzeit von CO_2 weltweit? Unter Verwendung der Variabilitätsverweilzeitbeziehung wurden die globalen troposphärischen und stratosphärischen CO_2-Verweilzeiten für den Zeitraum 2006-2015 auf 28,4±18,2 bzw. 458,6±115,1 (Mittelwert ± eine Standardabweichung) geschätzt. CO_2 hat in der nördlichen Hemisphäre im Vergleich zur südlichen Hemisphäre eine kürzere Verweilzeit, was auf eine größere Aufnahme durch die Vegetation zurückzuführen ist.

(3) Wie ist der stratosphärische Ethantrend? Es ist ein allgemein rückläufiger Trend bei stratosphärischem Ethan im Zeitraum 2006-2016 zu beobachten, mit zwei Spitzenwerten in den Jahren 2010 und 2013, die möglicherweise durch mehr Probenahmen über Nordamerika und Asien verursacht wurden, wo die Ethanemissionen Berichten zufolge ansteigen aufgrund von Öl- und Gasemissionen. Die Ergebnisse von Modellsimulationen am gleichen Probenahmeort zeigten, dass im Modell die Ethankonzentration in der Stratosphäre um etwa 10% (Median) unterschätzt wurde. Das Modell, das auf den besten aktuellen Schätzungen des Emissionsinventars basiert, erfasst einige ähnliche Trends wie die Beobachtungen, wie z. B. Rückgang in den Jahren 2006-2009, Spitzenwerte in den Jahren 2010 und 2013, aber die absoluten Ethanwachstumsraten sind bei Modellsimulationen viel niedriger als bei den Messungen.

CONTENTS

1. INTRODUCTION

1.1 The Atmosphere

The Earth's atmosphere is characterized into different regions by temperature and pressure (Figure 1.1). The lowest layer, the troposphere, extends from the earth's surface to ~12 km altitude, its temperature decreases with height and vertical mixing is fast. The stratosphere extends from the tropopause (see section 1.2) to ~50 km altitude and has slow vertical mixing and increase of temperature with height. The troposphere and the stratosphere are studied as the lower atmosphere. Above them, the mesosphere and the thermosphere are known as the upper atmosphere.

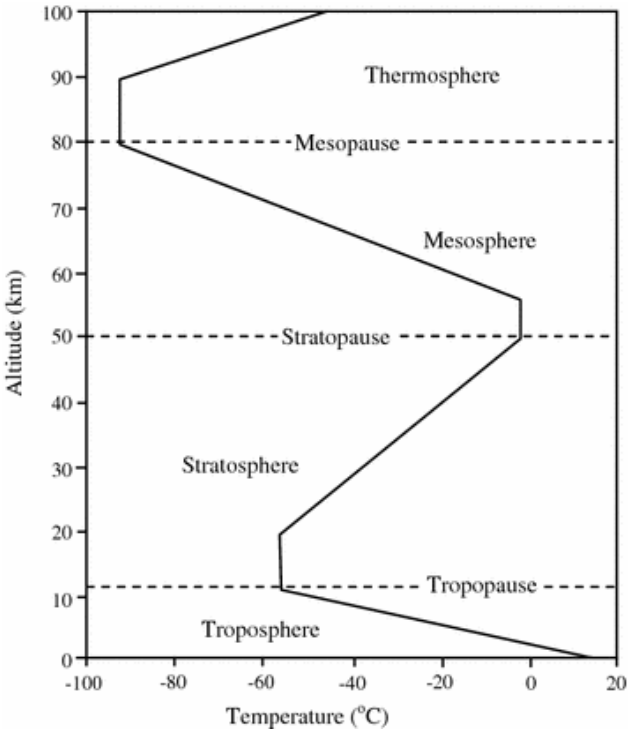

Figure 1.1 Layers of the atmosphere. This figure is taken from Chandrappa and Chandra Kulshrestha (2016), used with permission ©Springer Nature.

1.2 Stratosphere-Troposphere Exchange (STE)

The troposphere and the stratosphere have different physical and chemical characteristics, e.g. chemical composition, temperature gradients, circulation, etc. (Stohl, 2003). The dividing layer between them is termed the tropopause and it has multiple definitions. The thermal tropopause is defined as the lowest altitude where the temperature lapse rate < 2 K km^{-1} (WMO, 1957). The potential vorticity (PV)-based dynamical tropopause can be defined with three-dimensional temperature and wind data (Gettelman et al., 2011), and it is conserved under adiabatic and frictionless conditions (Ertel, 1942;Wirth, 1995). The chemical tropopause is defined with the vertical gradients and values of chemical compounds (Pan et al., 2004), such as O_3 (Bethan et al., 1996), N_2O (Assonov et al., 2013), O_3-CO correlation (Fischer et al., 2000;Hoor et al., 2002;Zahn and Brenninkmeijer, 2003).

STE has been studied and reviewed in many previous studies (Holton et al., 1995;Stohl, 2003;Bönisch et al., 2009;Hoor et al., 2010;Gettelman et al., 2011). Figure 1.2 illustrates the currently accepted general transport scheme in the Northern Hemisphere up to 25 km. The global circulation can be described by an upwelling flow from the tropical upper troposphere to the stratosphere, transport to the extratropical stratosphere through the Brewer-Dobson Circulation (red outline) or isentropic exchange (red or orange wavy arrows), descending (or poleward) to the middle and high latitudes in the troposphere. The Brewer-Dobson circulation (Dobson et al., 1929;Brewer, 1949;Dobson, 1956) plays an important role in STE and can significantly influence the lifetimes of chemical compounds (especially ozone-depleting substances and greenhouse gases), the recovery of stratospheric ozone, background reservoirs for STE and climate change (Butchart, 2014b;Gettelman et al., 2011). The STE is a bidirectional process, which can be seen as the subtropical jet stream (a belt of high-speed winds flowing above subtropical regions) due to Rossby wave (or as planetary waves, occurred in rotating fluids) breaking can

trigger convection and transport air into both directions (the troposphere and the stratosphere).

The upper troposphere and lower stratosphere (UTLS) is a coupling layer connecting the troposphere and the stratosphere. It is normally considered as the region ±5 km around the tropopause. UTLS is not only important for STE, but also for chemistry, dynamic and radiation of the troposphere and the stratosphere, and climate feedbacks (Gettelman et al., 2011;Holton et al., 1995;Solomon et al., 2010). In this PhD project, the aircraft measurement data were collected in the UTLS region (at ~10 km height).

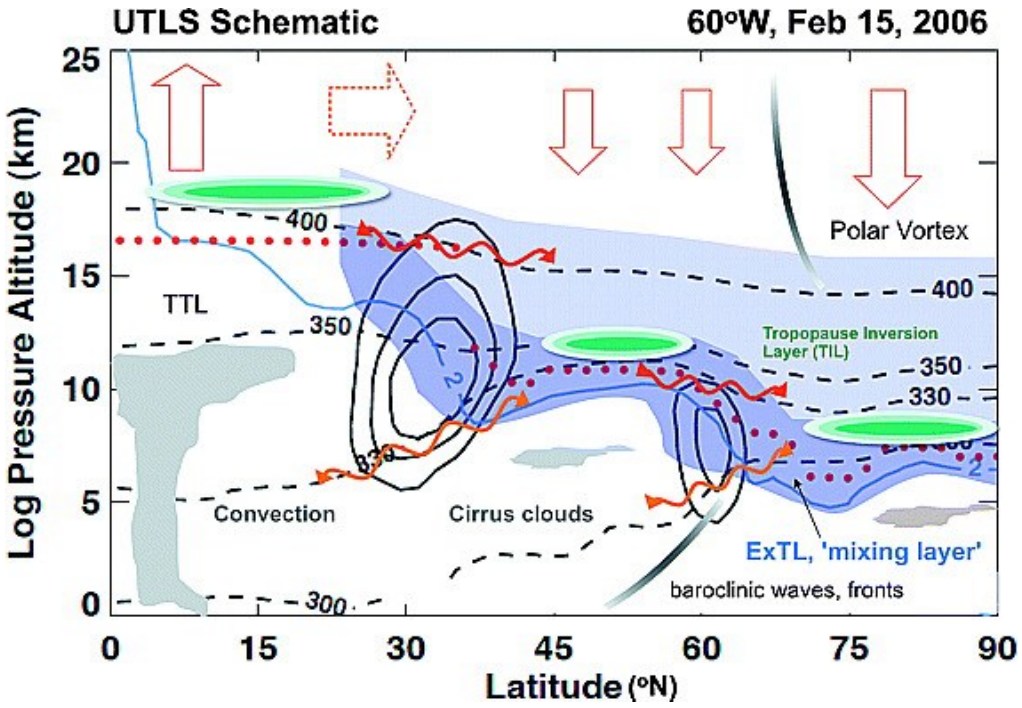

Figure 1.2 Schematic illustration of STE, taken from Gettelman et al. (2011) Figure 1, used with permission ©John Wiley and Sons.

1.3 Atmospheric radicals (OH, Cl)

Hydroxyl (OH) and chlorine (Cl) radicals are important for atmospheric oxidation processes. They react with many chemical compounds in the atmosphere, including methane, volatile organic compounds, carbon monoxide, and ozone-depleting substances. Primary OH radicals can be formed by the photodissociation of ozone in the presence of water vapor (Levy, 1971;Lelieveld et al., 2016):

$$O_3 + h\nu \rightarrow O(^1D) + O_2 \ (\lambda < 330 \text{ nm}) \quad \text{(R 1)}$$

$$O(^1D) + H_2O \rightarrow 2OH \quad \text{(R 2)}$$

Secondary OH radical formation (mostly generated through NO_x , O_x and OVOC oxidation mechanisms) lead to ~67% of global OH formation whereby the NO_x mechanism predominates in polluted environments and contributes greatly (~33%) to the global OH formation (Lelieveld et al., 2016). Figure 1.3 shows a simplified schematic of the formation and loss processes of OH and HO_2 in the remote troposphere. Dashed lines indicate pathways that become important at high NO_x concentrations, and solid lines indicate background conditions.

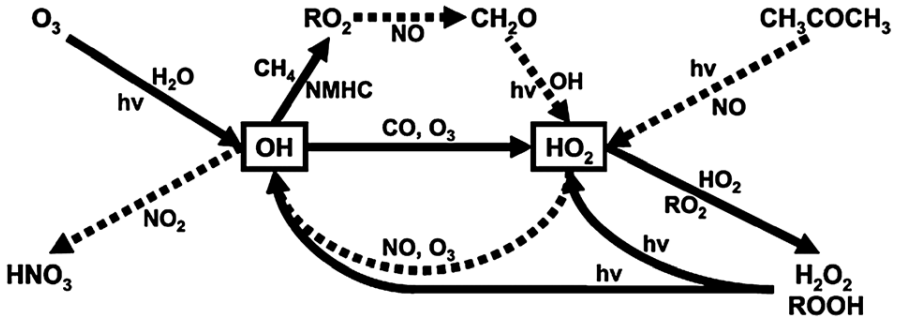

Figure 1.3 Simplified formation and loss scheme of HOx in the remote troposphere. Figure from Stone et al. (2012), used with permission © Royal Society of Chemistry.

OH radical concentrations can be either measured directly (e.g. by laser-induced fluorescence spectroscopy) (Fuchs et al., 2012) or estimated indirectly, such as by models (Lelieveld et al., 2016), from relationships of hydrocarbon measurements (Jobson et al., 1998;Williams et al., 2001;Li et al., 2018). Many ground based measurements or model simulations have been used to estimate mean OH radical concentrations of (1-7) × 10^6 molecules cm^{-3} with temporal and spatial variations (Heard et al., 2006;Hosaynali Beygi et al., 2011;Lelieveld et al., 2016). Stratospheric OH radicals were estimated as part of this PhD project with global aircraft measurements to be 1.1×10^5 ($\sigma = 0.8 \times 10^5$) molecules cm^{-3}, which is ten times lower than tropospheric OH concentrations (Li et al., 2018).

Chlorine radicals (or atoms) are more abundant in the stratosphere than the troposphere (Gromov et al., 2018). Chlorinated compounds (e.g. CFCs, HCFCs) act as major sources for Cl free radicals. In the stratosphere, the C-Cl bonds of these chlorinated compounds are broken down by high energy UV radiation (normally <290nm) and this process releases chlorine radicals. As an efficient catalyst (Molina, 1996), Cl radicals are responsible for ozone destruction, especially in polar regions, through the following reactions:

$$ClO + O \rightarrow Cl + O_2 \quad \text{(R 3)}$$

$$Cl + O_3 \rightarrow ClO + O_2 \quad \text{(R 4)}$$

$$\text{net: } O + O_3 \rightarrow 2O_2 \quad \text{(R 5)}$$

Tropospheric Cl concentrations are estimated to be low (~100 molecules cm^{-3}) (Gromov et al., 2018) whereas stratospheric Cl concentrations are > 1,000 molecules cm^{-3} (Li et al., 2018;Lelieveld et al., 1999;Park et al., 2010;Gromov et al., 2018).

1.4 IAGOS-CARIBIC observations

Observations of atmospheric trace gases in the UTLS region, such as CH_4, CO_2, SF_6, C_2H_6, HCN, CH_3Cl and halocarbons, are achieved by aircraft, balloons, or satellites, e.g. IAGOS-CARIBIC, SCIAMACHY, MOZAIC, TOMS, MIPAS, ACE, ATMOS, TRACE-A, START, HALOE, CONTRAIL, SPURT, ER-2 projects or campaigns (Baker et al., 2011;Schuck et al., 2009;Umezawa et al., 2015;Glatthor et al., 2009;González Abad et al., 2011;Pan et al., 2010;Schuck et al., 2012;Diallo et al., 2017;Sawa et al., 2008;Engel et al., 2006).

The IAGOS-CARIBIC project (**I**n-service **A**ircraft for a **G**lobal **O**bserving **S**ystem-**C**ivil **A**ircraft for the **R**egular **I**nvestigation of the atmosphere **B**ased on an **I**nstrument **C**ontainer) is an aircraft based scientific project with the aim of monitoring long-term global atmospheric physics and chemistry (Brenninkmeijer et al., 2007;Karu, 2019). The flight altitudes are ~10 km. The first phase (CARIBIC -1) started in 1997 and stopped in 2002. The second phase (CARIBIC -2) started in 2004 with more instrumentation and more frequent flights on board a Lufthansa A340 aircraft. From mid-2020, CARIBIC -2 stopped and the third phase (CARIBIC -3) is in preparation which will involve moving to the Lufthansa A350 aircraft with greater capacity for instrumentation and a longer flight range. CARIBIC -2 had 19 instruments on board, with more than 100 species being measured, including ozone, carbon dioxide, water vapor, aerosols, etc. Figure 1.4 shows the flight paths of CARIBIC -2 until April 2014. Within this PhD project, all the results are derived from analysis of the CARIBIC -2 data set.

Each CARIBIC -2 flight normally consisted of four flight sequences. Installed in the airplane container are two types of whole air samplers: HIRES and TRAC. HIRES consists of eighty-eight stainless steel flasks (1.2 L each) and each TRAC consists of fourteen glass sampling flasks (2.7 L each). During each flight, one HIRES and two TRACs are on board to collect air samples, thus in total 116 samples are collected. These

samples are transported to the laboratory at the Max Planck Institute for Chemistry, where three GCs with different detectors (FID, ECD, AED) measure greenhouse gases (GHGs) (Schuck et al., 2009), volatile organic compounds (VOCs) (Baker et al., 2010;Karu et al., 2020b) in the air samples.

Many studies have reported the atmospheric compositions in the UTLS region based on IAGOS-CARIBIC data. The Asian monsoon anticyclone promotes a fast transport from the tropics to mid-latitudes in the UTLS. That was confirmed by the study from Schuck et al. (2012), which presented distributions of CH_4 mixing ratios and fluxes over different regions in the UTLS, and in summer a CH_4 maximum over Asian regions was observed. Assonov et al. (2013) showed an application of N_2O measurements in the UTLS to distinguish upper tropospheric and STE-affected air. Baker et al. (2016) used relationships among measured hydrocarbons and explored strong chlorine radical chemistry over Asia. Thorenz et al. (2017) reported maximum concentrations of some trace gases and particles between 10°N and 10°S due to strong surface sources and rapid vertical transport. Umezawa et al. (2014) observed strong influence by biomass burning in South America and Africa, and domestic biofuel emission in South Asia with the CH_3Cl and CO measurements in the UTLS. Later Umezawa et al. (2015) estimated the stratospheric lifetime of CH_3Cl to be 35±7 years with a tracer-tracer correlation. Karu et al. (2020a) estimated COS lifetime (atmospheric: 2.1 ± 1.3 years and stratospheric: 47 ± 16 years) and a total flux of 118 ± 39 Gg (S) yr^{-1} into the stratosphere with observations in the UTLS.

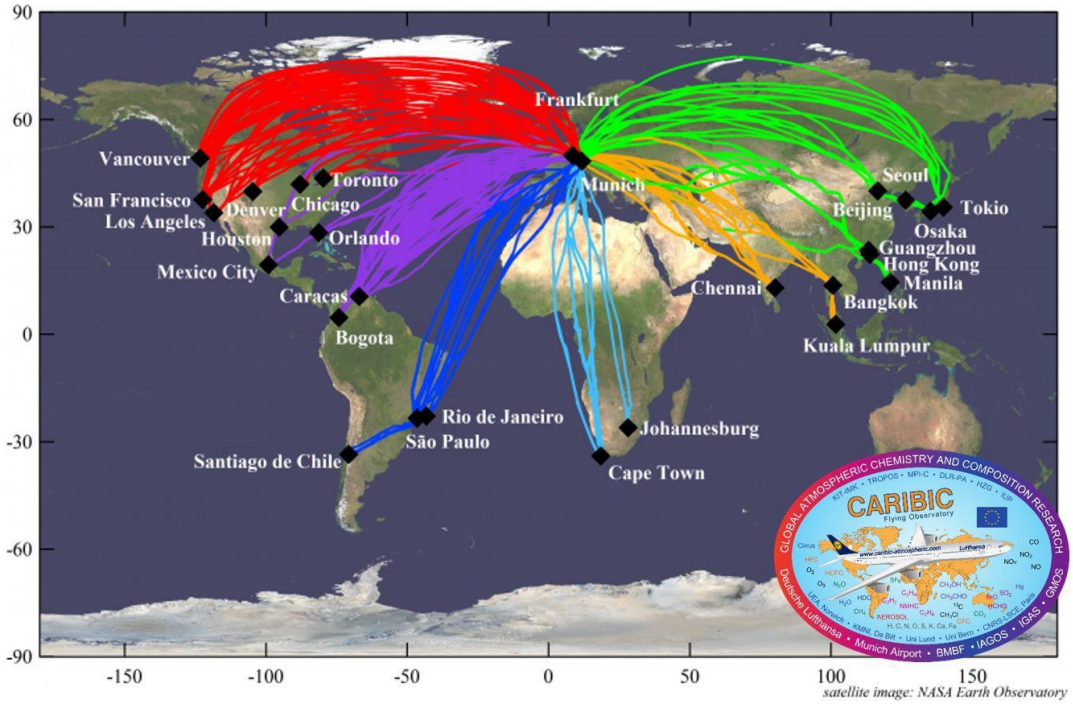

Figure 1.4 Flight paths of CARIBIC -2.

1.5 Atmospheric residence time

The atmospheric residence time (or lifetime) of a trace gas is normally estimated from its burden and known sinks. For the compounds with simple loss processes in the atmosphere, e.g. CFCs by photodissociation, CO and some VOCs by reaction with OH radicals, the lifetimes are relatively easy to estimate if the photolysis rates or OH reaction rate coefficients are known. Eq. 1.1 shows the lifetime of a compound with respect to OH sink following a second-order reaction.

$$\tau = \frac{1}{k[OH]} \qquad \text{(Eq. 1.1)}$$

Estimating residence time becomes difficult for gases with multiple loss processes, e.g. removal processes of CO_2 and carbonyl sulfide (COS), which include important contributions from the uptake by vegetation and ocean, which cover timescales from minutes to centuries.

Junge (1974) presented an inverse correlation between residence time of trace gases and their variabilities (hereinafter as "variability-residence time relationship"). This included many important atmospheric gases, such as CO_2, CH_4, N_2O, with range of residence times from 0.01 to 10^7 years. Subsequent studies (Jobson et al., 1998;Jobson et al., 1999;Volk et al., 1997) have improved the approach and applied it on field measurements in the troposphere and the stratosphere. These works have concluded that the "b" factor in the equation (details see Chapter 3) indicates the remoteness of sources, and pointed out the influence of Cl atoms on the approach. Further studies have examined this approach with various trace gases in different locations (Williams et al., 2000;Pollmann et al., 2016), mostly targeting OH radical estimations.

In this PhD project, the improved variability-residence time relationship approach was applied to estimate the atmospheric and stratospheric residence time of COS and CO_2 with the CARIBIC data set and NOAA ground site observations.

2. TROPOSPHERIC OH AND STRATOSPHERIC OH AND CL CONCENTRATIONS DETERMINED FROM CH_4, CH_3CL, AND SF_6 MEASUREMENTS

This work has been published as Li et al. (2018):

Li, M., Karu, E., Brenninkmeijer, C., Fischer, H., Lelieveld, J., and Williams, J.: Tropospheric OH and stratospheric OH and Cl concentrations determined from CH_4, CH_3Cl, and SF_6 measurements, Nature Climate and Atmospheric Science, 1, 2018.

I am the first-author of this work and my contribution to this work includes developing the concepts of effective OH concentration and its relationship with mean age of air, analyzing all the data (including estimating tropospheric and stratospheric OH, stratospheric Cl concentrations), making all the figures and tables, and writing the manuscript together with Prof. Williams.

The following text and figures quoted (within "") from page 12 to page 32 are exactly the same as published on Li et al. (2018) which is cited on page 11.

"Abstract

The hydroxyl (OH) radical is the key oxidant in the global atmosphere as it controls the concentrations of toxic gases like carbon monoxide and climate relevant gases like methane. In some regions, oxidation by chlorine (Cl) radical is also important, and in the stratosphere both OH and Cl radicals impact ozone. An empirical method is presented to determine effective OH concentrations in the troposphere and lower stratosphere, based on CH_4, CH_3Cl and SF_6 data from aircraft measurements (IAGOS-CARIBIC) and a ground based station (NOAA). Tropospheric OH average values of 10.9×10^5 (σ = 9.6×10^5) molecules cm^{-3} and stratospheric OH average values of 1.1×10^5 ($\sigma = 0.8\times10^5$) molecules cm^{-3} were derived over mean ages derived from SF_6. Using CH_4 led to higher OH estimates due to the temperature dependence of the CH_4 + OH reaction in the troposphere and due to the presence of Cl in the stratosphere. Exploiting the difference in effective OH calculated from CH_3Cl and CH_4 we determine the main altitude for tropospheric CH_4 oxidation to be 4.5~10.5km and the average Cl radical concentration in the lower stratosphere to be 1.1×10^4 ($\sigma = 0.6\times10^4$) molecules cm^{-3} (with a 35% measurement uncertainty). Furthermore, the data are used to examine the temporal trend in annual average stratospheric OH and Cl radical concentration between 2010 and 2015. 2013 showed highest stratospheric OH and lowest Cl but no clear temporal trend was observed in the data in this period. These data serve as a baseline for future studies of stratospheric circulation changes.

Introduction

The hydroxyl radical (OH) is the most important oxidant in the troposphere and lower stratosphere. It initiates removal from the atmosphere of toxic gases such as carbon monoxide (CO), radiatively active gases such as methane (CH_4), tropospheric ozone precursors such as volatile organic compounds (VOCs) and NOx ($NO + NO_2$), and stratospheric ozone-depleting compounds such as hydrochlorofluorocarbons (HCFCs) (Lelieveld et al., 2008;Montzka et al., 2011b). Therefore, it plays a key role in the atmospheric oxidation capacity, air quality and climate (Patra et al., 2014).

One source of atmospheric OH is the reaction of O^1D, a minor product in the photolysis of ozone, with H_2O (Levy, 1971;Heard and Pilling, 2003). An even larger source in terms of gross OH formation is recycling from its reaction products, which maintains the atmospheric oxidation efficiency (Lelieveld et al., 2016). Despite its low ambient concentration (< 1pptv), and its short atmospheric lifetime (<1 s), the first valid OH measurements (by FAGE-LIF) were reported as early as the mid-1980s at ground level (Hard et al., 1986). Measurements were later extended to the upper troposphere and lower stratosphere with balloons (Stimpfle and Anderson, 1988) and the high-altitude ER2 research aircraft (Wennberg et al., 1994), in parallel with alternative measurement methods such as differential optical absorption spectroscopy DOAS (Perner, 1976), mass spectrometry via $H_2{}^{34}SO_4$ (Eisele and Tanner, 1991) and ^{14}CO radioactive counting techniques(Felton et al., 1988). These in-situ measurements are broadly consistent with regional scale indirect OH determinations using the depletion of hydrocarbons over multi-hour timescales (Mckeen et al., 1990;Blake et al., 1993) and with empirical assessments based on the variability lifetime relationship (Williams et al., 2000;Williams et al., 2001).

Although OH concentrations at a given point in space and time can now be measured reliably at high frequency to examine local photochemistry, it is difficult to relate such

OH concentrations that vary strongly with actinic flux and H_2O, to longer lived species transported zonally in the troposphere and eventually into the stratosphere. To address this, advanced models have been applied to make indirect estimates of the global OH concentration based on methyl chloroform (CH_3CCl_3) and ^{14}CO data (Lelieveld et al., 2016;Rigby et al., 2017;Patra et al., 2014;Montzka et al., 2011b;Prinn et al., 2005;Krol and Lelieveld, 2003). However, such models inevitably contain in-built assumptions, including uncertain emissions inventories as well as transport and deposition parameterizations that may differ from real world conditions.

In this study, we have developed and applied an empirical data based method to estimate the "effective OH concentration" that has acted in the troposphere and lower stratosphere over longer (yearly) timescales between 2008-2015. Our approach uses long term measurements of three species (SF_6, CH_3Cl and CH_4) made at the ground and monthly at 10-12 km altitude during long distance commercial aircraft flights. SF_6 measurements are used to derive the mean air age of the airborne samples, i.e. of the trace compounds contained therein, so that the initial surface mixing ratios of CH_3Cl and CH_4, upon emission, can be determined from the surface network and compared with the OH affected samples taken at altitude. Knowing the age of the sampled air, the net change in concentration and the reaction rate coefficient allows an "effective OH" concentration to be calculated assuming OH is the only sink. Both CH_3Cl and CH_4 are predominately removed from the atmosphere by OH although reaction rates are relatively slow (atmospheric lifetimes are about one year (Montzka et al., 2011a) and 8-10 years (Prinn et al., 2005) respectively). CH_3Cl is mostly emitted from tropical vegetation (Yokouchi et al., 2002) and is the most abundant natural source of stratospheric chlorine (Santee et al., 2013;Umezawa et al., 2014). The greenhouse gas CH_4 is emitted from wetlands, ruminants, rice fields, landfills and fossil fuel use, and atmospheric concentrations have increased strongly over the past 200 years (Baker et al., 2012;Turner et al., 2017). In the context of this study an important difference between CH_3Cl and CH_4 is that the rates of reaction with OH and Cl are much more dependent on temperature in the case of CH_4. Using this data based approach we may empirically determine a representative annual "effective OH concentration" for the troposphere and the lower stratosphere. Furthermore, we may look for indications of temporal trends in OH and hence changes

in global oxidation capacity. Finally, by exploiting the reaction rate differences between CH_3Cl and CH_4 we can even attempt to determine the height in the troposphere where CH_4 oxidation by OH is largest and estimate Cl radical concentration in the lowermost stratosphere.

Results

OH concentration as a function of mean age

The derived "effective OH concentration" experienced by an air parcel will be hereafter shortened to OH_{eff}, and depending on the air age be referred to as tropospheric OH_{eff} (age <100 days) and stratospheric OH_{eff} (age >200 days). The rationale is that an air sample collected in the upper troposphere – lower stratosphere (UTLS) region can be regarded as a mixture of two major largescale airflows (Bönisch et al., 2009;Ray et al., 2014;Garny et al., 2014). The first is the fast transport of air from the tropical tropopause layer (TTL) to the extra tropics (Fig.1 blue lines) which normally takes place within 0.3 years (~100 days), while the second pathway (Fig.1 red lines) is the slower downwelling transport from the "overworld" (potential temperature > 380 K) into the lowermost stratosphere which is associated with the lower branch of the Brewer-Dobson circulation (BDC). Note that the compounds within the lower stratosphere of the northern hemisphere are predominately influenced by the BDC and not the northern mid-latitude emissions (~10%) (Orbe et al., 2015). In order to simplify interpretation of the results and to apply our analysis to the region of highest airborne data coverage we use only samples collected between 30°-60°N in the UTLS region (Fig. 1 box).

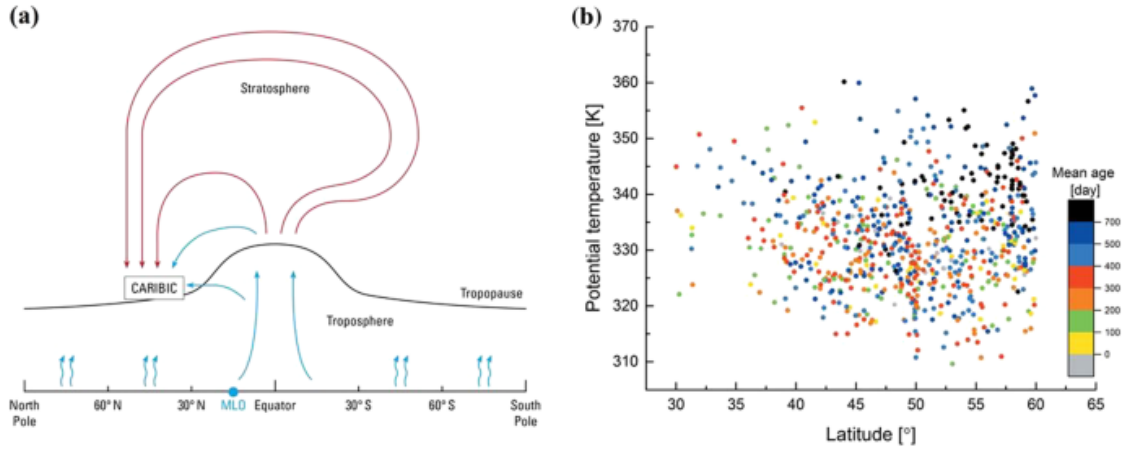

Figure 1 (a) A schematic representation of the major atmospheric transport pathways associated with CARIBIC samples between 30°-60°N. The blue arrows indicate fast transport from ground to the tropical tropopause, the red arrows indicate downward transport from the stratosphere into the lowermost stratosphere. The box indicates CARIBIC flight sampling altitude. The NOAA observation station at Mauna Loa (MLO) is marked in blue. (b)Scatterplot of all samples' latitude versus potential temperature, color-coded with mean age.

Figure 2 shows the OH_{eff} derived from both CH_3Cl (black boxes) and CH_4 (red boxes) and OH_r (real OH, blue boxes) derived from OH_{eff} and stratospheric Cl (eq.4, see Method) as a function of mean air age. The tropospheric (mean age <100 days) mean OH_{eff} from both species is significantly larger (by a factor of 6 on average) than the lower stratospheric (mean age >200 days) mean OH_{eff}. Air with a mean age of between 100-200 days appears to be influenced by both troposphere and stratosphere, and accordingly OH_{eff} for both species in this age range lies between the younger (tropospheric) and older (stratospheric) values. Median tropospheric OH_{eff} were 9.93×10^5 and 2.63×10^6 molecules cm^{-3} for CH_3Cl and CH_4 respectively, whereas median stratospheric values from 200-1100 days were 1.69×10^5 and 3.35×10^5 molecules cm^{-3}. Tropospheric OH_{eff} values exhibit a much larger variability than stratospheric values, likely due to the strong sources and sinks of both molecules in the tropical troposphere, including weak seasonal variations that impact the term $[A]_g - [A]_C$ in eq.1. Stratospheric OH_r exhibits smaller variation compared to stratospheric OH_{eff} and is rather constant for samples with mean age between 200 and 700 days with a median value of 1.0×10^5 molecules cm^{-3}, whereas for samples older than 700 days, OH_r decreases due to the decrease of ozone, water vapor

and molecule density in the upper stratosphere. Median, average and standard deviation data are given numerically in Table 1(a).

Interestingly, OH_{eff} calculated using the CH_4 data was consistently higher than using CH_3Cl data. The tropospheric median OH_{eff} derived from CH_3Cl for years 2008-2015 is 9.9×10^5 molecules cm^{-3} which matches the tropospheric mean OH concentration of 1.1×10^6 molecules cm^{-3} reported from a recent global modelling study (Lelieveld et al., 2016). However, the median tropospheric OH_{eff} derived from CH_4, 2.6×10^6 molecules cm^{-3}, is between two and three times larger. Intuitively this seems unreasonable since both measurements stem from the same air sample and therefore must render the same "effective OH concentration" assuming there is no additional reagent inputs. One

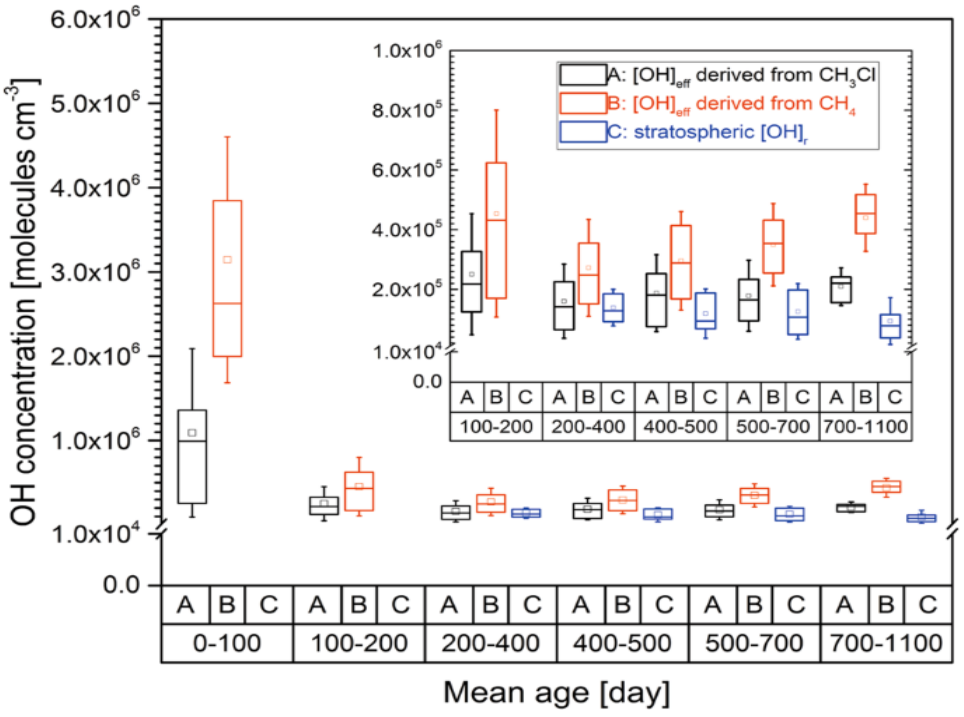

Figure 2 OH abundance (OH_{eff}, OH_r) derived from CH_3Cl and CH_4 for different mean age groups over all years (2008-2015 for OH_{eff}, 2010-2015 for OH_r), the inserted figure excludes the troposphere to expand the concentration scale. Box plots with the median (horizontal solid line in the box) and the mean (square in the box) gives the 25% and 75% percentiles and whisker in dashed line indicates one standard deviation. Number of samples >12 for each group.

possible explanation for this apparent discrepancy is that loss processes besides OH remove CH_4 from the atmosphere but are then calculated as OH in this approach. For example, the reaction with chlorine radicals (Cl) with CH_4 has been shown to be significant in Asian pollution outflow(Baker et al., 2016). The aforementioned paper reported the presence of radicals in the ratio [Cl]:[OH] of 9~16 Cl:10^3 OH, and since the reaction rate of CH_4 with Cl is ~32 times faster than that with OH (for CH_3Cl it is only 10 times faster) (DeMore, 1997), an apparent overestimation of OH_{eff} by about 30-50% can ensue. However, such high Cl radical concentrations have only been seen under very specific conditions (lofted coastal pollution outflow) and so this cannot explain the OH_{eff} difference in the global tropospheric data. An alternative explanation for the discrepancy is the strong temperature dependence of reaction 2, as CH_4 oxidation by OH occurs much more rapidly in the warmer lower atmosphere. Assuming that the OH_{eff} from CH_3Cl is correct (as it is lower and in agreement with previous global estimates), we may determine at which temperature (and therefore which altitude) CH_4 oxidation mainly occurs. By this method, we calculate that most tropospheric oxidation of CH_4 occurs at circa 7km (4.5~10.5km, 220~260K). OH radical abundance reaches an optimum just above the boundary layer (2-4km) where the water concentration and photon fluxes are high and the flux of reactive sink species from the surface is decreasing. In addition, a second OH optimum occurs in the outflow region of clouds (10km) (Lange et al., 2001) where uplifted and lightning generated NOx enhances OH levels through the reaction of HO_2 with NO. Therefore the 4.5~10.5km height derived in this study likely represents an average of the effects of both OH maxima regions. This empirical estimate concurs with the model derived report that OH concentrations are at maximum in the free troposphere owing to recycling by NO_x (Lelieveld et al., 2016). A recent global modelling study using comprehensive chemistry (Lelieveld et al., 2016) suggests that OH is relatively high in the 4.5-10.5km altitude range, which was attributed to OH recycling rather than primary formation. The model derived distribution is supported by this work.

Table 1 Statistical values (median, mean, one standard deviation (STD)) of (a) derived OH_{eff} and stratospheric OH_r for different mean age groups; (b) chlorine radical in the stratosphere during 2010-2015 (unit in 10^3 molecules cm^{-3}); and (c) stratospheric OH_r in the stratosphere during 2010-2015 (unit in 10^4 molecules cm^{-3}).

(a)

Mean age [day]		0-100	100-200	200-400	400-500	500-700	700-1100
OH_{eff} derived from CH_3Cl ($\times10^5$ molecules cm^{-3})	Median	9.9	2.2	1.4	1.8	1.6	2.2
	Mean	10.9	2.5	1.6	1.9	1.8	2.1
	STD	9.6	2.0	1.2	1.3	1.2	0.6
OH_{eff} derived from CH_4 ($\times10^5$ molecules cm^{-3})	Median	26.3	4.3	2.5	2.9	3.5	4.5
	Mean	31.4	4.5	2.7	3.0	3.5	4.4
	STD	14.1	3.4	1.6	1.7	1.4	1.1
stratospheric OH_r ($\times10^4$ molecules cm^{-3})	Median			13.0	8.8	9.7	9.0
	Mean			12.8	10.3	11.1	9.9
	STD			7.6	7.5	8.1	7.0

(b)

	2010	2011	2012	2013	2014	2015
Median	10.4	11.6	12.6	6.9	8.2	9.7
Mean	11.7	10.9	12.1	7.3	10.0	11.3
STD	6.9	4.9	6.8	5.1	5.7	6.4

(c)

	2010	2011	2012	2013	2014	2015
Median	9.2	8.2	11.9	12.8	5.4	9.3
Mean	11.8	9.5	12.1	12.4	8.5	9.6
STD	7.8	7.9	8.2	7.9	6.9	5.1

Stratospheric Cl radical

Figure 3 shows the annual Cl radical concentration derived from air samples with age larger than 200 days in the stratosphere over the time period 2010-2015. The average Cl concentration over all periods is 1.1 (±0.6)×10^4 molecules cm^{-3}. Even though this result is five times higher compared to a 24h average Cl concentration of 2.40×10^3 molecules cm^{-3} for 14-18.5 km height (Park et al., 2010), it is more comparable to lower stratospheric Cl concentration of 5×10^3~3×10^4 molecules cm^{-3} estimated by CO/C_2H_6 ratio (Lelieveld et al., 1999). Our result is also in close agreement with a recent model estimation (Gromov et al., 2018) based on isotopic ratios of methane and CO that yielded 1.6×10^4 molecules cm^{-3} for the lowermost stratosphere. No significant variation during this timeframe is observed in our dataset, although in 2013 Cl concentrations were lower than in the other years. Note that due to other minor loss processes (e.g. reaction with O^1D, photodissociation (Minschwaner and Manney, 2015)) in the stratosphere and mesosphere for both molecules, there is a slight overestimation of stratospheric Cl concentration. Mean, median and one standard deviation data are given in Table 1(b).

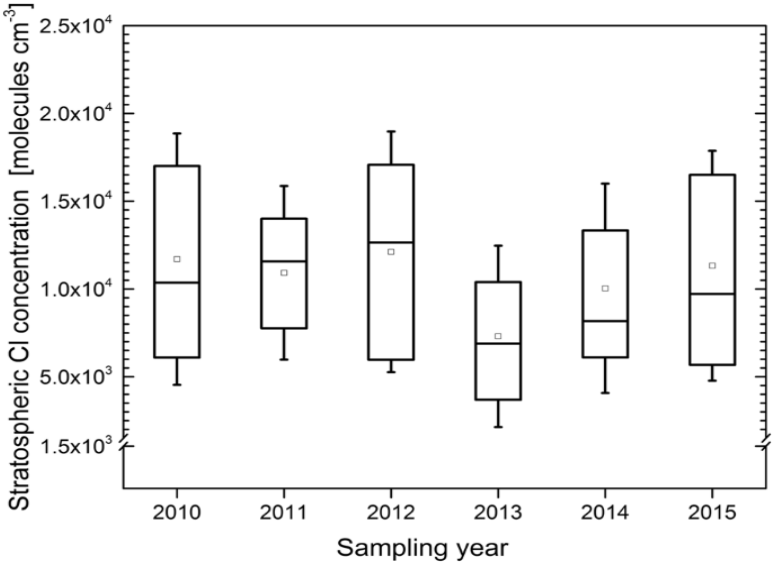

Figure 3 Annual trend (2010-2015) of stratospheric chlorine radical concentration derived from samples with mean age larger than 200 days. Box plots with the median (horizontal solid line in the box) and the mean (square in the box) gives the 25% and 75% percentiles and whisker in dashed line indicates one standard deviation. Number of samples > 12 for each group.

Stratospheric OH radical

Figure 4 presents the annual average stratospheric OH_r as a function of sampling year rather than the mean air age shown in Figure 2. Data are from samples with age larger than 200 days to be classed as stratospheric. The overall stratospheric OH_r of 1.1 (±0.8) $\times 10^5$ molecules cm^{-3} for the years 2010-2015 is derived. Median average OH values generally vary within 0.8~1.3$\times 10^5$ molecules cm^{-3} with an exceptionally low median value of 5.4$\times 10^4$ in the year 2014, statistical details see Table 1(c). No clear trend is apparent in the dataset, and the highest value was found for 2013.

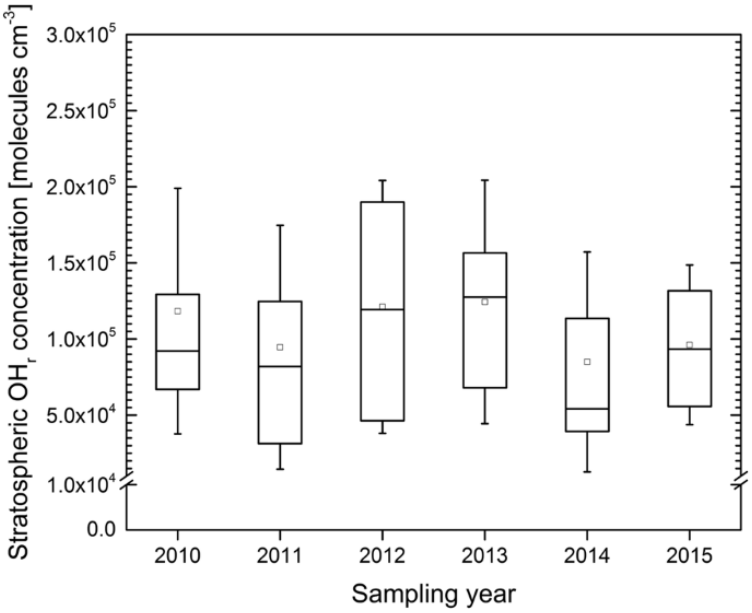

Figure 4 Annual trend (2010–2015) of stratospheric OHr concentration derived from samples with mean age larger than 200 days. Box plots with the median (horizontal solid line in the box) and the mean (square in the box) give the 25 and 75% percentiles and whisker in dashed line indicates one standard deviation. Number of samples > 12 for each group

Discussion

This study presents a new empirical method of monitoring the effective OH concentration in the global troposphere and lower stratosphere over long periods. The method also delivers the mean altitude range for tropospheric CH_4 oxidation and the effective Cl radical concentration in the lower stratosphere. These parameters are all useful measures of the overall atmospheric oxidizing capacity and markers for future circulation changes. Provided that high quality, long term monitoring of these three gases continues, the impact of future global events can be assessed in these terms. For example, a volcanic eruption, a change in global CFC emission rates, or a change in stratospheric circulation patterns can lead to changes in UV radiation, stratospheric chlorine loading, and water vapor, all of which can significantly impact the derived metrics.

This method is built on three key assumptions. The first is that both CH_3Cl and CH_4 are predominantly oxidized by OH. While this is true for the troposphere and the lower stratosphere, over longer timescales (>500 days) air masses can be expected to also enter the upper stratosphere as part of the Brewer-Dobson circulation. At these higher altitudes a minor photolysis sink for CH_3Cl and the reaction of O^1D radicals with CH_4 could lead to a small overestimation of the calculated effective OH. Indeed, in Figure 2 a tendency to higher OH_{eff} in older air can be seen in the CH_4 derived OH results. By only considering data within certain age ranges (0-100 days troposphere and 200-400 days lower stratosphere) the impact of additional loss mechanisms is limited. The second assumption is that this time segregation does delineate troposphere (0-100 days), mixed troposphere-stratosphere (100-200 days) and stratosphere (>200 days). This assumption is supported by the trend in OH variability measured in the three categories. The third assumption made here is that the tropospheric effective OH using CH_3Cl is correct and CH_4 derived OH is high because of either Cl radicals (in the stratosphere) or the temperature dependence of the reaction (in the troposphere). Support for this assumption

comes from the fact that the CH_3Cl estimate is lower than that of CH_4 (additional chemistry leads to overestimation), no other significant loss rates are known, and the CH_3Cl estimate more closely matches the most recent global model studies.

Uncertainties and sensitivities of this method are important to consider. Different to variations which show statistical distributions of the results, uncertainties are the differences between the measured values and the true values, whereas sensitivities represent how much output values will be affected by the input values. Firstly, there is an instrumental uncertainty. By considering the measurement errors of SF_6, CH_4, CH_3Cl measurements at ground level and by aircraft and reaction rates k_{OH} and k_{Cl}, measurement uncertainties are calculated by error propagation for mean age, OH_{eff} derived from CH_4 and CH_3Cl, stratospheric Cl and stratospheric OH_r of 8%, 10%, 22%, 35% and 37%, respectively. Secondly the choice of the source region could influence the calculation. An ideal tracer for the mean age calculation should be well mixed in the source region so that its mixing ratio time series can be used to derive initial concentrations. Since SF_6 is not perfectly well mixed globally (i.e. there is a weak NH/SH gradient and a slight latitude dependence in each hemisphere), an average mixing ratio should be applied to represent the source region. Therefore we chose the average SF_6 mixing ratio in the northern hemisphere (NH) as determined by the NOAA network since our samples were collected in northern mid-latitudes. The mean age results were also derived from individual source regions, namely Mauna Loa (MLO, 19.5°N), Cape Matatula (SMO, 14.3°S), Niwot Ridge (NWR, 40.052°N), Pt. Barrow (BRW, 71.3°N), Mace Head (MHD, 53°N) and 20°S to 20°N region, but the overall average NH SF_6 observation gave the most positive mean age values for our aircraft measurements. A ±0.05 ppt difference of SF_6 mixing ratios in different tropospheric source regions corresponds to 0.17 years difference for the derived mean age. Thirdly we consider the sensitivity of calculation to the temperature-dependent reaction rates. We use two temperatures (216K and 250K) to represent the average temperatures in the troposphere and stratosphere. By varying these temperatures by ±5K, the reaction rate of the reaction CH_3Cl+OH is less sensitive (variation of -14% ~ 11%) than that of the reaction CH_4+OH (variation of -17% ~ 33%) (see Table S1 in the supplementary material). Fourthly, sensitivity of seasonal cycles of CH_4, CH_3Cl in source region. Both CH_4, CH_3Cl have

seasonal cycles in the troposphere with amplitudes of ca. 1% and 5%, respectively. When examining their temporal concentration in the lowermost stratosphere (Fig.S2 in the supplementary material) with the N_2O concentration(Boering et al., 1996), seasonal variations of CH_4 have been damped out (linear correlation in each N_2O group) while those of CH_3Cl are attenuated but still visible. By varying ±5% of CH_3Cl in the source region, the OH_{eff} of samples with age ~70 days and larger than 700 days change ~80% and ~25%, respectively. Finally, in this study OH is calculated as a second order reaction (see Eqs. 2 and 3 in Method). Alternatively one can use the pseudo first order approach in which OH is assumed to be constant Ac= Ag*exp(-R*k*OH) (6) and this produces fractionally higher values (<1%).

It should be noted that the now well established methyl chloroform (MCF) derived global mean OH requires several important assumptions, for example concerning MCF emissions (at least before 2000), ocean uptake and stratospheric loss. Furthermore, MCF is declining rapidly as emissions have stopped, and it does not provide height information, nor indications about Cl abundance. Other relatively long-lived halocarbons have been considered to complement the MCF method, but these OH estimates are also dependent on the source estimates. Therefore, our new, independent method should be acknowledged as an important complementary source of information on OH and Cl.

The radical abundances derived here represent multiday average effective concentrations that are derived directly from long lived atmospheric gas measurements. Therefore this work provides an important ground truth dataset for comparison with modelling approaches, and oxidant levels that can be used in conjunction with rate coefficients to derive lifetime estimates for other atmospheric species. This valuable information is obtained from relatively inaccessible regions using measurements of only three molecules. Provided the aircraft and ground based measurements continue, then future OH and Cl oxidant changes induced by major volcanos or stratospheric circulation changes should be captured by applying this method. This work provides the empirical methodological approach and the baseline for future studies.

Methods

Data set. Whole air samples of IAGOS-CARIBIC (In-service Aircraft for a Global Observing System-Civil Aircraft for the Regular Investigation of the atmosphere Based on an Instrument Container) were collected at 10-12km in canisters during four flights monthly since 2008 and non-methane hydrocarbons and greenhouse gases were analyzed in laboratory at the Max Planck Institute for Chemistry, Mainz, Germany (Brenninkmeijer et al., 2007). Flight paths are shown in Fig.1(b). SF_6, CH_4 and CH_3Cl data of CARIBIC project were analyzed (Schuck et al., 2009;Baker et al., 2010;Brenninkmeijer et al., 2007;Umezawa et al., 2014) using GC-ECD (for SF_6) and GC-FID (for CH_4 and CH_3Cl) with measurement precisions of 1.5%, 0.17% and 1%, respectively. Ground station SF_6 data was taken from the monthly northern hemispheric NOAA/ESRL halocarbons flask program. CH_4 data is from the hourly NOAA ESRL Carbon Cycle Cooperative Global Air Sampling Network at Mauna Loa (Dlugokencky et al., 2017) and CH_3Cl data from the daily NOAA/ESRL halocarbons in situ program. NOAA used GC-FID for CH_4 and GC-ECD for SF_6 with precisions of 0.5% (SF_6) (Hall et al., 2011), 0.2% (CH_4) (Dlugokencky et al., 1994), respectively.

Mean age calculation. SF_6 is a long-lived industrial tracer with estimated global emissions of 7.4±0.6 Gg/yr (Rigby et al., 2010) and has negligible sinks in the troposphere and stratosphere. Consequently, the atmospheric mixing ratio of SF_6 has been observed to increase steadily for the past three decades(IPCC, 2007) with a growth rate of 0.27 ppt/yr. In several previous studies, this species has been used to determine the "mean age" of air samples collected at altitude (Waugh, 2002;Engel et al., 2008;Ray et al., 2014;Hall and Plumb, 1994). This "mean age" is the term given to the time since the SF_6 mixing ratio measured from the aircraft is equivalent to the SF_6 measured in the surface source region, or in other words it indicates the average transit time between air leaving the surface until it is measured. We used the monthly northern hemispheric SF_6

observations from NOAA/ESRL halocarbons flask program as the initial SF_6 concentrations and a second-order polynomial fitting was applied for the time series (years 2005-2016) of SF_6 mixing ratio. Then we applied SF_6 mixing ratios by aircraft measurements to the fitting and found out the initial emission time. The difference of sampling time and initial emission time is the mean age. We excluded samples with calculated age less than 0 day (2.3% of total samples) that arise due to the higher mixing ratios of SF_6 in extratropical troposphere than that in the tropics (Bönisch et al., 2009). The spatial distribution of mean age can be found in Fig.1 (b). Absolute counts for each mean age group are shown in Fig. S1 in the supplementary material.

Effective OH calculation. The effective OH concentration $[OH]_{eff}$ was calculated according to equation (1).

$$[OH]_{eff} = \frac{[A]_g - [A]_c}{\Gamma \cdot k_{OH+A} \cdot [A]_g} \quad (1)$$

Where Γ is the mean age, $[A]_c$ is the mixing ratio of a compound A (in this case either CH_4 or CH_3Cl) sampled aloft by the CARIBIC aircraft at time t, and $[A]_g$ is the mixing ratio of A observed from the ground station at time t-Γ. Thus, $[A]_g - [A]_C$ equates to the average loss of A during a time period of Γ, and k_{OH+A} is the second-order reaction rate of compound A with the OH radical which is calculated for two temperatures (216K for Γ<100 days and 250K for Γ>100 days) corresponding to 11km and 40km height(National Oceanic Atmospheric Administration, 1976). In this calculation we assume that air with Γ<100 days has experienced predominately tropospheric conditions (average temperature of 216K), whereas air with Γ>100 days will have been transported to the stratosphere (average temperature of 250K).

The reactions and associated rates (Srinivasan, 2005;DeMore, 1997;Atkinson, 2003) are as follows:

$$CH_4 + OH \rightarrow CH_3 + H_2O \quad (2)$$

($k_{OH+CH_4,216K} = 6.9 \times 10^{-16}\ cm^3 s^{-1}$; $k_{OH+CH_4,250K} = 2.06 \times 10^{-15}\ cm^3 s^{-1}$)

$$CH_3Cl + OH \rightarrow CH_2Cl + H_2O \quad (3)$$

($k_{OH+CH_3Cl,216K} = 6.13 \times 10^{-15}\ cm^3 s^{-1}$; $k_{OH+CH_3Cl,250K} = 1.48 \times 10^{-14}\ cm^3 s^{-1}$)

Stratospheric Cl and OH radical calculation. Effective OH concentrations for the lower stratosphere, see Figure 1, were consistently higher when calculated from CH_4, similar to the tropospheric values described above. However, in the stratosphere, the differential reaction rate of Cl with CH_4 and CH_3Cl is a viable explanation for the relatively constant offset in calculated OH_{eff} as chlorine radical production at high altitudes (>10 km) occurs over wide areas due to photolysis of chlorine containing compounds. For this calculation, we assume loss of CH_4 (or CH_3Cl):

$$k_{OH+A} \cdot [OH]_r + k_{Cl+A} \cdot [Cl] = k_{OH+A} \cdot [OH]_{eff\text{-}A} \quad (4)$$

where $[OH]_r$ is the real OH concentration in the stratosphere, [Cl] is the chlorine radical concentration, $[OH]_{eff\text{-}A}$ is the effective OH derived from compound A in this study. Applying Eq.4 for CH_4 and CH_3Cl, then [Cl] can be expressed as:

$$[Cl] = \frac{[OH]_{eff\text{-}CH_4} - [OH]_{eff\text{-}CH_3Cl}}{\frac{k_{Cl+CH_4}}{k_{OH+CH_4}} - \frac{k_{Cl+CH_3Cl}}{k_{OH+CH_3Cl}}} \quad (5)$$

The ratios of k(Cl)/k(OH) are taken as 24 and 10 for CH_4 and CH_3Cl at 250K, respectively.

Supplementary Information

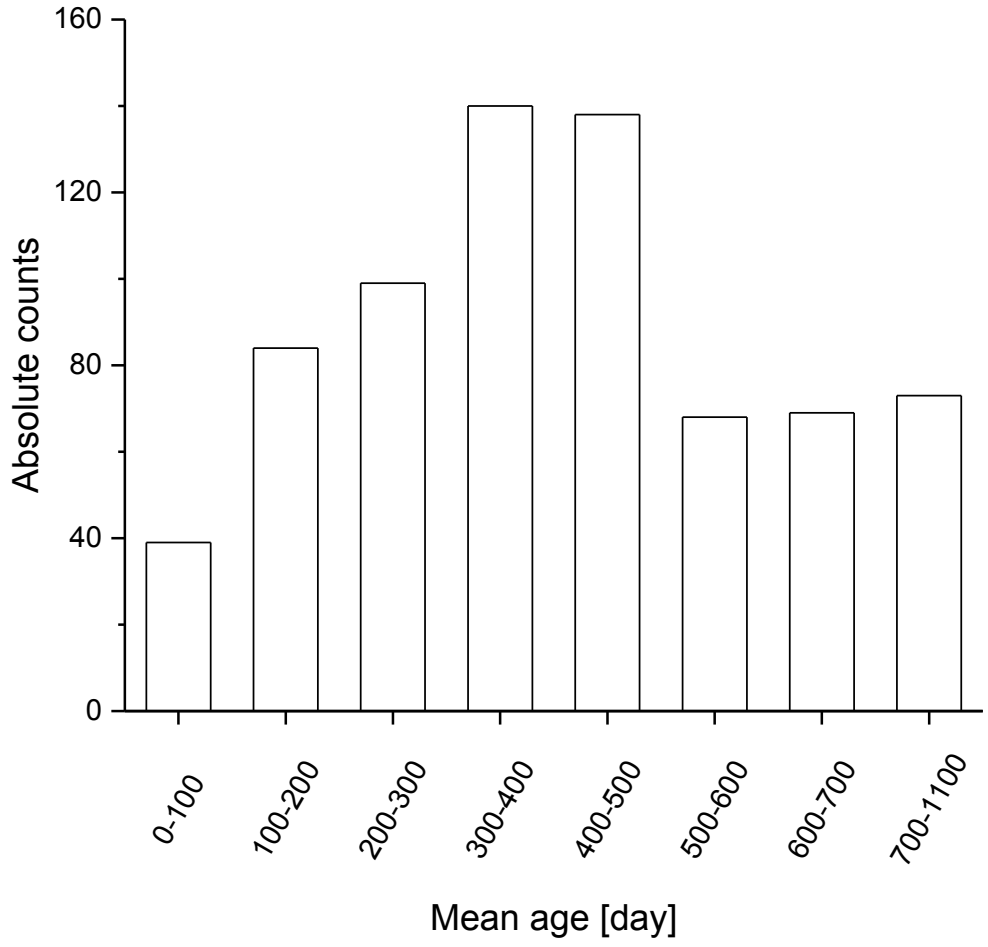

Figure S1. Total sample numbers for each mean age group.

Table S1. Sensitivity of reaction rates of CH_4+OH and CH_3Cl+OH to temperature variation.

		CH_4+OH	CH_3Cl+OH
Troposphere	$(k_{211K}-k_{216k})/k_{216k}$	-17%	-14%
	$(k_{221K}-k_{216k})/k_{216k}$	20%	16%
Stratosphere	$(k_{245K}-k_{250k})/k_{250k}$	-14%	-11%
	$(k_{255K}-k_{250k})/k_{250k}$	33%	11%

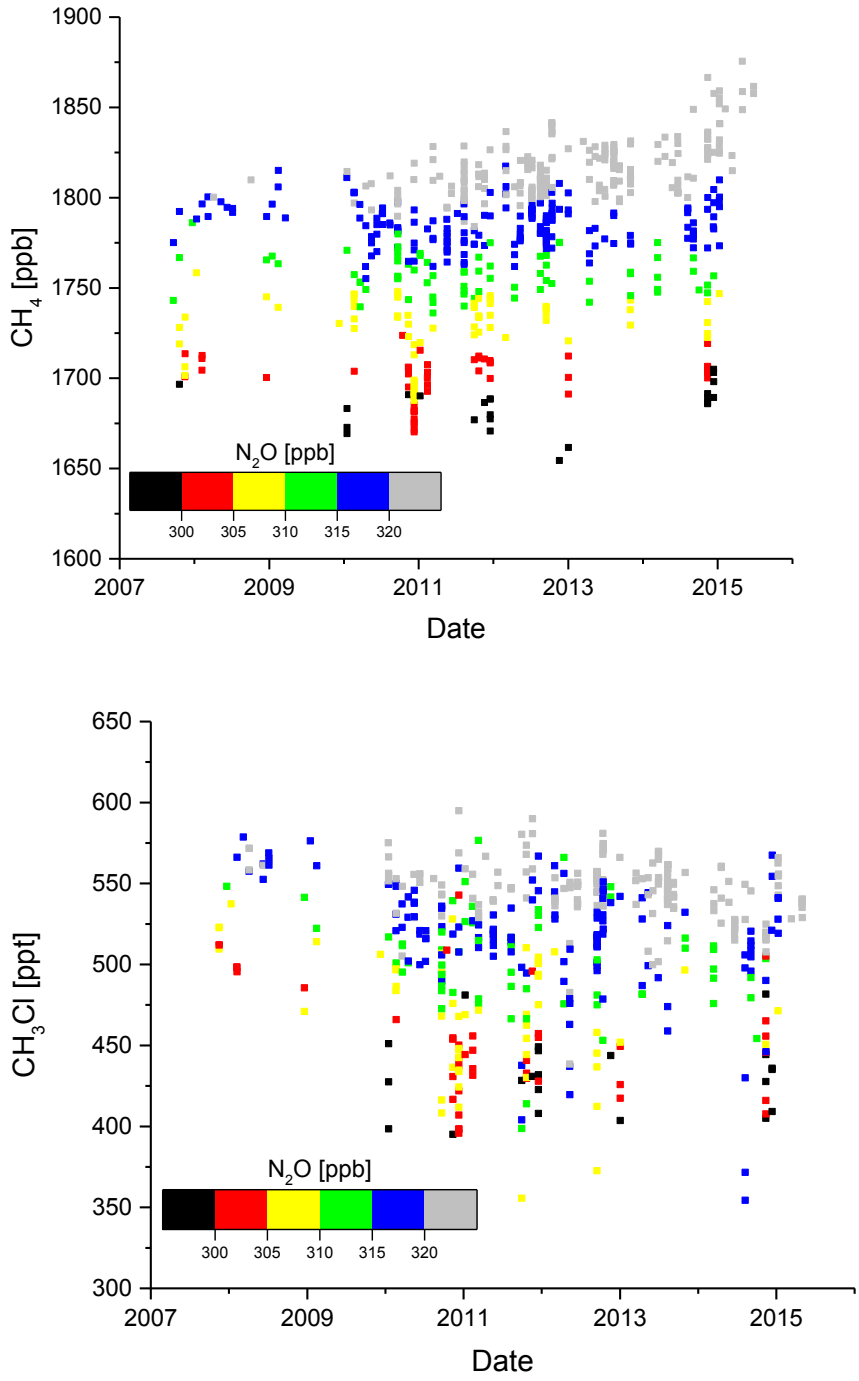

Figure S2. Temporal variation of CH_4 and CH_3Cl concentration in aircraft measurements color-coded with N_2O concentration. ”

3. THE EMPIRICALLY DETERMINED INTEGRATED ATMOSPHERIC RESIDENCE TIME OF CARBON DIOXIDE (CO_2)

This work is to be submitted as Li et al. (2020):

Li, M., Karu, E., Ciais, P., Lelieveld, J., and Williams, J.: The empirically determined integrated atmospheric residence time of carbon dioxide (CO_2), Proceedings of the National Academy of Sciences of the United States of America, to be submitted, 2020.

I am the first-author of this work and my contribution to this work includes assembling the data from NOAA and CARIBIC, quality control of the data, analyzing all the data (including performing variability-residence time relationship with NOAA and CARIBIC data in python, running Monte Carlo simulations, and analyzing trends of estimated residence times), making all of the figures and tables, and writing the manuscript together with Prof. Williams.

The following text and figures quoted (within "") from page 34 to page 62 are exactly the same as the manuscript which is cited on page 33.

"Abstract

The integrated atmospheric residence time (from combined effect of multiple removal processes) of carbon dioxide (CO_2) was empirically estimated as 28.4±18.2 (global troposphere), and 458.6±115.1 (stratosphere) years (mean ± one standard deviation), over 2006-2015 with four ground stations and aircraft observations. The tropospheric CO_2 residence time increases from north to south in latitude, the shortest times corresponding to the latitude of the boreal forest, and the longest to ocean dominated Southern Hemisphere (SH) high latitudes. The seasonal cycle in the residence time is larger in the southern than the northern hemispheric troposphere. The increase of CO_2 residence time in the SH suggests that either the southern carbon uptake capacity or the interhemispheric mixing time has been decreasing since the middle of 2013. Such global-scale assessments of the spatial and temporal variations of atmospheric CO_2 residence time can reveal and locate changes in climate-relevant processes, and improve prediction of future climate.

Introduction

Carbon dioxide (CO_2) is the most important radiatively active (greenhouse) gas in the Earth's atmosphere, besides water. Its current atmospheric mixing ratio (~410 ppmv in 2020) has increased by more than 40% compared to pre-industrial levels (280 ppmv) (Prentice et al., 2001), and present levels are more than double those found in glacial periods (ca. 190 ppmv) (Lüthi et al., 2008). The increase of CO_2 has been caused by historical emissions from fossil fuel burning and land use change, mainly deforestation. Global average mixing ratios are currently increasing at a rate of circa 2.5 ppmv per year. During the last decade, anthropogenic CO_2 emissions were on average 11 ± 0.8 PgC each year (Friedlingstein et al., 2019). To this total, fossil fuel emissions and cement production contribute 90% and land use change 10%. A fraction of CO_2 emitted by current and past anthropogenic emissions is persistently absorbed by land ecosystems (3.2 ± 0.6 PgC yr^{-1}) and the oceans (2.5 ± 0.6 PgC yr^{-1}) (Le Quéré et al., 2009), with most of the rest accumulating in the atmosphere. Land carbon uptake occurs as photosynthesis increases and fills in carbon pools at a faster rate than respiration and disturbances emissions depletes them. Ocean carbon uptake depends on air-sea exchange of CO_2, biogeochemical carbon cycling and mixing with the deep ocean.

The atmospheric removal processes (sinks) of carbon dioxide are planetary in scale and highly variable from one year to the next, reflecting mainly the response of tropical land carbon uptake to climate variability (Le Quéré et al., 2007). The residence time (or lifetime) of CO_2 in the atmosphere, both now and in future climate scenarios is notoriously difficult to determine. It cannot be described by a single number corresponding to an unique exponential residence time given that multiple processes operate on time scales going from hours to millennia to remove CO_2 from the atmosphere, unlike for instance the removal of a trace gas such as CH_4 or N_2O that is caused almost entirely by a single removal process and defines a single exponential lifetime. Current

estimates of the CO_2 residence time rely on impulse response simulations from coupled carbon-climate models to account for the multiplicity of removal processes (Joos et al., 2013). Coupled carbon-climate models mostly include representations of the photosynthesis response to CO_2 and climate, the turnover of carbon fixed by photosynthesis in ecosystem carbon pools, the solubility-driven dissolution of CO_2 in surface waters linked to ocean inorganic carbon chemistry and surface temperature, the mixing of surface waters with the deep ocean, and the perturbation of the ocean biological cycle (usually very small compared to physical mixing regarding in anthropogenic perturbation of air-sea CO_2 fluxes). These processes have typical time scales of decades. On longer time scales, other processes continue to remove an initial excess CO_2, such as long-term soil organic matter (e.g. peat and stable organic matter adsorbed on soil minerals) and woody biomass accumulation, the dissolution of seafloor carbonates, weathering reactions with carbonate and silicate rocks. The decay of CO_2 after an atmospheric pulse shows a rapid removal in the first decades, followed by a very slow decline on a century to millennium-scale. Joos et al. (2013) fitted three exponential functions to carbon-climate models pulse response functions and inferred three 'residence times': a first one of 4.3 years, corresponding to fast ocean and land removal processes, a second of 36.5 years for slow ocean and land removals, and a third one of 395 years for all other very slow processes.

Here we present results from an empirical method to derive the CO_2 residence time in the global troposphere and stratosphere. This method determines a residence time directly from measurements of atmospheric CO_2 concentration variability relative to the one of a suite of other globally distributed trace gases. The conceptual approach was first conceived by Junge (1974), who showed the atmospheric variability of tropospheric trace gases is inversely proportional to their residence time (hereafter referred to as the variability-residence time relationship). Junge (1974) demonstrated that the relationship held for trace gases with residence times ranging from 10^{-2} – 10^{4} years, thus including CO_2. This method has been previously applied to short-lived species from tropospheric field measurement data (Colman et al., 1998;Williams et al., 2000;Williams et al., 2001), and stratospheric observations (Jobson et al., 1999) to derive understanding of atmospheric radical abundances. We now apply this method to surface based, upper

tropospheric and stratospheric datasets to determine the CO_2 residence time on a global scale over ten years of observations. We evaluate the approach by using measurements to derive the residence time of COS (carbonyl sulfide) and in the case of the stratosphere, use an alternative residence time estimation method. This approach allows monthly residence times of CO_2 (and COS) to be calculated and changes in residence time between 2006-2015 at four ground stations and in the stratosphere to be examined.

Materials and Methods

Data collection.

Tropospheric measurement data (January 2006 – December 2015) of carbon dioxide (CO_2), carbonyl sulfide (COS), methane (CH_4), methyl chloride (CH_3Cl), nitrous oxide (N_2O), ethane (C_2H_6), propane (C_3H_8), trichlorofluoromethane (CFC-11), dichlorodifluoromethane (CFC-12) and chlorodifluoromethane (HCFC-22) at Pt. Barrow (BRW, 71.3° N, 156.6° W, 11 m a.s.l.), Mauna Loa (MLO, 19.5° N, 155.6° W, 3397 m a.s.l.), Cape Matatulu (SMO, 14.3° S, 170.6° W, 42 m a.s.l.), and Palmer Station, Antarctica (PSA, 64.9° S, 64° W, 10 m a.s.l.) was provided by the National Oceanic and Atmospheric Administration (NOAA). Daily measurement data are used, and when not available, we used discrete data (~weekly) instead. Observation data (May 2006 – December 2015) of CO_2, COS, N_2O, CH_4, C_2H_6, C_3H_8 and CH_3Cl in the northern hemispheric UTLS region was provided by the analysis of air samples collected during global flights in the IAGOS-CARIBIC project (Brenninkmeijer et al., 2007).

NOAA/ESRL program.

Gas chromatographs (GCs) are used to measure atmospheric halocarbons and trace gases by NOAA (www.esrl.noaa.gov/gmd/hats/index.html). In this study, we focus on CO_2, COS, N_2O, CH_4, C_2H_6, C_3H_8 , CFC-11, CFC-11, HCFC-22 and CH_3Cl for the analysis and used daily data of all compounds from NOAA for the time Jan 2006 to Dec 2015. The compounds and their corresponding measurement precision are listed below. In order to represent the global tropospheric trends, data from four ground sites (MLO, SMO, BRW, PSA) has been included. MLO and BRW are in the Northern Hemisphere, SMO and PSA are in the Southern Hemisphere, MLO and SMO are in the tropics and BRW and PSA are in the polar regions.

IAGOS-CARIBIC.

Canister samples were collected during flights in the UTLS region (at 10-12 km height) (Brenninkmeijer et al., 2007) and analyzed in the laboratory with GC-ECD (for greenhouse gases) (Schuck et al., 2009) and GC-FID (for non-methane hydrocarbons) (Baker et al., 2010;Umezawa et al., 2014). In this study, we included the data of CO_2, N_2O, CH_4, C_2H_6, C_3H_8 and CH_3Cl collected in the Northern Hemisphere during 2006.01-2015.12. Stratospheric samples with potential velocity (PV) higher than 2, defining the location of the tropopause, were selected. Data with values below detection limits was excluded.

Table 1. Spatial coverage of samples (a, b) and measurement precision (c).

a. Spatial coverage of northern hemispheric samples.

	Range
Latitude	0.4 ~ 77.4° N
Longitude	122.3° W ~ 141.77° E

b. Spatial coverage of stratospheric samples.

	Range
Latitude	17.2 ~ 77.4° N
Longitude	122.3° W ~ 138.7° E

c. Measurement precision.

compound	CO_2	N_2O	CH_4	C_2H_6	C_3H_8	CH_3Cl
precision	0.08%	0.15%	0.17%	0.2%	0.8%	1%

Variability-residence time relationship.

The variation (standard deviation) of atmospheric trace gases observed within time and space has an inverse relationship with the residence time of corresponding trace gases. This relationship has been corroborated by many observations, both in the troposphere and the stratosphere (Junge, 1974;Colman et al., 1998;Jobson et al., 1999;Williams et al., 2001). The relationship can be expressed as:

$$S_{\ln X} = A\tau^{-b} \quad \text{(Eq.1)}$$

Where $S_{\ln X}$ in the left side of the equation represents the standard deviation of the natural logarithm of observed mixing ratios of trace gases within time and space. At the right-hand side of the equation, the terms 'A' and 'b' indicate fitting parameters, and 'τ' represents the atmospheric residence time of trace gases. The 'b' factor indicates the remoteness of sampling from local source (Jobson et al., 1999). The residence times (or lifetimes) of all trace gases applied in this study have been adopted from the WMO (WMO, 2011), SPARC (Ko et al., 2013) and IPCC (IPCC, 2007) reports and the atmospheric OH lifetime (Table 2).

A schematic illustration of the relationship is shown in Figure 1. Red dots indicate the compounds whose variabilities and residence time are known, the greed dots (either CO_2 or COS) indicate that the variability is known and the residence time is the target. To ensure the quality, only when the relationship has good correlation ($R^2 > 0.5$) and more than three compounds are available for the curve fitting, then the estimated CO_2 or COS residence time is output.

A programming code in Python (3.6) was written to input, process and output the data. R^2 distributions of filtered output data are shown in Figure 2.

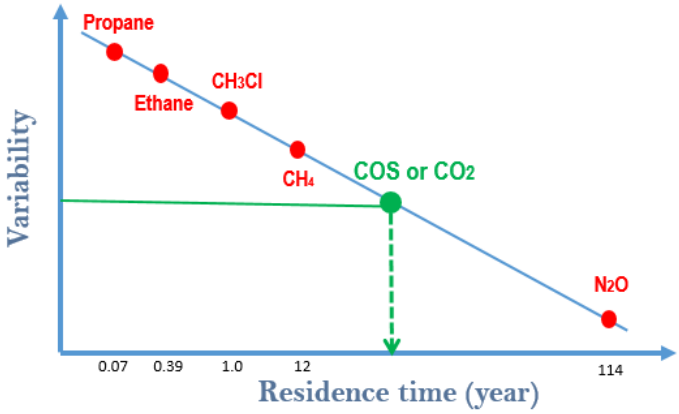

Figure 1 Schematic illustration of variability-residence time relationship and CO_2 (or COS) residence time estimation.

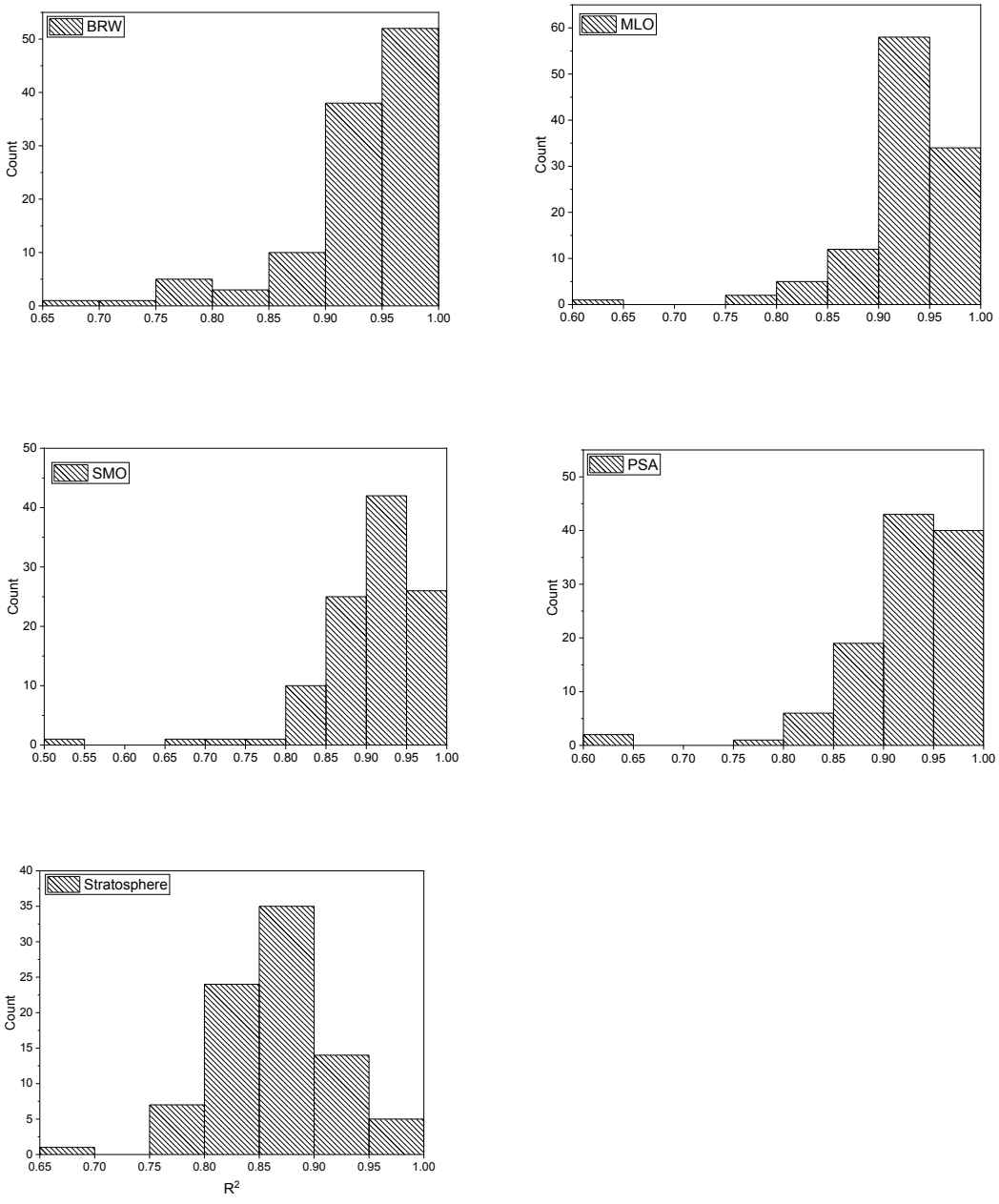

Figure 2 R^2 distributions of filtered data in the stratosphere and at MLO, SMO, PSA and BRW.

Table 2. Atmospheric residence time.

Compound	Residence time / Lifetime (year)
N_2O	114*
CH_3Cl	1.0*
CH_4	12.0**
C_2H_6	0.39***
C_3H_8	0.07***
CFC-11	45.0*
CFC-12	100.0*
HCFC-22	11.9*

*from WMO (2011) report (WMO, 2011) and SPARC report (Ko et al., 2013).

** from IPCC (2007) report (IPCC, 2007).

***estimated based on OH radical concentration (6.2×10^5 molecules/cm^3) which is the average of the global tropospheric OH concentration (1.13×10^6 molecules/cm^3) (Lelieveld et al., 2016) and the global stratospheric OH concentration (1.1×10^5 molecules/cm^3) (Li et al., 2018), reaction rates with OH (Atkinson, 2003;Krasnoperov and Michael, 2004) at 250K.

Tracer-tracer correlation (Plumb and Ko relationship).

A tracer-tracer correlation between two long lived atmospheric species allows the estimation of the stratospheric residence time of a constituent if the stratospheric residence time of the other is known, as described by Plumb and Ko in 1992 (Plumb and Ko, 1992), and later applied in other observations (Barkley et al., 2008). For deriving the stratospheric residence time of CO_2, the correlation between CO_2 and N_2O has been used. The residence time of N_2O in the stratosphere is relatively well known, globally estimated as 114 years (τ_y), thus it allows to calculate the CO_2 stratospheric residence time (τ_x).

$$\tau_x = \frac{\overline{MR_x}}{\overline{MR_y}} \times |m| \times \tau_y \qquad \text{(Eq.2)}$$

A potential vorticity, PV > 2PVU, filter was used to distinguish the stratospheric from the tropospheric air samples. The slopes (m) were computed for each month separately, and $\overline{MR_x}$ and $\overline{MR_y}$ correspond to the mean mixing ratios of CO_2 and N_2O of the corresponding month, respectively.

Data processing.

All the measurement data were grouped by a fixed period (monthly or yearly) and the standard deviation (variation) of each compound in this period (monthly or yearly) was calculated (n >10 for each). For estimating CO_2 residence time with variability-residence time relationship, a linear regression algorithm in Python (3.6) was programmed to fit the natural logarithm (ln) of the standard deviations of all the compounds expect CO_2 and their atmospheric residence time (Table 1), i.e. ln(standard deviation) versus ln(atmospheric residence time). The CO_2 variations were only input into the linear regressions which have good correlation ($R^2 > 0.5$), and the CO_2 residence time was calculated by month or year. For the stratospheric CO_2 residence time estimation with two independent methods, stratospheric northern hemispheric samples were identified with potential velocity (PV) higher than 2 PVU. Outliers which are out of the range of [Q1-1.5 × IQR, Q3+1.5 × IQR] (Q1: the first quartile; IQR: the interquartile range = Q3-

Q1; Q3: the third quartile) were excluded. The trend, seasonality and 95% confidence interval were achieved with the help from the open source library "Prophet" designed for time series analysis (Taylor and Letham, 2018).

Monte Carlo simulation.

We have randomly generated 1,000 different values varying ± 10% for each residence time of the compounds listed in Table. In total 5,000 residence times for the 5 compounds were input into the programming code together for estimation of the yearly CO_2 residence time at BRW, MLO, SMO, PSA, and in NH and the stratosphere. For each location listed above, I calculated the difference between the original residence time and the newly estimated residence time (Table 3).

Trend analysis.

The trend analysis model ("Prophet") can detect abrupt change points in a real time series dataset. The input argument 'changepoint_prior_scale' can be manually changed to avoid overfitting or underfitting. We fitted the trends under ten scales (L1, L2, L3, …, L10) which covers from overfitting to underfitting. This gives the uncertainty and confidence interval of the trend analysis. In the main text, the average value of ten fitting scales (black line in corresponding figures) was used to represent the trend of each station. Uncertainties of trend analysis (difference from average to maximum and minimum) of each station are analyzed. The mean uncertainties for BRW, MLO, SMO and PSA are 6.2%, 0.5%, 2.9%, and 3.2%, respectively.

Results

We first examined the variability-residence time dependence for data taken over ten years from two ground-based stations in the Northern Hemisphere (NH) (NOAA sites – Barrow (BRW), Alaska and Mauna Loa (MLO), Hawaii) and from aircraft samples collected in the upper troposphere and lower stratosphere (UTLS) of the NH (IAGOS-CARIBIC project). The five chemical species common to both datasets namely ethane (C_2H_6), propane (C_3H_8), methyl chloride (CH_3Cl), methane (CH_4) and nitrous oxide (N_2O) are used to generate the variability-residence time dependence according to the method developed by Jobson et al. (1998). The atmospheric residence times of these species vary from less than a month to over 100 years (Table 1). The ten-year datasets of Barrow, of Mauna Loa and the airborne NH have similar gradients in the variability - residence time dependency (b factors: 0.72, 0.67 and 0.60, respectively) and they are all above 0.5, typical of remote background tropospheric observations (Jobson et al., 1999). This relationship confirms that the datasets are not affected by local sources. Instead the variability is caused by various physical and chemical processes occurring in the airmass prior to measurement. Due to the relatively long residence times of the species used here, all sources and sinks on a hemispheric to global scale may impact the measured variability. Similar gradients (b factors) are generated when using data from the SH and stratosphere: Samoa (SMO), Palmer Station Antarctica (PSA), and the stratosphere: 0.63, 0.66, and 0.58, respectively, all $R^2 \geq 0.87$.

Having established the aforementioned relationships we may now calculate empirically the atmospheric residence time of CO_2 and COS using ground and aircraft measurements. COS is chosen in addition to CO_2 as it has a similar terrestrial photosynthetic sink distribution to CO_2 but a better constrained atmospheric residence time, so that it can be used to validate the approach. The measurement variability is determined and the residence time interpolated from the relationship shown in Figure 3.

The COS residence time inferred from BRW is between 0.82 - 1.57 years and the one inferred from Mauna Loa is slightly longer, 1.8 - 2.8 years. These values are in good agreement with previous studies which have determined atmospheric residence times between 1.5 – 3.0 years; and a global residence time of 2.1 years (Montzka et al., 2007;Karu et al., 2020a). Using the same method, we inferred an annual CO_2 residence time varying between 6 and 12 years at BRW and between 15 and 20 years at Mauna Loa. The average CO_2 residence time at MLO is longer than that at BRW, because global circulation is generally zonal, MLO is less influenced by the strong seasonal uptake of boreal and arctic sinks influencing BRW in summer. Using the entire NH dataset from aircraft measurements, including data from both the troposphere and the stratosphere, we inferred a CO_2 residence time of global NH atmosphere (troposphere and stratosphere) between 200 and 400 years (Figure 3b). The stratosphere is more isolated from the strong terrestrial and oceanic sinks than any surface stations and the CO_2 residence time relative to CO_2 removal from this reservoir is longer. At BRW, the annual CO_2 residence time shows an analogous temporal trend to the COS residence time (Figure 3b), a compound which shares similar vegetation uptake sinks with CO_2 (Montzka et al., 2007). In 2013, both CO_2 and COS show an increase in the residence time inferred from atmospheric concentration variability. In this year a severe drought was recorded with a high percentage of drought impacted areas in Alaska in 2013 (Figure 4). I therefore surmise that the drought has weakened the land carbon uptake capacity within the area influencing the BRW station during that year.

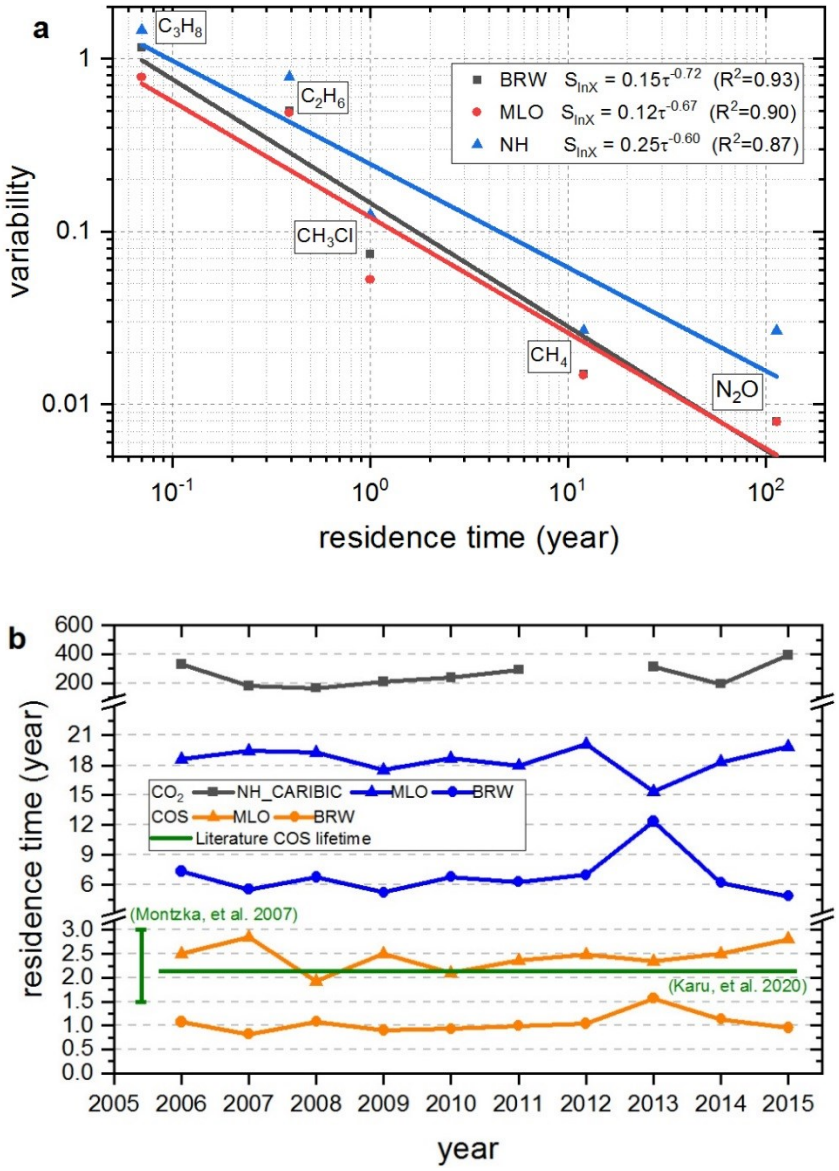

Figure 3 (a) variability – residence time relationship inferred from concentration records at the ground station BRW (black line), MLO (red line) and all the northern hemispheric air samples (thereinafter NH) collected from IAGOS-CARIBIC including both tropospheric and stratospheric samples (blue line) during 2006.01-2015.12 (n > 800 for each point); (b) annual CO_2 residence time at BRW, MLO and NH, COS residence time at BRW and values from other studies (Montzka et al., 2007;Karu et al., 2020a) (n > 10 for each year).

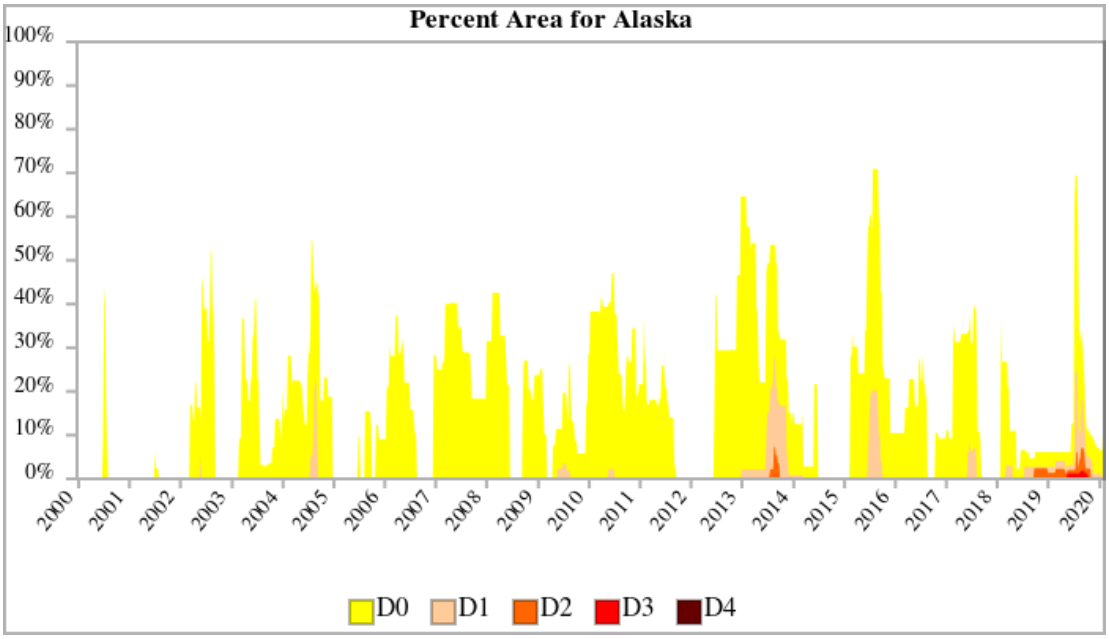

Figure 4 Droughts in Alaska from 2000 to 2020. D0: abnormally dry, D1: moderate drought, D2: severe drought, D3: extreme drought, D4: exceptional drought. Figure Source: https://www.drought.gov/drought/states/alaska

The results shown in Figure 5 are based on yearly data, meaning that the variability comes from all measurements taken during the year. Colman et al. (1998) have applied the same method (with C_2H_6 and CH_3Cl as well) and derived the residence time of CH_3Br (0.8 ± 0.1 years) based only on a ca. one-month of data. We therefore extend this residence time determination method for longer-lived compounds (such as CO_2 and COS) to the monthly scale, to determine the seasonal dependence of their residence times. I first determined the COS residence time at BRW and MLO (Figure 5a) which was highest in April and May, and lowest in August and September. The steep decrease from April to September corresponds to the period of highest photosynthetic uptake in the NH. Similar seasonal trends are also seen for the CO_2 residence time at BRW and MLO

(Figure 5b). The CO_2 residence time in the stratosphere is approximately an order of magnitude longer (Figure 5c).

For the stratospheric data it was possible to apply an alternative approach to determine the CO_2 residence time to provide a check on the empirical estimation. This involved a tracer-tracer correlation to a species with a well-established stratospheric residence time (in this case for N_2O of 114 years) (Plumb and Ko, 1992). The stratospheric CO_2 residence time estimated with the two independent methods is in reasonably good agreement (Figure 6) and the monthly trends are similar (Figure 5c), although the variability-based method gives on average lower values.

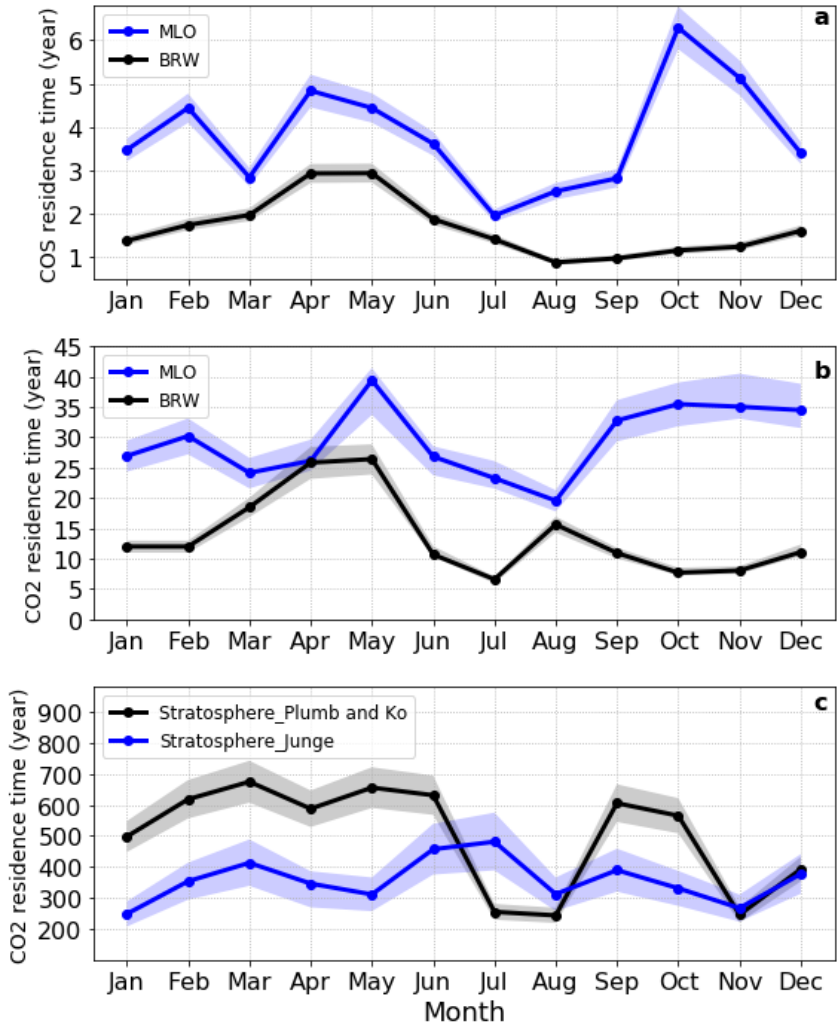

Figure 5 Monthly mean (a) COS residence time at MLO and BRW; (b) CO_2 residence time at MLO and BRW; (c) stratospheric CO_2 residence time derived from two independent methods (Junge, Plumb and Ko, Supplementary Materials) during 2006.01-2015.12. Uncertainties indicated with shaded area are estimated with Monte Carlo simulations for variability-residence time (Junge) method (max-min as shaded, n = 1000 for each month at each site) and ±10% variation of N_2O lifetime for Plumb and Ko method.

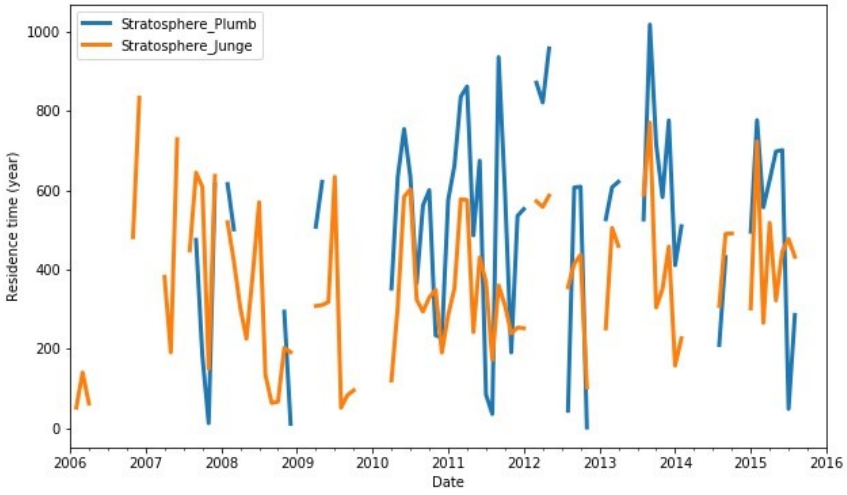

Figure 6 Stratospheric CO_2 residence time comparison between the two methods.

We now extend the analysis to the global scale. Figure 7 shows the CO_2 residence time derived from four surface stations (two in the NH and two in the SH), the corresponding trend, the seasonality, and the 95% confidence interval when processed as described in the previous section. Generally, the calculated CO_2 residence time increases from north to south in latitude, with BRW indicating the shortest and PSA in Antarctica the longest CO_2 residence time among four sites. This is consistent with the greater proportion of landmass in the NH, which globally is approximately twice as effective at removing CO_2 than the oceans during peak growing season (Le Quéré et al., 2009). The integrated CO_2 residence time at all four sites shows a slowly declining trend over 2006-2015. At PSA, the integrated CO_2 residence time decreases the fastest among the four sites at 0.58 years/year (until June 2013). An independent study of the Southern Ocean carbon budget (Landschützer et al., 2015) showed the carbon uptake from the Southern Ocean which is the strongest oceanic sink for CO_2, has strengthened from 2002 through 2011, and this is consistent with the observed decrease in CO_2 residence time. The increase of CO_2 residence time at PSA and SMO since mid-2013 may indicate the carbon uptake capacity in the SH (from ocean or landmass) has been saturated or the interhemispheric mixing

time has been decreasing (Patra et al., 2011) and more CO_2 being transported into the SH from the NH.

The CO_2 residence time at SMO and PSA shows peaks in October (Figure 7c,d, Figure 8) and decreases from October until February. This seasonal cycle corresponds to the increased CO_2 uptake by land and ocean biota during the SH spring-summer, which effectively shortens the residence time until February. The derived integrated CO_2 residence time increases in September-October, which can be caused by increasing CO_2 emissions from hemisphere-wide biomass burning at this time. These act to suppress the variability caused by the photosynthetic sink and lead to longer empirically estimated CO_2 residence times. At the two northern hemispheric sites MLO and BRW, CO_2 residence time decreases from April to July during the NH summer when photosynthetic uptake of terrestrial vegetation is peaking. The seasonal variation in CO_2 residence time is much weaker in the NH (max-min: Δ 15 years NH compared Δ 50 years SH, Figure 8).

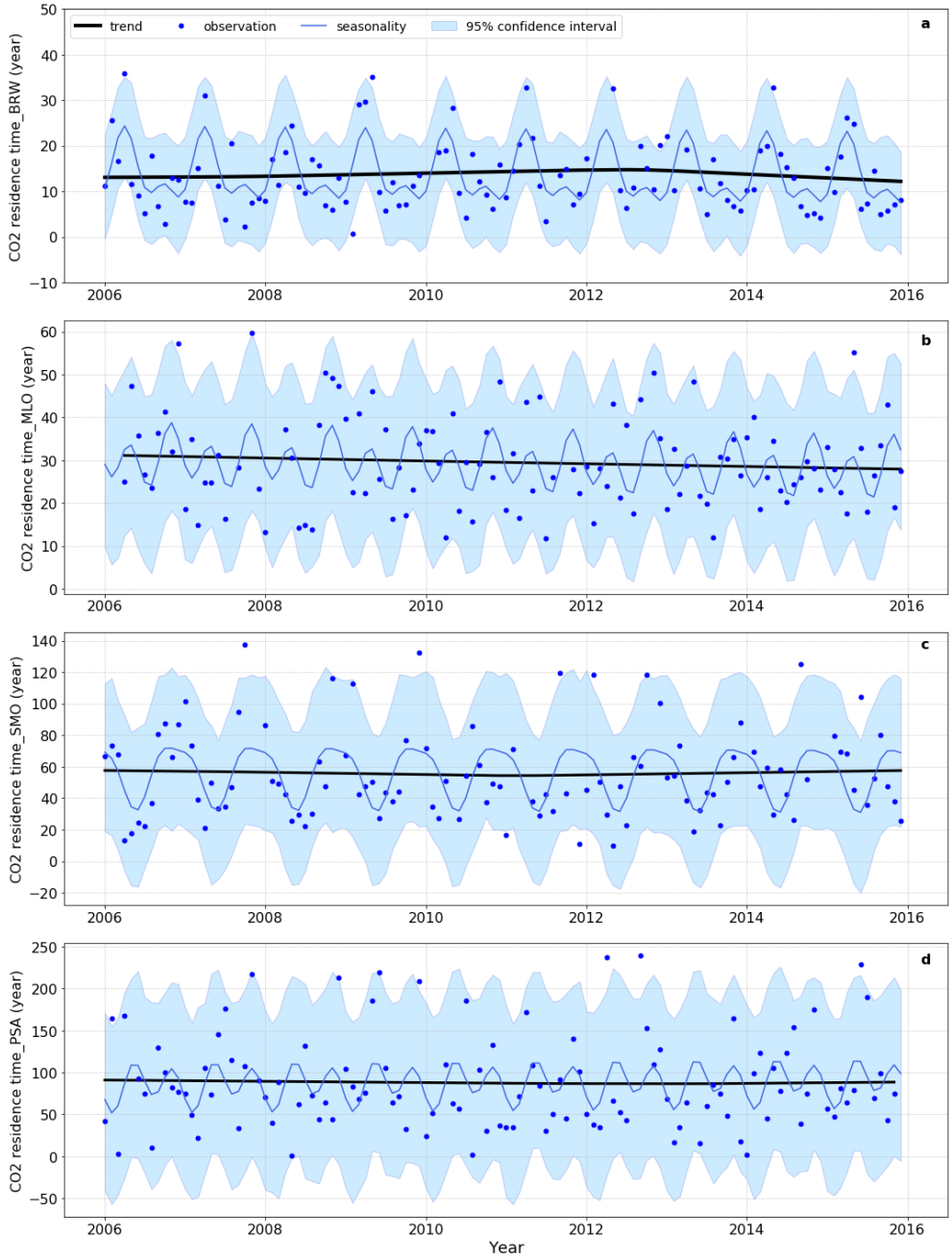

Figure 7 Trend, seasonality, 95% confidence interval of CO_2 residence time at BRW (a), MLO (b), SMO (c) and PSA (d) over time. Observational values (blue dots) are calculated with the variability-residence time (Junge) method (n > 10).

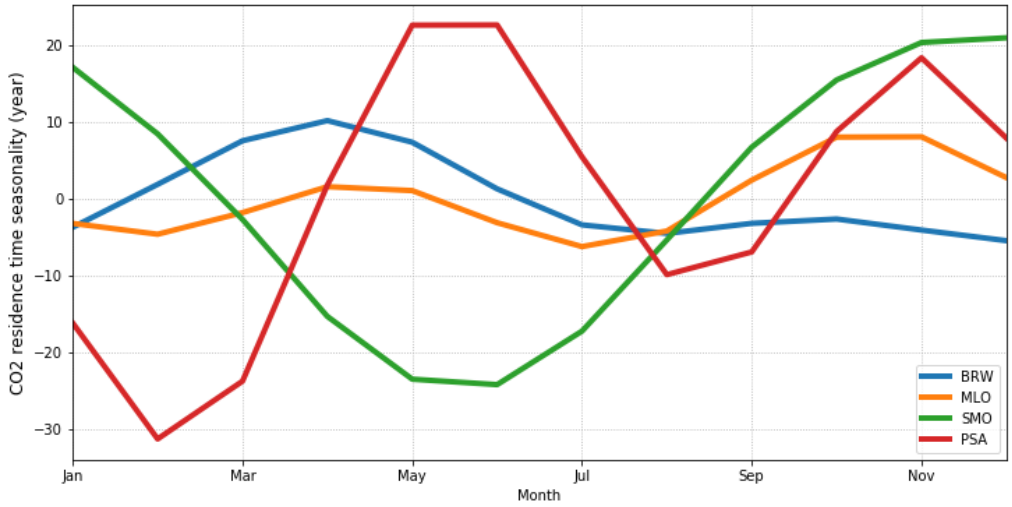

Figure 8 "Prophet" model estimation of seasonality of CO_2 residence time at BRW, MLO, SMO and PSA over 2006-2015.

Discussion

Based on the temporal variance of CO_2 and other species, we empirically derived the integrated atmospheric CO_2 residence time in the global troposphere (surface), whole Northern Hemisphere (troposphere and stratosphere), and stratosphere as 28.4 ± 18.2, 258.6 ± 74.6, and 458.6 ± 115.1 years (mean ± one standard deviation), respectively, over 2006-2015. Two previous modelling studies have estimated CO_2 residence times on the global scale (Joos et al., 2013;Pierrehumbert, 2014). Both used three timescales (from decadal to millennial) as tuning parameters to fit the exponential results of either an impulse response function (IRF) (Joos et al., 2013) or radiative forcing (Pierrehumbert, 2014) of CO_2 from their models. The three timescales were calculated as 4.3, 36.5, and 394.4 years by Joos et al. (2013) and 8.7, 93.3, 645.9 years by Pierrehumbert (2014). Significant discrepancy is found between these two studies, but the underlying reasons remain unclear because the values of the models calculated timescales do not have real world process-based meaning. In this study, the integrated atmospheric residence time of CO_2 for the global troposphere (surface) is 28.4 years, which lies between the two shortest timescales from the models (Joos et al., 2013;Pierrehumbert, 2014), and the integrated stratospheric residence time (458.6 years) is comparable to the longest timescale from Joos et al. (2013) and Pierrehumbert (2014). These results help indicate to which processes the timescales correspond: the first two shortest timescales represent slow ocean and land (vegetation) removal, and the longest timescale represents for all other very slow processes (such as soil organic matter and woody biomass accumulation, the dissolution of seafloor carbonates, weathering reactions with carbonate and silicate rocks).

As the latitudes of the four ground sites are to a first approximation evenly distributed across the globe (from 71.3° N, 19.5° N to 14.3° S, 64.9° S), we have taken the average tropospheric CO_2 residence time over the four sites (28.4 years) as representative of the

global tropospheric residence time. As the air in the stratosphere is mixed via the Brewer Dobson circulation on relatively short timescales (ca. 2-5 years) (Randel et al., 1993;Butchart, 2014a), the derived stratospheric CO_2 residence time (458.6 years) can be taken as representative for the whole stratosphere (including both hemispheres), although only air samples collected in the northern hemispheric stratosphere were used.

Being remote from local sources is an important precondition for applying the variability-residence time relationship method to derive atmospheric residence times. The airborne stratospheric data is by its very nature distant from the surface sources and the sampling protocols and the background stations minimize local influence on the data as evidenced by the similarity in variability-residence time dependencies (b factors). From Figure 3, physical and chemical processes occurring in the air masses reaching the measurement sites induce variability in the data inversely proportional to the species residence time. Williams et al. (2000) considered the spatial extent of the regions influencing variability for species with different residence times. By assuming an instrumental precision of 1% similar to that of the measurements used here, it was shown that the variability is sensitive to sources within a space encompassing between 4 and 5 atmospheric residence times of the species. For short-lived species, this is an important consideration when generating the variability residence time plot since longer lived species can be impacted by sources further afield. However, for a species with a residence time of 25 days (e.g., propane, the shortest lived species used here) and assuming a constant 5 m s^{-1} wind speed, then these species can be affected by sources and sinks over 54,000 km distance from the detector, equivalent to the size of the hemisphere. Longer lived species are influenced over correspondingly longer distances. Hamrud (1983) used a two-dimensional numerical model to examine the influence of source and sink distributions on variability. While establishing the general feature of decreasing variability for increasing residence time the model study indicated that large uncertainties can arise when source distributions are not equivalent, particularly for anthropogenic compounds. In our study the chemical species chosen are all influenced by hemisphere-wide sources and sinks. Unfortunately the Hamrud model study was not able to assess CO_2 residence times since the model did not include the seasonal variations in the biological sources and sinks. Thus further model studies are needed, ideally with

three dimensional models run over longer time periods. To minimize any possible local influence and source inhomogeneity issues in this study, we 1) excluded results when the curve fitting coefficient (R^2) of the variability-residence time relationship is <0.5, thus reducing uncertainty from source-sink distribution because if one or more species used are influenced by local sources or sinks, R^2 will decrease; 2) tested the robustness of the approach by adding three long-lived species and removing the two shortest lived species from the variability-residence time plot. Little difference is found between the CO_2 residence time at BRW (Figure 9) based on the method with five compounds (N_2O, CH_4, CH_3Cl, C_2H_6, and C_3H_8) and with only three compounds (N_2O, CH_4, CH_3Cl). However the difference becomes larger (~25% on average) when three long-lived species are added (CFC-11, CFC-12, and HCFC-22). Therefore we estimate an uncertainty of ~25% related to the choice of compounds used for the variability-residence time relationship. Uncertainties from the residence times used for the variability-residence time relationship are estimated to be ~2-4% for the troposphere, and ~4-5% for the NH and stratosphere by applying 1,000 Monte Carlo simulations randomly for each region (see Methods section, *Monte Carlo simulation,* and Table 3). Uncertainties of the trend analysis are 0.5% ~ 6.2% depending on sites (see Methods section *Trend analysis*, and Fig.10 a,b). Thus we estimate an overall uncertainty of 35% for the integrated atmospheric CO_2 residence time calculated by this method.

It is important to note that the method to determine integrated CO_2 atmospheric residence time is based on the relative variation of monthly or annual data. Each point is independently derived from data within a confined timeframe. Therefore, long-term trends in CO_2 related very slow processes affecting the removal of anthropogenic CO_2 will have little effect on the variability and hence the residence time calculated. In the case of CO_2 whose atmospheric residence time is determined by multiple removal processes acting on different time scales, this approach constrains the residence time with respect to the short-lived pools (surface ocean absorption, plants and litter) rather than the slow pools that operate over longer timescales. This metric is therefore particularly useful for the assessment of rapid environmental change. The residence times generated by this method support the recently reported decreases in CO_2 ocean uptake in the Southern Hemisphere (Landschützer et al., 2015). It is therefore expected that application

of this analysis to further measurement stations worldwide can help locate regions where climate relevant processes are changing and gauge their impact."

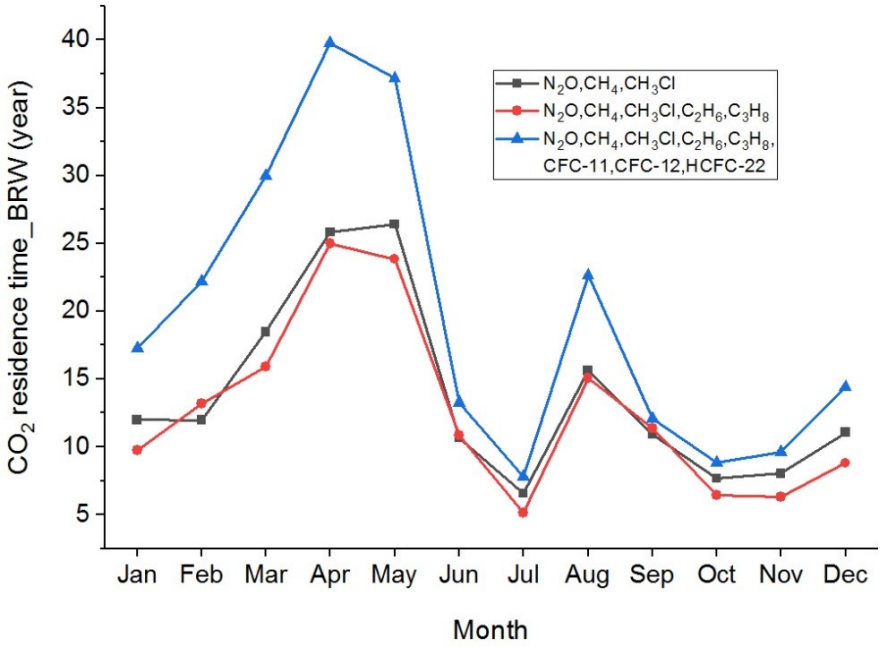

Figure 9 Comparison of CO_2 residence time at BRW among three different combinations of compounds. Three combinations of compounds to define the variability-residence time relationship were used to test how much uncertainty comes from the choice of compounds. Choice #1 uses only three long-lived compounds (N_2O, CH_4, and CH_3Cl); Choice #2 adds two short-lived compounds based on choice #1 (N_2O, CH_4, CH_3Cl, C_2H_6, and C_3H_8); Choice #3 adds three long-lived and anthropogenic compounds (CFC-11, CFC-12, and HCFC-22).

Table 3. Monte Carlo simulation results.

YEAR	MEDIAN (MIN,MAX) DIFFERENCE IN %					
	BRW	MLO	SMO	PSA	NH	Stratosphere
2006	2.1(0,7.9)	2.5(0.0,8.7)	2.5(0,8.7)	2.3(0,8.7)	4.2(0,15.4)	4.7(0,17.6)
2007	2.0(0,7.8)	2.5(0.0,8.7)	2.5(0,8.7)	3.1(0,9.7)	3.9(0,13.5)	4.4(0,15.7)
2008	2.0(0,7.9)	2.5(0.0,8.8)	2.5(0,8.8)	2.3(0,8.7)	3.7(0,15.2)	4.4(0,18.2)
2009	2.0(0,7.7)	2.5(0.0,8.4)	2.5(0,8.4)	3.3(0,10.6)	4.0(0,16.4)	4.6(0,19.0)
2010	2.1(0,7.9)	2.5(0.0,8.6)	2.5(0,8.6)	2.8(0,8.8)	4.1(0,16.8)	4.5(0,18.4)
2011	2.0(0,7.8)	2.5(0.0,8.6)	2.5(0,8.6)	3.0(0,9.7)	4.2(0,17.1)	4.7(0,18.8)
2012	2.1(0,8.0)	2.5(0.0,8.9)	2.5(0,8.9)	3.7(0,12.8)	4.7(0,18.9)	5.0(0,20.5)
2013	2.4(0,8.2)	2.4(0.0,8.3)	2.4(0,8.3)	3.0(0,9.6)	4.1(0,16.6)	4.6(0,17.9)
2014	2.0(0,7.9)	2.5(0.0,8.7)	2.5(0,8.7)	3.0(0,9.5)	3.9(0,15.4)	4.0(0,16.5)
2015	1.9(0,7.7)	2.5(0.0,8.6)	2.5(0,8.6)	2.9(0,9.4)	4.3(0,17.2)	4.6(0,18.1)

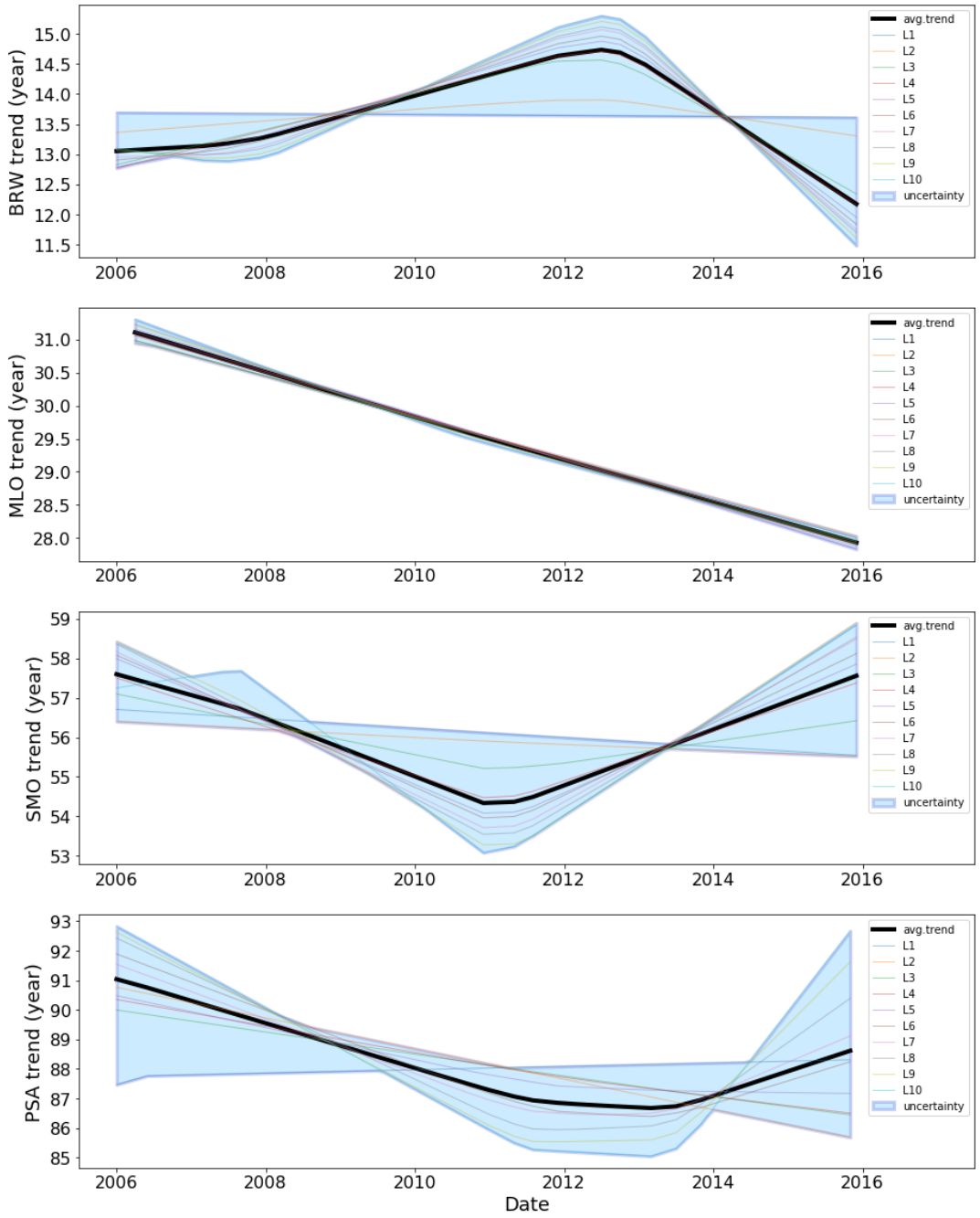

Figure 10 (a) Trends of CO_2 residence times at BRW, MLO, SMO and PSA estimated with ten fitting scales (L1, L2, …, L10), their average (black line) and uncertainty (blue shadow).

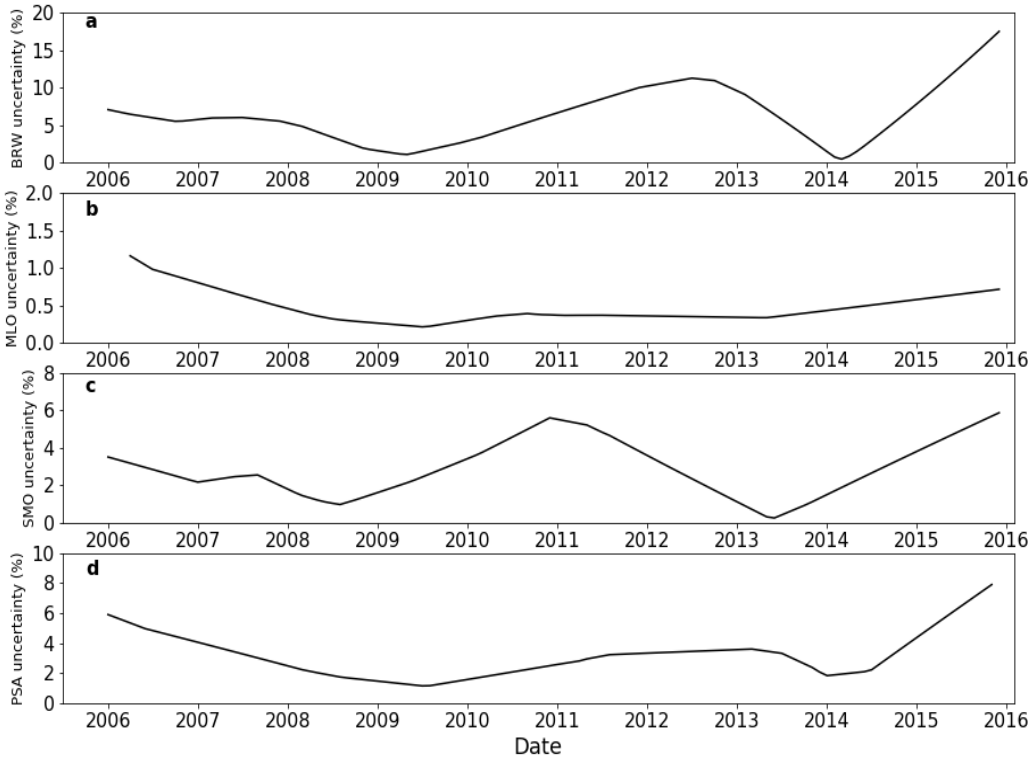

Figure 10 (b) Uncertainties of trend analysis of CO_2 residence times at BRW, MLO, SMO and PSA."

4. STRATOSPHERIC ETHANE TREND ANALYSIS

My contribution to this work includes assembling the observation and model data, analyzing all the data, making all the figures and tables, drafting the chapter. Prof. Williams revised the chapter.

4.1 Introduction

Ethane, the second most abundant hydrocarbon in the atmosphere after methane, has major sources from natural gas and oil production (~60%), biofuel combustion (20%) and biomass burning (18%), and 80% of its emissions are from the Northern Hemisphere (Xiao et al., 2008). Its major atmospheric sink is the reaction with the OH radical in the atmosphere. Ethane is an important precursor of atmospheric PAN (peroxyacetyl nitrate) which has a major effect on tropospheric ozone distributions, and thus further impacts air quality (Rudolph, 1995;González Abad et al., 2011). Due to the seasonal variation of the photochemically generated OH radicals, ethane has a global lifetime of 80 days, with a minimum in summer (~2 months) and a maximum in winter (~10 months) (Xiao et al., 2008). Ethane has been reported with notably different temporal growth rates (or trends) over global ground stations, with an increase in the Northern Hemisphere of 0.42±0.19 Tg/yr during 2009-2014 (Helmig et al., 2016). González Abad et al. (2011) presented seasonal, latitudinal and hemispheric variations of ethane in the upper troposphere with measurements from the ACE campaign and GEOS-Chem model data. They concluded that the seasonal trend could be explained by emissions (anthropogenic and biomass burning) and destruction rates. Glatthor et al. (2009) used ethane data derived from MIPAS/ENVISAT limb emission spectra from 54 days of observations at pressure levels of 200 hPa (10.5~12.6 km) and 125hPa (13.5~15.5km) during 2003 and 2004, to investigate emission plumes and vertical profiles.

Although many previous studies have attempted to understand the distributions, emissions and lifetimes of ethane in the troposphere for particular intensive measurement campaigns, long-term trend analysis is missing. In this chapter, a long-term trend of stratospheric ethane is presented and the observational trend is compared with global model simulations.

4.2 Observed trends

4.2.1 Ground observations

The trend and seasonality analysis algorithm ("Prophet") used in this study has been described in detail elsewhere (Taylor and Letham, 2018). It was applied to the same CARIBIC-2 and NOAA ground station datasets as used throughout this study (Li et al., 2020). It has been shown that the "Prophet" algorithm performs well for non-continuous time series data, as is the case for the aircraft data. To test whether this algorithm also performs well for ground station datasets, the ethane trend (concentration versus time) and seasonality at Iceland were estimated by two independent algorithms ("Prophet", and the other one from NOAA, see: www.esrl.noaa.gov/gmd/ccgg/mbl/crvfit/crvfit.html) with the same dataset from NOAA. Figure 4.1 shows the comparison between the results from the two algorithms. Ethane seasonality is well captured by both algorithms (Figure 4.1). The variations of the ethane trend during 2009.05 – 2014.05 estimated by both algorithms match very well, whereas the slopes of the trends have some notable differences. The NOAA algorithm estimated 46.2 ppt/yr, and 37.0 ppt/yr was estimated by the "Prophet" algorithm, thus a 20% difference exists between the two algorithms. A clear decreasing ethane trend from 2014.06 is observed at Iceland with the "Prophet" algorithm.

Some studies have focused on ethane trend analysis with either ground based sampling or ground based FTIRs (Fourier Transform Infrared Spectrometers) from solar and lunar measurements. A summary of these studies are shown in Table 4.1a. Angelbratt et al. (2011) reported that the trends of C_2H_6 partial column at four European sites (Jungfraujoch, Zugspitze, Harestua and Kiruna) during 1996-2006 were -1.09 ~ -2.11 %/year. Simpson et al. (2012) concluded a strong global ethane decline of 21% over 26 years (1984-2010), with stronger decline occurred from 1984 to 1999 (-7.2±1.7 ppt/yr)

than from 2000 to 2010 (-1.9±1.3 ppt/yr). Franco et al. (2015) showed the ethane trend at Jungfraujoch was -0.92%/year during 1994-2008, followed by a strong positive trend of 4.9%/year during 2009-2014, which may be related to the growth of shale gas exploitation in North America. Helmig et al. (2016) calculated a mean ethane growth rate of 2.9-4.7%/year during 2009.05-2014.05 at 32 northern hemispheric ground measurement sites, and concluded that North American oil and gas development was the primary source of the increasing emission of ethane. Franco et al. (2016) compared the ethane total column change at six sites across the Northern Hemisphere for the period of 2003-2008 and 2009-2014, and revealed a sharp increase of 3-5%/year during 2009-2014 compared with 2003-2008, which is associated with oil and gas industry emission. They also estimated a 1.2 Tg/year increase of anthropogenic ethane emission from the North America during 2008-2014. In summary, the data analyses to date are consistent and show an increased emission of ethane globally, with a specific rapid increase associated with oil and gas exploration in the US.

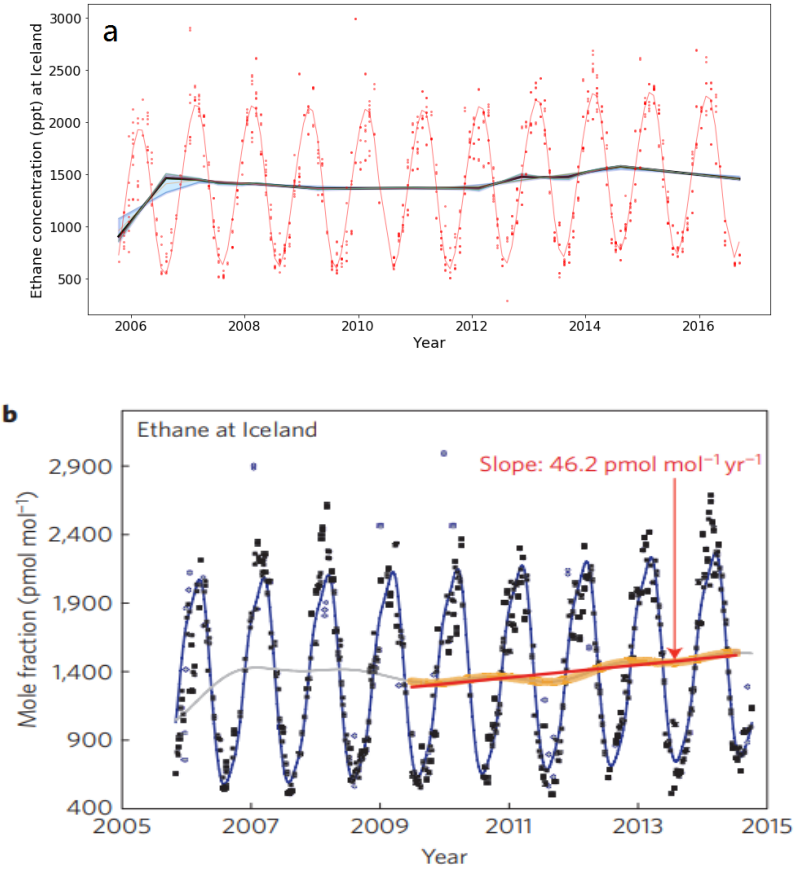

Figure 4.1 Ethane seasonality and trend at Iceland estimated by (a) "Prophet" algorithm (light blue shadow indicates uncertainty from trend fitting); and (b) NOAA algorithm, figure from Helmig et al. (2016).

Table 4.1 Summary of studies reporting ethane trends in the troposphere (a) and stratosphere (b).

Trends (%/year)	Time period	References
(a) Tropospheric trends		
-1.09 ~ -2.11 (four European sites)	1996-2006	Angelbratt et al. (2011)
-0.81 (global)	1986-2010	Simpson et al. (2012)
-0.92 (Jungfraujoch)	1994-2008	Franco et al. (2015)
4.9 (Jungfraujoch)	2009-2014	Franco et al. (2015)
2.9-4.7 (32 ground sites)	2009-2014	Helmig et al. (2016)
3-5 (six sites, ethane total column)	2009-2014 compared with 2003-2008	Franco et al. (2016)
(b) Stratospheric trends		
-3.31 ~ 0.43 (stratospheric column)	2000-2005	Gardiner et al. (2008)
-1.75±1.30 (8-16km above Jungfraujoch)	2004-2008	Franco et al. (2015)
-1.0±0.2 (8-21km above Jungfraujoch)	1995-2009	Helmig et al. (2016)
9.4±3.2 (8-16km above Jungfraujoch)	2009-2013	Franco et al. (2015)
6.0±1.1 (8-21km above Jungfraujoch)	2009-2015	Helmig et al. (2016)

4.2.2 Stratospheric observations

While ground based stations will be affected by upwind, the stratospheric samples offer a more inherently averaged global perspective. Stratospheric ethane trend, estimated with all the CARIBIC samples taken in the northern hemispheric lowermost stratosphere with PV>2 PVU during 2006-2016, is shown in Figure 4.2. Blue light shadow indicates the uncertainty from the trend analysis, which is described in Materials and Methods section of Chapter 3 under "Trend analysis". The black line indicates the average trend from ten trend analysis fittings. Pie charts show the spatial composition of the samples taken from three phases (separated by red lines). The uncertainty of the estimated stratospheric ethane trend is shown in Figure 4.3.

There are three possible reasons for an observed trend: 1) a change in emissions from a emission category, a place, or continent, 2) a change in sinks (e.g. OH variation), 3) a change in the mixing between stratosphere and troposphere.

As shown in Figure 4.2, during phase 1 (2006.02~2012.04), stratospheric ethane shows a rather constant decrease at rate of 6.9%/year, with a small turnover peaking in 2010. This is followed by a drastic trend change in phase 2 (2012.04~2013.03) which displayed an increased rate of 42.7%/year, and in phase 3 (2013.03~2014.09) there was a decrease at a rate of 25.9%/year. Considering that CARIBIC flew on a global scale and the flights are not evenly distributed over regions, I cannot immediately conclude that the observed stratospheric trends represent changes in global ethane emissions or sinks. Some of the derived trends may be the result of a sampling bias, dependent on when certain regions were sampled. To investigate the real causes of the observed trend, the spatial compositions of sampling during three phases (shown as pie charts in Figure 4.2) were compared. Asia, America and Europe are the largest ethane emitters in the world, contributing ~80% of ethane emissions in the Northern Hemisphere (Xiao et al., 2008). In phase 1, more samples were collected over the rest of the Northern Hemisphere, and only 11.1% were made over Asia. Compared to phase 1, samples of phase 2 were collected more over Asia and America, and this may contribute to an apparent increase of the observed trend because ethane emissions in Asia were increasing as documented

in the emissions inventory EDGAR v4.3.2_VOC_spec database (Huang et al., 2017) and a sharp increase of oil and gas emissions in the North America was observed (Helmig et al., 2016). In phase 3, fewer samples were collected over Asia, and more from the rest of the continents of the Northern Hemisphere, but the decreasing trend in phase 3 is still much more than that in phase 1. In order to verify and quantify this sampling bias associated trend, the measured trend data are compared to results from a global model where the modelled data are extracted at the same latitude, longitude, altitude and time as the original measurement (discussed in section 4.3.2). The model incorporates all known emissions via the emission inventory so any deviations between model and measurements are indicators of hitherto unknown emissions or atmospheric processes. The distributions of sampling cannot explain completely the changes in the observed trend.

To the best of my knowledge, there are only three studies reporting the stratospheric (or upper tropospheric) ethane trends (Gardiner et al., 2008;Franco et al., 2015;Helmig et al., 2016), all from fourier transform spectrometer measurements. A summary of these studies are shown in Table 4.1b. Gardiner et al. (2008) presented annual trend in stratospheric ethane column (relative to year 2000) at six sites varying from 0.43 to -3.31%/year until year 2005. Franco et al. (2015) calculated ethane trends at 8-16 km measured at Jungfraujoch of -1.75±1.30 (for 2004-2008) and 9.4±3.2 (for 2009-2013) %/year, indicating an 11% sharp increase since 2009. Helmig et al. (2016) showed that UTLS column (8-21km) measured at Jungfraujoch was decreasing at -1.0±0.2%/year (1995-2009) and started a sharp increase at rate of 6.0±1.1%/year since 2009 until 2015, while the difference in trend growth rate between the two time periods is smaller for mid-tropospheric column (3.6-8 km): -0.8±0.3%/year (1995-2009) and 4.2±1.0%/year (2009-2015).

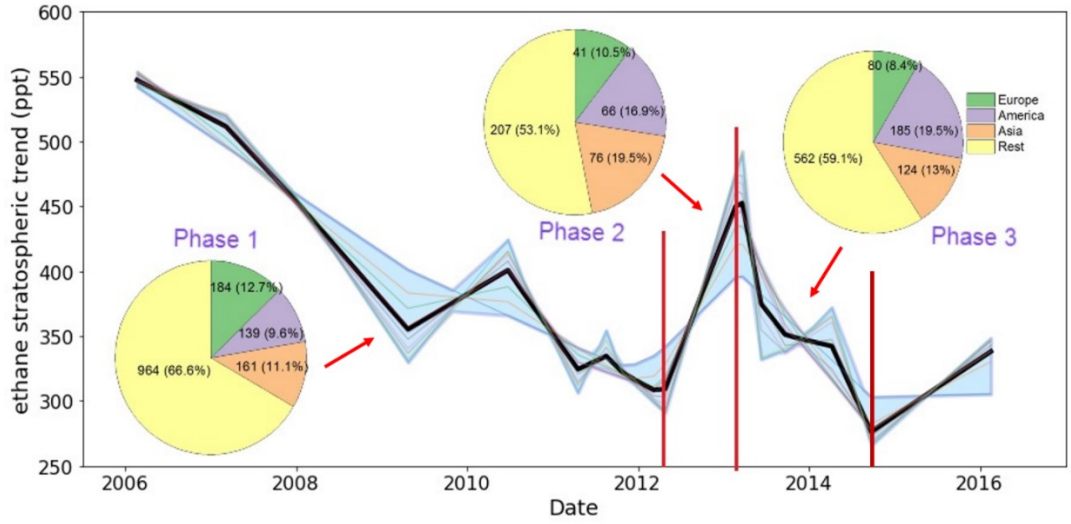

Figure 4.2 Ethane stratospheric trend and flights spatial compositions.

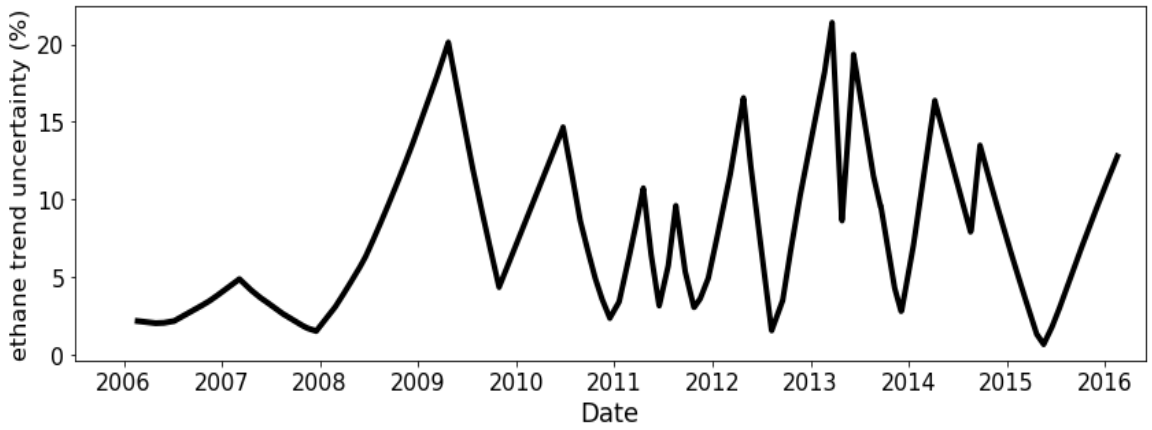

Figure 4.3 Uncertainty of stratospheric ethane trend analysis, indicated as blue shadow in Figure 4.2 .

In order to understand what the driving factors for the observed trend are, stratospheric trends of some other compounds measured from the same samples are shown in Figure 4.4. Some of these compounds share major emission sources with ethane, e.g. methane and propane are also emitted strongly from fossil fuel production, while other compounds to a lesser extent, e.g. i-butane and CO are emitted more from fossil fuel combustion. All these compounds share their major sink namely the oxidation with OH radical. Both ethane and methane show an increase from early 2012 until early 2013, indicating an enhanced fossil fuel emission, possibly from oil and gas production over North America (see section 4.2.1). A decrease of ethane, methane and propane occurred from spring to autumn in 2014, whereas not the case for i-butane and CO. This may rule out the influence of changes in atmospheric OH concentration (assuming sources of i-butane and CO not changing much), since this would cause all the aforementioned compounds to change in a manner consistent with a changing common sink.

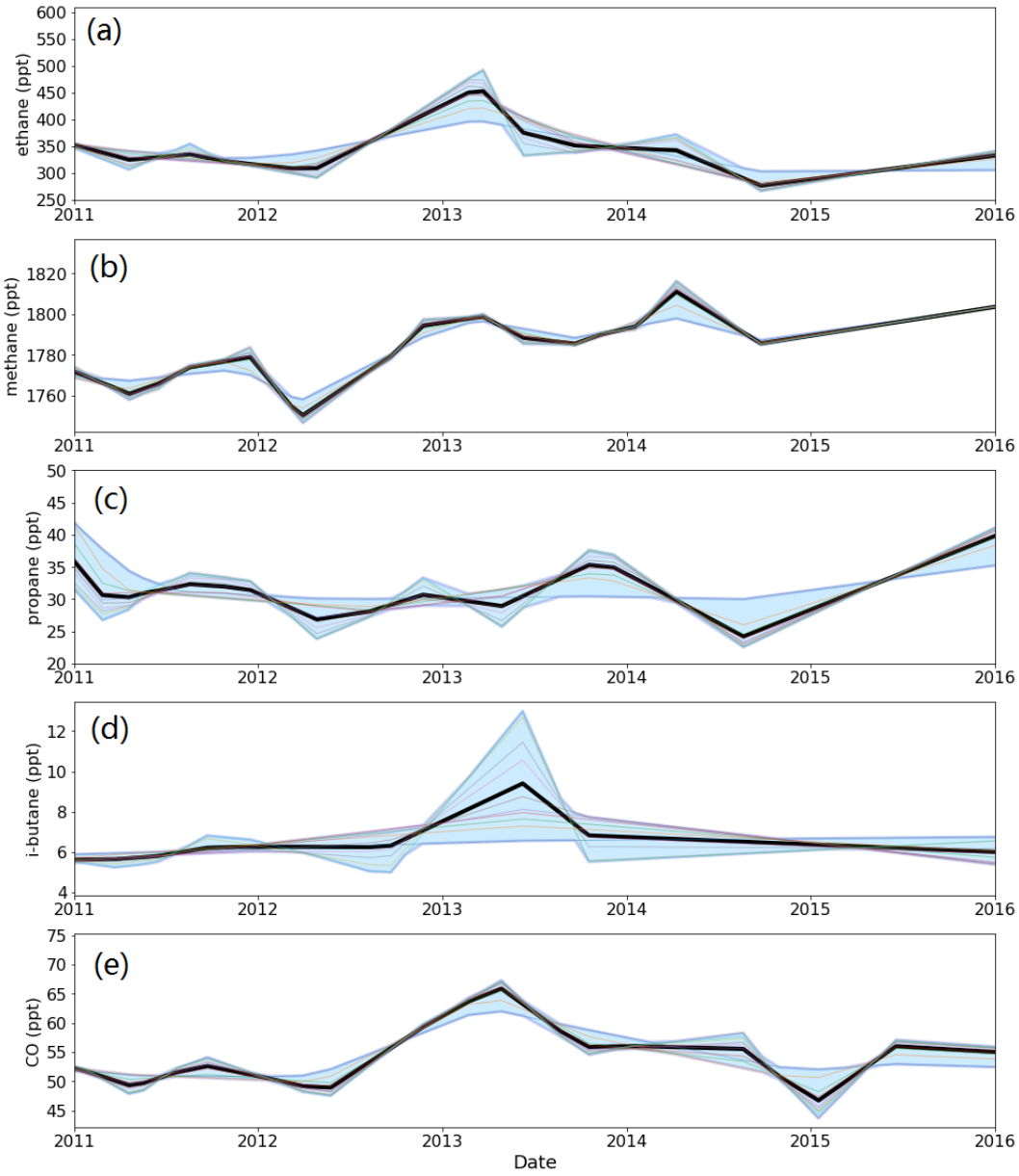

Figure 4.4 Stratospheric trends of (a) ethane, (b) propane, (c) methane, (d) i-Butane and (e) CO during 2011-2016.

4.3 Model simulations

4.3.1 EMAC model description

The EMAC (ECHAM/MESSy Atmospheric Chemistry) model is capable of modelling the chemistry and dynamics of the troposphere and the stratosphere, and some recent updates of the model (version 2.51) have been made and described in (Jöckel et al., 2016). In this study, hindcast simulations (RC1SD-base-10a) in a spatial resolution of 2.8°×2.8° in latitude and longitude, and vertical resolution of 90 model levels reaching up to 0.01 hPa (~80 km) were conducted. Gas-phase chemistry considered in the RC1SD-base-10a simulations includes methane, alkanes and alkenes up to C_4, ozone, odd nitrogen, some selected non-methane hydrocarbons (NMHCs), halogen chemistry, heterogeneous reactions, etc. In total, 310 reactions of 155 species are included in the model.

Two emission inventory data sets are considered in the simulations: one is MACCity (Granier et al., 2011;Diehl et al., 2012) which has a resolution of 0.5°×0.5° and considers a seasonal cycle (monthly resolved) covering the period 1950 to 2010. Starting in 2000, the data set is based on the "MACCity" emissions (Granier et al., 2011), and followed by the IPCC AR5 RCP 8.5 scenario for 2005 and 2010. The other data set is ACCMIP (Lamarque et al., 2010) and AR5 RCP 6.0 data (Fujino et al., 2006) which prescribe monthly values (without seasonal variability) that have been linearly interpolated from annual emission fluxes. From the year 2000, the emissions from the RCP 6.0 scenario are used. The emission inventories include six sectors (road, land, shipping, agricultural waster burning, aviation and biomass burning), and heights are characterized by the vertically distributed ground-based emission fluxes (Pozzer et al., 2009). For RC1SD-base-10a simulations, emissions until 2011 are from MACCity and from 2012 ACCMIP+RCP 6.0 were used.

In this study, two types of simulations were conducted: (1) constant meteorology and constant emission (hereafter climatology), sampled at the CARIBIC sampling location. Any trends (or changes) detected in this simulation would be caused by different sample location/timing. (2) real meteorological conditions from ECMWF and the emissions described above, sampled at the CARIBIC sampling location.

4.3.2 Comparison between model and observation

Figure 4.5 shows ethane stratospheric trends from observation and the two types of model simulations as described above. The trend from climatology (Figure 4.5 b) is relatively flat, with small fluctuations that represent changes from sampling location. Figure 4.5 (c) shows the modelled ethane trend with real meteorology and emissions. It is clear that the model underestimated ethane concentration and trend. On the other hand, the model captures some similar trend features as the observations, e.g. the decreasing trend until 2009, a peak about Δ50 ppt in middle 2010, and a peak appeared in early 2013. A further improvement of the model simulation to match the trend of the observations is needed, and this will be discussed in outlook section.

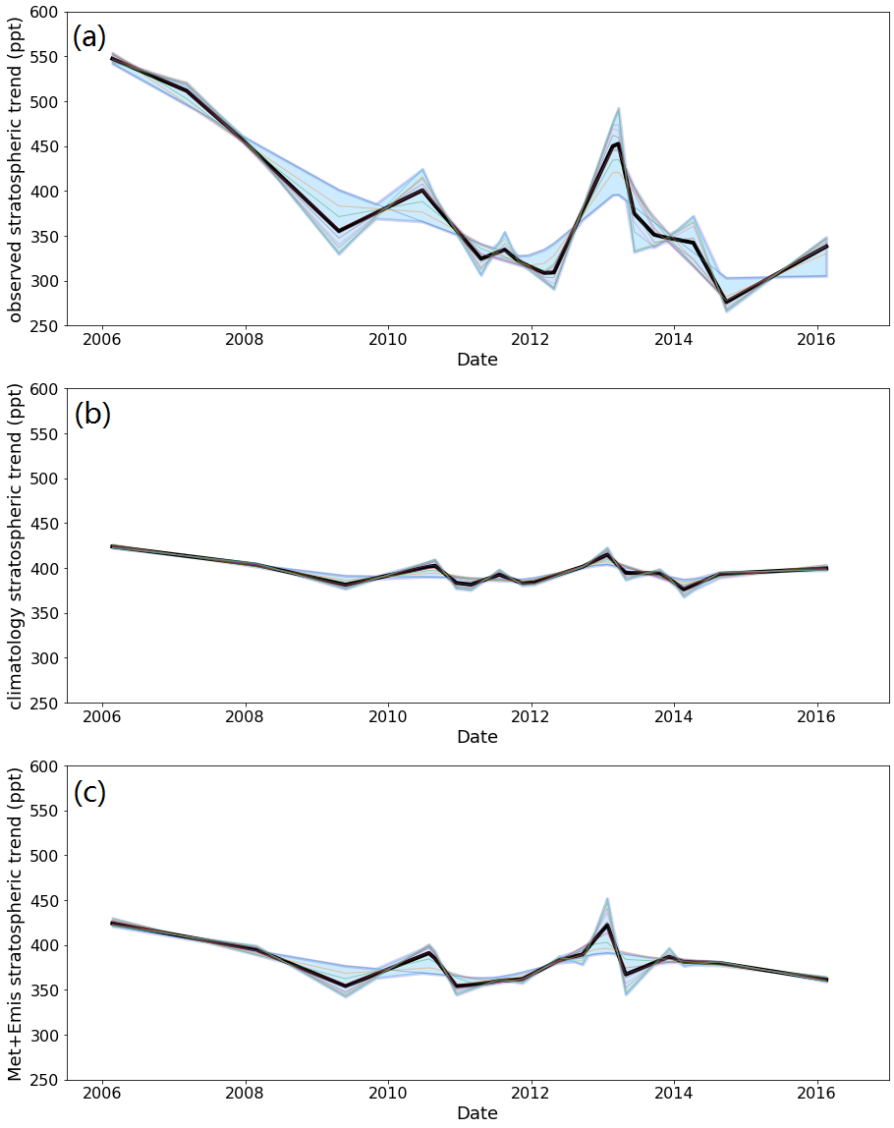

Figure 4.5 Ethane stratospheric trends from (a) observation; (b) model simulations with climatology; (c) model simulations with real meteorology and emissions.

5. CONCLUSIONS AND OUTLOOK

In this PhD project, some empirical methodologies are developed and applied to global long-term airborne observations. They help to address some key questions in atmospheric sciences.

(1) What are the concentrations of OH and Cl radicals in the UTLS region and do they change with time? Multi-year global abundance of two key atmospheric (including tropospheric and stratospheric) radicals: OH and Cl, were estimated. No temporal trend was observed. These results are useful for understanding sinks and lifetimes of reactive compounds, troposphere-stratosphere exchange, and climate change. Future studies can apply similar methods to estimate other radicals, e.g. Br, which is important for stratosphere. This will require better measurements of compounds that react fast with Br radical. Apart from radical abundance, comprehensive studies on understanding global atmospheric oxidation capacity including both the troposphere and the stratosphere are needed.

(2) How does the residence time of CO_2 vary across the globe? CO_2 has multiple removal processes in the atmosphere. The spatial and temporal distributions of the residence time of CO_2 in the troposphere and stratosphere were estimated for different stations and hemispheres. This will help to improve our current

understanding on global carbon cycle and the changing climate. Future studies can investigate what the driving factors (e.g. changes in emissions, land or ocean sinks) for the variation of CO_2 residence time are, by combining with other climate-related parameters. The method (variability-residence time relationship) can be a more robust analysis of the influence from source-sink distribution changes than with three-dimensional climate models since they are based directly on data.

(3) How is the stratospheric ethane trend? Stratospheric ethane trends were determined from an observational UTLS dataset and interpreted with help from model simulations. A general decreasing trend from 2006 to 2016 is observed, with two peaks in 2010 and 2013. The state-of-the-art global model applied, underestimated ethane concentration and its variability. Model simulations can be improved by tuning the emissions from different regions, and try to match the observations.

(4) It is clear to see that long-term observations on global atmospheric chemistry and physics are very important for monitoring climate change, and changes in human activities. Future studies can combine advanced statistical methods (such as machine learning algorithms) to understand what causes the observed trends. Apart from benefiting atmospheric sciences, long-term observations can help to understand health effects from different trace gases or climate change, and their socio-economic effects. The presented data-based methods can be an early warning system for rapid changes in planetary scale processes.

A. LIST OF PUBLICATIONS

Atmospheric chemistry-related:

1. **Li, M**., Karu, E., Brenninkmeijer, C., Fischer, H., Lelieveld, J., and Williams, J.: Tropospheric OH and stratospheric OH and Cl concentrations determined from CH_4, CH_3Cl, and SF_6 measurements, *Nature Climate and Atmospheric Science*, 1, 2018.
2. **Li, M.**, Karu, E., Ciais, P., Lelieveld, J., and Williams, J.: The empirically determined atmospheric residence time of carbon dioxide (CO_2), *Proceedings of the National Academy of Sciences of the United States of America, to be submitted*, 2020.
3. Karu, E., **Li, M.**, Ernle, L., Brenninkmeijer, C. A., Lelieveld, J., and Williams, J.: Atomic emission detector with gas chromatographic separation and cryogenic pre-concentration (CryoTrap-GC-AED) for trace gas measurement, *Atmospheric Measurement Techniques Discussion*, 2020a. (Appendix 1)
4. Karu, E., **Li, M.**, Ernle, L., Brenninkmeijer, C. A., Lelieveld, J., and Williams, J.: Carbonyl sulfide (OCS) in the UTLS region: estimates of lifetimes and fluxes, *Geophysical Research Letters*, in review, 2020b. (Appendix 2)
5. Hong, Z.*, **Li, M.***, Wang, H., Xu, L., Hong, Y., Chen, J., Chen, J., Zhang, H., Zhang, Y., Wu, X., Hu, B., and Li, M.: Characteristics of atmospheric volatile organic compounds (VOCs) at a mountainous forest site and two urban sites in the southeast of China, *Science of The Total Environment*, 657, 1491-1500, 2019. (*these authors contributed equally to this work)
6. **Li, M.**, Pozzer, A., Lelieveld, J., Williams, J.: Stratospheric ethane trend during 2006-2016, in preparation.

Indoor chemistry-related:

1. **Li, M.**, Weschler, C. J., Bekö, G., Wargocki, P., Lucic, G., and Williams, J.: Human Ammonia Emission Rates under Various Indoor Environmental Conditions, *Environmental Science & Technology*, 54, 5419-5428, 2020b.
2. Bekö, G., Wargocki, P., Wang, N., **Li, M.**, Weschler, C. J., Morrison, G., Langer, S., Ernle, L., Licina, D., Yang, S., Zannoni, N., and Williams, J.: The Indoor Chemical Human Emissions and Reactivity project (ICHEAR): Overview of experimental methodology and preliminary results, *Indoor Air*, 2020.
3. Wang, N., Zannoni, N., Ernle, L., Bekö, G., Wargocki, P., **Li, M.**, Weschler, C. J., and Williams, J.: Total OH reactivity of emissions from humans: in-situ measurement and budget analysis, *Environmental Science & Technology*, in review, 2020.

B. CURRICULUM VITAE

EDUCATION

04. 2018 - 12.2020	PhD student, Max Planck Institute for Chemistry, Johannes Gutenberg-Universität Mainz, Germany
10. 2015 - 01.2018	M.Sc Environmental Science, University of Frankfurt, Germany
04. 2015 - 10.2015	B.Sc Environmental Engineering, TU Braunschweig, Germany
09. 2009 - 07.2013	B.Sc Environmental Science, Fujian Normal University, China

RESEARCH PROJECTS

Mar. 2017- present	IAGOS - CARIBIC (Civil Aircraft for the Regular Investigation of the Atmosphere Based on an Instrument Container)
Apr-May. 2019	Indoor Chemical Human Emissions and Reactivity (ICHEAR)
Feb. 2019	Breath Analysis on human excitement, Portugal

CONFERENCE

Nov. 2020	Oral presentation, Indoor Air 2020, virtual
Apr. 2019	Oral presentation, European Geosciences Union (EGU) General Assembly 2019, Vienna, Austria
Dec. 2018	Poster presentation, American Geophysical Union (AGU) fall meeting 2018, Washington, D.C. USA

SOCIAL CONTRIBUTION

Apr. 2021	Convener of EGU2021 session (How to find funding and write a research grant)
Apr. 2020 - present	Representative of EGU Early Career Scientists in Atmospheric Sciences Division
	Editor of EGU blog of Atmospheric Sciences Division
Sep.- Nov. 2020	Organized EGU webinars “Making geoscience societies more inclusive” and “Publishing and Careers at Nature Research”
Jun. 2020	Expert Reviewer for IPCC AR6 WGI Second Order Draft

C. LIST OF FIGURES

D. LIST OF TABLES

E. ACKNOWLEDGEMENTS

First of all, I want to give great thanks to my supervisors. Jonathan knows how to motivate and inspire me. He is always there for discussing science, giving advice for career paths, or small talk. Many of the ideas of this project are inspired or supported by him. He also shows me how to be open-minded with new ideas and voice from others. Thorsten is always generous and helpful to give me insightful ideas on my project and support, especially during my PAC meetings.

Secondly, I want to thank all of my colleagues and collaborators. I got numerous support from ORSUM group, Paul Crutzen Graduate School and CARIBIC team, especially from Einar, Claus, Carl, Thomas, Rolf, Sergy, Tobi, Karin, Nora, Jeannie and Ute. I want to thank Horst and John for attending my PAC meetings and gave comments and ideas, and thank Andrea for running EMAC model and discussion. The team members from Porto and ICHEAR projects offered me great knowledge in indoor chemistry, which is quite different as atmospheric science. I thank the graphic office (Dominic) and the communications department (Simone, Neli, Susanne) for their help whenever I need them.

Thirdly, I give great thanks to my friends for always being there for me. Many old friends are still there with me and many colleagues become new friends, e.g. Einar, Nora, Christof (or -ph), Jake, Alex, Steven, Bruna, Neli, Akima, Tobi, Rong, Marco, Kai, Najin, Leslie, etc. They all brought me joy and support.

Last but not least, I want to give my deepest thank to my family, especially my grandfather who passed away in the week when I had a work accident in Denmark. He was a traditional person and wanted me to settle down somewhere close to him, but he never mentioned this to me, instead he always told me to pursue my dreams and that he will be supporting me no matter how far I go. I feel guilty for not visiting him often due to my study in Germany. This taught me to cherish and appreciate what I have now.

F. REFERENCES

Angelbratt, J., Mellqvist, J., Simpson, D., Jonson, J. E., Blumenstock, T., Borsdorff, T., Duchatelet, P., Forster, F., Hase, F., Mahieu, E., De Mazière, M., Notholt, J., Petersen, A. K., Raffalski, U., Servais, C., Sussmann, R., Warneke, T., and Vigouroux, C.: Carbon monoxide (CO) and ethane (C2H6) trends from ground-based solar FTIR measurements at six European stations, comparison and sensitivity analysis with the EMEP model, Atmos. Chem. Phys., 11, 9253-9269, 10.5194/acp-11-9253-2011, 2011.

Assonov, S. S., Brenninkmeijer, C. A. M., Schuck, T., and Umezawa, T.: N_2O as a tracer of mixing stratospheric and tropospheric air based on CARIBIC data with applications for CO_2, Atmospheric Environment, 79, 769-779, 10.1016/j.atmosenv.2013.07.035, 2013.

Atkinson, R.: Kinetics of the gas-phase reactions of OH radicals with alkanes and cycloalkanes, Atmos. Chem. Phys., 3, 2233-2307, 10.5194/acp-3-2233-2003, 2003.

Baker, A. K., Slemr, F., and Brenninkmeijer, C. A. M.: Analysis of non-methane hydrocarbons in air samples collected aboard the CARIBIC passenger aircraft, Atmos. Meas. Tech., 3, 311-321, 10.5194/amt-3-311-2010, 2010.

Baker, A. K., Schuck, T. J., Slemr, F., van Velthoven, P., Zahn, A., and Brenninkmeijer, C. A. M.: Characterization of non-methane hydrocarbons in Asian summer monsoon outflow observed by the CARIBIC aircraft, Atmospheric Chemistry and Physics, 11, 503-518, 10.5194/acp-11-503-2011, 2011.

Baker, A. K., Schuck, T. J., Brenninkmeijer, C. A. M., Rauthe-Schöch, A., Slemr, F., van Velthoven, P. F. J., and Lelieveld, J.: Estimating the contribution of monsoon-related biogenic production to methane emissions from South Asia using CARIBIC observations, Geophysical Research Letters, 39, 10.1029/2012gl051756, 2012.

Baker, A. K., Sauvage, C., Thorenz, U. R., van Velthoven, P., Oram, D. E., Zahn, A., Brenninkmeijer, C. A. M., and Williams, J.: Evidence for strong, widespread chlorine radical chemistry associated with pollution outflow from continental Asia, Sci Rep, 6, 36821, 10.1038/srep36821, 2016.

References

Barkley, M. P., Palmer, P. I., Boone, C. D., Bernath, P. F., and Suntharalingam, P.: Global distributions of carbonyl sulfide in the upper troposphere and stratosphere, Geophysical Research Letters, 35, 10.1029/2008gl034270, 2008.

Bethan, S., Vaughan, G., and Reid, S.: A comparison of ozone and thermal tropopause heights and the impact of tropopause definition on quantifying the ozone content of the troposphere, Quarterly Journal of the Royal Meteorological Society, 122, 929-944, 1996.

Blake, N. J., Penkett, S. A., Clemitshaw, K. C., Anwyl, P., Lightman, P., Marsh, A. R. W., and Butcher, G.: Estimates of atmospheric hydroxyl radical concentrations from the observed decay of many reactive hydrocarbons in well-defined urban plumes, Journal of Geophysical Research: Atmospheres, 98, 2851--2864, 10.1029/92JD02161, 1993.

Boering, K. A., Wofsy, S. C., Daube, B. C., Schneider, H. R., Loewenstein, M., Podolske, J. R., and Conway, T. J.: Stratospheric Mean Ages and Transport Rates from Observations of Carbon Dioxide and Nitrous Oxide, Science, 274, 1340, 1996.

Bönisch, H., Engel, A., Curtius, J., Birner, T., and Hoor, P.: Quantifying transport into the lowermost stratosphere using simultaneous in-situ measurements of SF_6 and CO_2, Atmos. Chem. Phys., 9, 5905-5919, 10.5194/acp-9-5905-2009, 2009.

Brenninkmeijer, C. A. M., Crutzen, P., Boumard, F., Dauer, T., Dix, B., Ebinghaus, R., Filippi, D., Fischer, H., Franke, H., Frieβ, U., Heintzenberg, J., Helleis, F., Hermann, M., Kock, H. H., Koeppel, C., Lelieveld, J., Leuenberger, M., Martinsson, B. G., Miemczyk, S., Moret, H. P., Nguyen, H. N., Nyfeler, P., Oram, D., O'Sullivan, D., Penkett, S., Platt, U., Pupek, M., Ramonet, M., Randa, B., Reichelt, M., Rhee, T. S., Rohwer, J., Rosenfeld, K., Scharffe, D., Schlager, H., Schumann, U., Slemr, F., Sprung, D., Stock, P., Thaler, R., Valentino, F., van Velthoven, P., Waibel, A., Wandel, A., Waschitschek, K., Wiedensohler, A., Xueref-Remy, I., Zahn, A., Zech, U., and Ziereis, H.: Civil Aircraft for the regular investigation of the atmosphere based on an instrumented container: The new CARIBIC system, Atmos. Chem. Phys., 7, 4953-4976, 10.5194/acp-7-4953-2007, 2007.

Brewer, A.: Evidence for a world circulation provided by the measurements of helium and water vapour distribution in the stratosphere, Quarterly Journal of the Royal Meteorological Society, 75, 351-363, 1949.

Butchart, N.: The Brewer-Dobson circulation, Reviews of Geophysics, 52, 157-184, 10.1002/2013rg000448, 2014a.

Butchart, N.: The Brewer‐Dobson circulation, Reviews of geophysics, 52, 157-184, 2014b.

Chandrappa, R., and Chandra Kulshrestha, U.: Major Issues of Air Pollution, in: Sustainable Air Pollution Management: Theory and Practice, edited by: Chandrappa, R., and Chandra Kulshrestha, U., Springer International Publishing, Cham, 1-48, 2016.

References

Colman, J. J., Blake, D. R., and Rowland, F. S.: Atmospheric Residence Time of CH3Br Estimated from the Junge Spatial Variability Relation, Science, 281, 392, 10.1126/science.281.5375.392, 1998.

DeMore, W. B. S., S.P.; Golden, D.M.; Hampson, R.F.; Kurylo, M.J.; Howard, C.J.; Ravishankara, A.R.; Kolb, C.E.; Molina, M.J.: Chemical kinetics and photochemical data for use in stratospheric modeling. Evaluation number 12, 1 - 266, 1997.

Diallo, M., Legras, B., Ray, E., Engel, A., and Añel, J. A.: Global distribution of CO2 in the upper troposphere and stratosphere, Atmos. Chem. Phys., 17, 3861-3878, 10.5194/acp-17-3861-2017, 2017.

Diehl, T., Heil, A., Chin, M., Pan, X., Streets, D., Schultz, M., and Kinne, S.: Anthropogenic, biomass burning, and volcanic emissions of black carbon, organic carbon, and SO2 from 1980 to 2010 for hindcast model experiments, Atmos. Chem. Phys. Discuss., 2012, 24895-24954, 10.5194/acpd-12-24895-2012, 2012.

Dlugokencky, E. J., Steele, L. P., Lang, P. M., and Masarie, K. A.: The growth rate and distribution of atmospheric methane, Journal of Geophysical Research: Atmospheres, 99, 17021--17043, 10.1029/94JD01245, 1994.

Dlugokencky, E. J., Crotwell;, A. M., Lang;, P. M., and Mund, J. W.: Atmospheric Methane Dry Air Mole Fractions from quasi-continuous measurements at Mauna Loa, Hawaii, 1986-2016, Version: 2017-01-20,Path: ftp://aftp.cmdl.noaa.gov/data/trace_gases/ch4/in-situ/surface/, 2017.

Dobson, G. M. B., Harrison, D., and Lawrence, J.: Measurements of the amount of ozone in the Earth's atmosphere and its relation to other geophysical conditions.—Part III, Proceedings of the Royal Society of London. Series A, Containing Papers of a Mathematical and Physical Character, 122, 456-486, 1929.

Dobson, G. M. B.: Origin and distribution of the polyatomic molecules in the atmosphere, Proceedings of the Royal Society of London. Series A. Mathematical and Physical Sciences, 236, 187-193, 1956.

Eisele, F. L., and Tanner, D. J. J.: Ion-assisted tropospheric OH measurements, J. Geophys. Res., 96, 9295–9308, 10.1029/91JD00198, 1991.

Engel, A., Bönisch, H., Brunner, D., Fischer, H., Franke, H., Günther, G., Gurk, C., Hegglin, M., Hoor, P., Königstedt, R., Krebsbach, M., Maser, R., Parchatka, U., Peter, T., Schell, D., Schiller, C., Schmidt, U., Spelten, N., Szabo, T., Weers, U., Wernli, H., Wetter, T., and Wirth, V.: Highly resolved observations of trace gases in the lowermost stratosphere and upper troposphere from the Spurt project: an overview, Atmos. Chem. Phys., 6, 283-301, 10.5194/acp-6-283-2006, 2006.

References

Engel, A., Möbius, T., Bönisch, H., Schmidt, U., Heinz, R., Levin, I., Atlas, E., Aoki, S., Nakazawa, T., Sugawara, S., Moore, F., Hurst, D., Elkins, J., Schauffler, S., Andrews, A., and Boering, K.: Age of stratospheric air unchanged within uncertainties over the past 30 years, Nature Geoscience, 2, 28-31, 10.1038/ngeo388, 2008.

Ertel, H.: Ein neuer hydrodynamischer Wirbelsatz, Met. Z., 59, 277-281, 1942.

Felton, C. C., Sheppard, J. C., and Campbell, M. J.: Measurements of the diurnal OH cycle by a 14C-tracer method, Nature, 335, 53-55, 10.1038/335053a0, 1988.

Fischer, H., Wienhold, F. G., Hoor, P., Bujok, O., Schiller, C., Siegmund, P., Ambaum, M., Scheeren, H. A., and Lelieveld, J.: Tracer correlations in the northern high latitude lowermost stratosphere: Influence of cross-tropopause mass exchange, Geophysical Research Letters, 27, 97-100, 10.1029/1999gl010879, 2000.

Franco, B., Bader, W., Toon, G. C., Bray, C., Perrin, A., Fischer, E. V., Sudo, K., Boone, C. D., Bovy, B., Lejeune, B., Servais, C., and Mahieu, E.: Retrieval of ethane from ground-based FTIR solar spectra using improved spectroscopy: Recent burden increase above Jungfraujoch, Journal of Quantitative Spectroscopy and Radiative Transfer, 160, 36-49, 10.1016/j.jqsrt.2015.03.017, 2015.

Franco, B., Mahieu, E., Emmons, L. K., Tzompa-Sosa, Z. A., Fischer, E. V., Sudo, K., Bovy, B., Conway, S., Griffin, D., Hannigan, J. W., Strong, K., and Walker, K. A.: Evaluating ethane and methane emissions associated with the development of oil and natural gas extraction in North America, Environmental Research Letters, 11, 044010, 10.1088/1748-9326/11/4/044010, 2016.

Friedlingstein, P., Jones, M. W., O'Sullivan, M., Andrew, R. M., Hauck, J., Peters, G. P., Peters, W., Pongratz, J., Sitch, S., Le Quéré, C., Bakker, D. C. E., Canadell, J. G., Ciais, P., Jackson, R. B., Anthoni, P., Barbero, L., Bastos, A., Bastrikov, V., Becker, M., Bopp, L., Buitenhuis, E., Chandra, N., Chevallier, F., Chini, L. P., Currie, K. I., Feely, R. A., Gehlen, M., Gilfillan, D., Gkritzalis, T., Goll, D. S., Gruber, N., Gutekunst, S., Harris, I., Haverd, V., Houghton, R. A., Hurtt, G., Ilyina, T., Jain, A. K., Joetzjer, E., Kaplan, J. O., Kato, E., Klein Goldewijk, K., Korsbakken, J. I., Landschützer, P., Lauvset, S. K., Lefèvre, N., Lenton, A., Lienert, S., Lombardozzi, D., Marland, G., McGuire, P. C., Melton, J. R., Metzl, N., Munro, D. R., Nabel, J. E. M. S., Nakaoka, S. I., Neill, C., Omar, A. M., Ono, T., Peregon, A., Pierrot, D., Poulter, B., Rehder, G., Resplandy, L., Robertson, E., Rödenbeck, C., Séférian, R., Schwinger, J., Smith, N., Tans, P. P., Tian, H., Tilbrook, B., Tubiello, F. N., van der Werf, G. R., Wiltshire, A. J., and Zaehle, S.: Global Carbon Budget 2019, Earth Syst. Sci. Data, 11, 1783-1838, 10.5194/essd-11-1783-2019, 2019.

Fuchs, H., Dorn, H. P., Bachner, M., Bohn, B., Brauers, T., Gomm, S., Hofzumahaus, A., Holland, F., Nehr, S., Rohrer, F., Tillmann, R., and Wahner, A.: Comparison of OH concentration measurements by DOAS and LIF during SAPHIR chamber experiments at high OH reactivity and low NO concentration, Atmos. Meas. Tech., 5, 1611-1626, 10.5194/amt-5-1611-2012, 2012.

References

Fujino, J., Nair, R., Kainuma, M., Masui, T., and Yuzuru, M.: Multi-gas Mitigation Analysis on Stabilization Scenarios Using Aim Global Model, The Energy Journal, Multi-Greenhouse Gas Mitigation and Climate Policy, 343-354, 2006.

Gardiner, T., Forbes, A., de Mazière, M., Vigouroux, C., Mahieu, E., Demoulin, P., Velazco, V., Notholt, J., Blumenstock, T., Hase, F., Kramer, I., Sussmann, R., Stremme, W., Mellqvist, J., Strandberg, A., Ellingsen, K., and Gauss, M.: Trend analysis of greenhouse gases over Europe measured by a network of ground-based remote FTIR instruments, Atmos. Chem. Phys., 8, 6719-6727, 10.5194/acp-8-6719-2008, 2008.

Garny, H., Birner, T., Bönisch, H., and Bunzel, F.: The effects of mixing on age of air, Journal of Geophysical Research: Atmospheres, 119, 7015-7034, 10.1002/2013jd021417, 2014.

Gettelman, A., Hoor, P., Pan, L. L., Randel, W. J., Hegglin, M. I., and Birner, T.: The Extratropical Upper Troposphere and Lower Stratosphere, Reviews of Geophysics, 49, 10.1029/2011rg000355, 2011.

Glatthor, N., von Clarmann, T., Stiller, G. P., Funke, B., Koukouli, M. E., Fischer, H., Grabowski, U., Höpfner, M., Kellmann, S., and Linden, A.: Large-scale upper tropospheric pollution observed by MIPAS HCN and C2H6 global distributions, Atmos. Chem. Phys., 9, 9619-9634, 10.5194/acp-9-9619-2009, 2009.

González Abad, G., Allen, N. D. C., Bernath, P. F., Boone, C. D., McLeod, S. D., Manney, G. L., Toon, G. C., Carouge, C., Wang, Y., Wu, S., Barkley, M. P., Palmer, P. I., Xiao, Y., and Fu, T. M.: Ethane, ethyne and carbon monoxide concentrations in the upper troposphere and lower stratosphere from ACE and GEOS-Chem: a comparison study, Atmospheric Chemistry and Physics, 11, 9927-9941, 10.5194/acp-11-9927-2011, 2011.

Granier, C., Bessagnet, B., Bond, T., D'Angiola, A., Denier van der Gon, H., Frost, G. J., Heil, A., Kaiser, J. W., Kinne, S., Klimont, Z., Kloster, S., Lamarque, J.-F., Liousse, C., Masui, T., Meleux, F., Mieville, A., Ohara, T., Raut, J.-C., Riahi, K., Schultz, M. G., Smith, S. J., Thompson, A., van Aardenne, J., van der Werf, G. R., and van Vuuren, D. P.: Evolution of anthropogenic and biomass burning emissions of air pollutants at global and regional scales during the 1980–2010 period, Climatic Change, 109, 163, 10.1007/s10584-011-0154-1, 2011.

Gromov, S., Brenninkmeijer, C. A. M., and Jöckel, P.: A very limited role of tropospheric chlorine as a sink of the greenhouse gas methane, Atmospheric Chemistry and Physics, 18, 9831-9843, 10.5194/acp-18-9831-2018, 2018.

Hall, B. D., Dutton, G. S., Mondeel, D. J., Nance, J. D., Rigby, M., Butler, J. H., Moore, F. L., Hurst, D. F., and Elkins, J. W.: Improving measurements of SF_6 for the study of atmospheric transport and emissions, Atmos. Meas. Tech., 4, 2441-2451, 10.5194/amt-4-2441-2011, 2011.

Hall, T. M., and Plumb, R. A.: Age as a diagnostic of stratospheric transport, Journal of Geophysical Research: Atmospheres, 99, 1059--1070, 10.1029/93JD03192, 1994.

References

Hamrud, M.: Residence time and spatial variability for gases in the atmosphere, Tellus B, 35B, 295-303, 10.1111/j.1600-0889.1983.tb00034.x, 1983.

Hard, T. M., Chan, C. Y., Mehrabzadeh, A. A., Pan, W. H., and O'Brien, R. J.: Diurnal cycle of tropospheric OH, Nature, 322, 617, 10.1038/322617a0, 1986.

Heard, D. E., and Pilling, M. J.: Measurement of OH and HO2 in the Troposphere, Chemical Reviews, 103, 5163-5198, 10.1021/cr020522s, 2003.

Heard, D. E., Read, K. A., Methven, J., Al-Haider, S., Bloss, W. J., Johnson, G. P., Pilling, M. J., Seakins, P. W., Smith, S. C., Sommariva, R., Stanton, J. C., Still, T. J., Ingham, T., Brooks, B., De Leeuw, G., Jackson, A. V., McQuaid, J. B., Morgan, R., Smith, M. H., Carpenter, L. J., Carslaw, N., Hamilton, J., Hopkins, J. R., Lee, J. D., Lewis, A. C., Purvis, R. M., Wevill, D. J., Brough, N., Green, T., Mills, G., Penkett, S. A., Plane, J. M. C., Saiz-Lopez, A., Worton, D., Monks, P. S., Fleming, Z., Rickard, A. R., Alfarra, M. R., Allan, J. D., Bower, K., Coe, H., Cubison, M., Flynn, M., McFiggans, G., Gallagher, M., Norton, E. G., O'Dowd, C. D., Shillito, J., Topping, D., Vaughan, G., Williams, P., Bitter, M., Ball, S. M., Jones, R. L., Povey, I. M., O'Doherty, S., Simmonds, P. G., Allen, A., Kinnersley, R. P., Beddows, D. C. S., Dall'Osto, M., Harrison, R. M., Donovan, R. J., Heal, M. R., Jennings, S. G., Noone, C., and Spain, G.: The North Atlantic Marine Boundary Layer Experiment(NAMBLEX). Overview of the campaign held at Mace Head, Ireland, in summer 2002, Atmos. Chem. Phys., 6, 2241-2272, 10.5194/acp-6-2241-2006, 2006.

Helmig, D., Rossabi, S., Hueber, J., Tans, P., Montzka, S. A., Masarie, K., Thoning, K., Plass-Duelmer, C., Claude, A., Carpenter, L. J., Lewis, A. C., Punjabi, S., Reimann, S., Vollmer, M. K., Steinbrecher, R., Hannigan, J. W., Emmons, L. K., Mahieu, E., Franco, B., Smale, D., and Pozzer, A.: Reversal of global atmospheric ethane and propane trends largely due to US oil and natural gas production, Nature Geoscience, 9, 490-495, 10.1038/ngeo2721, 2016.

Holton, J. R., Haynes, P. H., McIntyre, M. E., Douglass, A. R., Rood, R. B., and Pfister, L.: Stratosphere-troposphere exchange, Reviews of Geophysics, 33, 403--439, 10.1029/95RG02097, 1995.

Hoor, P., Fischer, H., Lange, L., Lelieveld, J., and Brunner, D.: Seasonal variations of a mixing layer in the lowermost stratosphere as identified by the CO-O3correlation from in situ measurements, Journal of Geophysical Research: Atmospheres, 107, ACL 1-1-ACL 1-11, 10.1029/2000jd000289, 2002.

Hoor, P., Wernli, H., Hegglin, M. I., and Bönisch, H.: Transport timescales and tracer properties in the extratropical UTLS, Atmospheric Chemistry and Physics, 10, 7929-7944, 10.5194/acp-10-7929-2010, 2010.

Hosaynali Beygi, Z., Fischer, H., Harder, H. D., Martinez, M., Sander, R., Williams, J., Brookes, D. M., Monks, P. S., and Lelieveld, J.: Oxidation photochemistry in the Southern Atlantic boundary layer: unexpected deviations of photochemical steady state, Atmos. Chem. Phys., 11, 8497-8513, 10.5194/acp-11-8497-2011, 2011.

References

Huang, G., Brook, R., Crippa, M., Janssens-Maenhout, G., Schieberle, C., Dore, C., Guizzardi, D., Muntean, M., Schaaf, E., and Friedrich, R.: Speciation of anthropogenic emissions of non-methane volatile organic compounds: a global gridded data set for 1970–2012, Atmos. Chem. Phys., 17, 7683-7701, 10.5194/acp-17-7683-2017, 2017.

IPCC: Climate Change 2007: Mitigation. Contribution of Working Group III to the Fourth Assessment Report of the Intergovernmental Panel on Climate Change [B. Metz, O.R. Davidson, P.R. Bosch, R. Dave, L.A. Meyer (eds)], Cambridge, United Kingdom and New York, NY, USA, 2007.

Jobson, B. T., Parrish, D. D., Goldan, P., Kuster, W., Fehsenfeld, F. C., Blake, D. R., Blake, N. J., and Niki, H.: Spatial and temporal variability of nonmethane hydrocarbon mixing ratios and their relation to photochemical lifetime, Journal of Geophysical Research: Atmospheres, 103, 13557-13567, doi:10.1029/97JD01715, 1998.

Jobson, B. T., McKeen, S. A., Parrish, D. D., Fehsenfeld, F. C., Blake, D. R., Goldstein, A. H., Schauffler, S. M., and Elkins, J. W.: Trace gas mixing ratio variability versus lifetime in the troposphere and stratosphere: Observations, Journal of Geophysical Research: Atmospheres, 104, 16091-16113, 10.1029/1999JD900126, 1999.

Jöckel, P., Tost, H., Pozzer, A., Kunze, M., Kirner, O., Brenninkmeijer, C. A. M., Brinkop, S., Cai, D. S., Dyroff, C., Eckstein, J., Frank, F., Garny, H., Gottschaldt, K. D., Graf, P., Grewe, V., Kerkweg, A., Kern, B., Matthes, S., Mertens, M., Meul, S., Neumaier, M., Nützel, M., Oberländer-Hayn, S., Ruhnke, R., Runde, T., Sander, R., Scharffe, D., and Zahn, A.: Earth System Chemistry integrated Modelling (ESCiMo) with the Modular Earth Submodel System (MESSy) version 2.51, Geosci. Model Dev., 9, 1153-1200, 10.5194/gmd-9-1153-2016, 2016.

Joos, F., Roth, R., Fuglestvedt, J. S., Peters, G. P., Enting, I. G., von Bloh, W., Brovkin, V., Burke, E. J., Eby, M., Edwards, N. R., Friedrich, T., Frölicher, T. L., Halloran, P. R., Holden, P. B., Jones, C., Kleinen, T., Mackenzie, F. T., Matsumoto, K., Meinshausen, M., Plattner, G. K., Reisinger, A., Segschneider, J., Shaffer, G., Steinacher, M., Strassmann, K., Tanaka, K., Timmermann, A., and Weaver, A. J.: Carbon dioxide and climate impulse response functions for the computation of greenhouse gas metrics: a multi-model analysis, Atmos. Chem. Phys., 13, 2793-2825, 10.5194/acp-13-2793-2013, 2013.

Junge, C. E.: Residence time and variability of tropospheric trace gases, Tellus, 26, 477-488, 10.1111/j.2153-3490.1974.tb01625.x, 1974.

Karu, E.: Atmospheric Sulfur Compounds in the Troposphere and Stratosphere Measured with an Atomic Emission Detector, Johannes Gutenberg-Universität Mainz, 2019.

Karu, E., Li, M., Ernle, L., Brenninkmeijer, C. A., Lelieveld, J., and Williams, J.: Carbonyl sulfide (OCS) in the UT/LS region: estimates of lifetimes and fluxes, Geophysical Research Letters, in review, 2020a.

References

Karu, E., Li, M., Ernle, L., Brenninkmeijer, C. A., Lelieveld, J., and Williams, J.: Atomic emission detector with gas chromatographic separation and cryogenic pre-concentration (CryoTrap-GC-AED) for trace gas measurement, Atmospheric Measurement Techniques Discussion, in review, 10.5194/amt-2020-199, 2020b.

Ko, M. K. W., Newman, P. A., Reimann, S., and Strahan, S. E.: SPARC Report on Lifetimes of Stratospheric Ozone-Depleting Substances, Their Replacements, and Related Species, SPARC, 256, 2013.

Krasnoperov, L., and Michael, J.: Shock tube studies using a novel multipass absorption cell: rate constant results for OH+ H2 and OH+ C2H6, The Journal of Physical Chemistry A, 108, 5643-5648, 2004.

Krol, M., and Lelieveld, J.: Can the variability in tropospheric OH be deduced from measurements of 1,1,1-trichloroethane (methyl chloroform)?, Journal of Geophysical Research: Atmospheres, 108, 10.1029/2002jd002423, 2003.

Lamarque, J. F., Bond, T. C., Eyring, V., Granier, C., Heil, A., Klimont, Z., Lee, D., Liousse, C., Mieville, A., Owen, B., Schultz, M. G., Shindell, D., Smith, S. J., Stehfest, E., Van Aardenne, J., Cooper, O. R., Kainuma, M., Mahowald, N., McConnell, J. R., Naik, V., Riahi, K., and van Vuuren, D. P.: Historical (1850–2000) gridded anthropogenic and biomass burning emissions of reactive gases and aerosols: methodology and application, Atmos. Chem. Phys., 10, 7017-7039, 10.5194/acp-10-7017-2010, 2010.

Landschützer, P., Gruber, N., Haumann, F. A., Rödenbeck, C., Bakker, D. C., Van Heuven, S., Hoppema, M., Metzl, N., Sweeney, C., and Takahashi, T.: The reinvigoration of the Southern Ocean carbon sink, Science, 349, 1221-1224, 2015.

Lange, L., Hoor, P., Helas, G., Fischer, H., Brunner, D., Scheeren, B., Williams, J., Wong, S., Wohlfrom, K. H., Arnold, F., Stroem, J., Krejci, R., Lelieveld, J., and Andreae, M. O.: Detection of lightning - produced NO in the midlatitude upper troposphere during STREAM 1998, Journal of Geophysical Research: Atmospheres, 106, 27777-27785, 10.1029/2001JD900210, 2001.

Le Quéré, C., Rödenbeck, C., Buitenhuis, E. T., Conway, T. J., Langenfelds, R., Gomez, A., Labuschagne, C., Ramonet, M., Nakazawa, T., Metzl, N., Gillett, N., and Heimann, M.: Saturation of the Southern Ocean CO2 Sink Due to Recent Climate Change, Science, 316, 1735, 10.1126/science.1136188, 2007.

Le Quéré, C., Raupach, M. R., Canadell, J. G., Marland, G., Le Quéré, C., Raupach, M. R., Canadell, J. G., Marland, G., Bopp, L., Ciais, P., Conway, T. J., Doney, S. C., Feely, R. A., Foster, P., Friedlingstein, P., Gurney, K., Houghton, R. A., House, J. I., Huntingford, C., Levy, P. E., Lomas, M. R., Majkut, J., Metzl, N., Ometto, J. P., Peters, G. P., Prentice, I. C., Randerson, J. T., Running, S. W., Sarmiento, J. L., Schuster, U., Sitch, S., Takahashi, T., Viovy, N., van der Werf, G. R., and Woodward, F. I.: Trends in the sources and sinks of carbon dioxide, Nature Geoscience, 2, 831-836, 10.1038/ngeo689, 2009.

References

Lelieveld, J., Bregman, A., Scheeren, H. A., Ström, J., Carslaw, K. S., Fischer, H., Siegmund, P. C., and Arnold, F.: Chlorine activation and ozone destruction in the northern lowermost stratosphere, Journal of Geophysical Research: Atmospheres, 104, 8201--8213, 10.1029/1998JD100111, 1999.

Lelieveld, J., Butler, T. M., Crowley, J. N., Dillon, T. J., Fischer, H., Ganzeveld, L., Harder, H., Lawrence, M. G., Martinez, M., Taraborrelli, D., and Williams, J.: Atmospheric oxidation capacity sustained by a tropical forest, Nature, 452, 737-740, 10.1038/nature06870, 2008.

Lelieveld, J., Gromov, S., Pozzer, A., and Taraborrelli, D.: Global tropospheric hydroxyl distribution, budget and reactivity, Atmos. Chem. Phys., 16, 12477-12493, 10.5194/acp-16-12477-2016, 2016.

Levy, H.: Normal atmosphere: Large radical and formaldehyde concentrations predicted, Science, 173, 141-143, 10.1126/science.173.3992.141, 1971.

Li, M., Karu, E., Brenninkmeijer, C., Fischer, H., Lelieveld, J., and Williams, J.: Tropospheric OH and stratospheric OH and Cl concentrations determined from CH_4, CH_3Cl, and SF_6 measurements, Nature Climate and Atmospheric Science, 1, 10.1038/s41612-018-0041-9, 2018.

Li, M., Karu, E., Ciais, P., Lelieveld, J., and Williams, J.: The empirically determined integrated atmospheric residence time of carbon dioxide (CO2), Proceedings of the National Academy of Sciences of the United States of America, to be submitted, 2020.

Lüthi, D., Le Floch, M., Bereiter, B., Blunier, T., Barnola, J.-M., Siegenthaler, U., Raynaud, D., Jouzel, J., Fischer, H., Kawamura, K., and Stocker, T. F.: High-resolution carbon dioxide concentration record 650,000–800,000 years before present, Nature, 453, 379, 10.1038/nature06949, 2008.

Mckeen, S. A., Trainer, M., Hsie, E. Y., Tallamraju, R. K., and Liu, S. C.: On the indirect determination of atmospheric OH radical concentrations from reactive hydrocarbon measurements, J. Geophys. Res., 95, 7493–7500, 10.1029/JD095iD06p07493, 1990.

Minschwaner, K., and Manney, G. L.: Derived methane in the stratosphere and lower mesosphere from Aura Microwave Limb Sounder measurements of nitrous oxide, water vapor, and carbon monoxide, Journal of Atmospheric Chemistry, 71, 253-267, 10.1007/s10874-015-9299-z, 2015.

Molina, M. J.: The role of chlorine in stratospheric chemistry, Pure Appl. Chem., 68, 1749-1756, 1996.

Montzka, S., Calvert, P., Hall, B., Elkins, J., Conway, T., Tans, P., and Sweeney, C.: On the global distribution, seasonality, and budget of atmospheric carbonyl sulfide (COS) and some similarities to CO2, Journal of Geophysical Research: Atmospheres, 112, 2007.

References

Montzka, S., Reimannander, S., Engel, A., Kruger, K., Simon, O. D., Sturges, W. T., Blake, D. R., Dorf, M. D., Fraser, P. J., Froidevaux, L., Jucks, K., Kreher, K., III, M. J. K., Mellouki, A., Miller, J., Nielsen, O. J., Orkin, V. L., Prinn, R. G., Rhew, R., Santee, M. L., Stohl, A., and Verdonik, D. P.: Ozone-Depleting Substances (ODSs) and Related Chemicals, Chapter 1 in Scientific Assessment of Ozone Depletion: 2010, World Meteorological Organization, 2011a.

Montzka, S. A., Krol, M., Dlugokencky, E., Hall, B., Jockel, P., and Lelieveld, J.: Small interannual variability of global atmospheric hydroxyl, Science, 331, 67-69, 10.1126/science.1197640, 2011b.

National Oceanic Atmospheric Administration: U.S. standard atmosphere, 1976, U.S. Government Printing Office, Washington, DC, 1976.

Orbe, C., Newman, P. A., Waugh, D. W., Holzer, M., Oman, L. D., Li, F., and Polvani, L. M.: Airmass Origin in the Arctic. Part I: Seasonality, Journal of Climate, 28, 4997-5014, 10.1175/JCLI-D-14-00720.1, 2015.

Pan, L. L., Randel, W. J., Gary, B. L., Mahoney, M. J., and Hintsa, E. J.: Definitions and sharpness of the extratropical tropopause: A trace gas perspective, Journal of Geophysical Research: Atmospheres, 109, 10.1029/2004jd004982, 2004.

Pan, L. L., Bowman, K. P., Atlas, E. L., Wofsy, S. C., Zhang, F., Bresch, J. F., Ridley, B. A., Pittman, J. V., Homeyer, C. R., Romashkin, P., and Cooper, W. A.: The Stratosphere–Troposphere Analyses of Regional Transport 2008 Experiment, Bulletin of the American Meteorological Society, 91, 327-342, 10.1175/2009BAMS2865.1, 2010.

Park, S., Atlas, E. L., Jiménez, R., Daube, B. C., Gottlieb, E. W., Nan, J., Jones, D. B. A., Pfister, L., Conway, T. J., Bui, T. P., Gao, R. S., and Wofsy, S. C.: Vertical transport rates and concentrations of OH and Cl radicals in the Tropical Tropopause Layer from observations of CO_2 and halocarbons: implications for distributions of long- and short-lived chemical species, Atmospheric Chemistry and Physics, 10, 6669-6684, 10.5194/acp-10-6669-2010, 2010.

Patra, P. K., Houweling, S., Krol, M., Bousquet, P., Belikov, D., Bergmann, D., Bian, H., Cameron-Smith, P., Chipperfield, M. P., Corbin, K., Fortems-Cheiney, A., Fraser, A., Gloor, E., Hess, P., Ito, A., Kawa, S. R., Law, R. M., Loh, Z., Maksyutov, S., Meng, L., Palmer, P. I., Prinn, R. G., Rigby, M., Saito, R., and Wilson, C.: TransCom model simulations of CH4 and related species: linking transport, surface flux and chemical loss with CH4 variability in the troposphere and lower stratosphere, Atmos. Chem. Phys., 11, 12813-12837, 10.5194/acp-11-12813-2011, 2011.

Patra, P. K., Krol, M. C., Montzka, S. A., Arnold, T., Atlas, E. L., Lintner, B. R., Stephens, B. B., Xiang, B., Elkins, J. W., Fraser, P. J., Ghosh, A., Hintsa, E. J., Hurst, D. F., Ishijima, K., Krummel, P. B., Miller, B. R., Miyazaki, K., Moore, F. L., Muhle, J., O'Doherty, S., Prinn, R. G., Steele, L. P., Takigawa, M., Wang, H. J., Weiss, R. F., Wofsy, S. C., and Young, D.:

Observational evidence for interhemispheric hydroxyl-radical parity, Nature, 513, 219-223, 10.1038/nature13721, 2014.

Perner, D. E., D. H.; Peatz, H. W.; Platt, U.; Roeth, E. P.; Volz, A. : OH - Radicals in the lower troposphere, Geophys. Res. Lett. , 3, 466–468, 10.1029/GL003i008p00466, 1976.

Pierrehumbert, R. T.: Short-Lived Climate Pollution, Annual Review of Earth and Planetary Sciences, 42, 341-379, 10.1146/annurev-earth-060313-054843, 2014.

Plumb, R. A., and Ko, M. K.: Interrelationships between mixing ratios of long ‐ lived stratospheric constituents, Journal of Geophysical Research: Atmospheres, 97, 10145-10156, 1992.

Pollmann, J., Helmig, D., Liptzin, D., Thompson, C. R., Hueber, J., Tans, P. P., and Lelieveld, J.: Variability analyses, site characterization, and regional [OH] estimates using trace gas measurements from the NOAA Global Greenhouse Gas Reference Network, Elementa: Science of the Anthropocene, 4, 10.12952/journal.elementa.000128, 2016.

Pozzer, A., Jöckel, P., and Van Aardenne, J.: The influence of the vertical distribution of emissions on tropospheric chemistry, Atmos. Chem. Phys., 9, 9417-9432, 10.5194/acp-9-9417-2009, 2009.

Prentice, I. C., Farquhar, G., Fasham, M., Goulden, M., Heimann, M., Jaramillo, V., Kheshgi, H., LeQuéré, C., Scholes, R., and Wallace, D. W.: The carbon cycle and atmospheric carbon dioxide, in, Cambridge University Press, 2001.

Prinn, R. G., Huang, J., Weiss, R. F., Cunnold, D. M., Fraser, P. J., Simmonds, P. G., McCulloch, A., Harth, C., Reimann, S., Salameh, P., O'Doherty, S., Wang, R. H. J., Porter, L. W., Miller, B. R., and Krummel, P. B.: Evidence for variability of atmospheric hydroxyl radicals over the past quarter century, Geophysical Research Letters, 32, 10.1029/2004gl022228, 2005.

Randel, W. J., Gille, J. C., Roche, A. E., Kumer, J. B., Mergenthaler, J. L., Waters, J. W., Fishbein, E. F., and Lahoz, W. A.: Stratospheric transport from the tropics to middle latitudes by planetary-wave mixing, Nature, 365, 533-535, 10.1038/365533a0, 1993.

Ray, E. A., Moore, F. L., Rosenlof, K. H., Davis, S. M., Sweeney, C., Tans, P., Wang, T., Elkins, J. W., Bönisch, H., Engel, A., Sugawara, S., Nakazawa, T., and Aoki, S.: Improving stratospheric transport trend analysis based on SF6 and CO2 measurements, Journal of Geophysical Research: Atmospheres, 119, 14,110-114,128, 10.1002/2014jd021802, 2014.

Rigby, M., Mühle, J., Miller, B. R., Prinn, R. G., Krummel, P. B., Steele, L. P., Fraser, P. J., Salameh, P. K., Harth, C. M., Weiss, R. F., Greally, B. R., O'Doherty, S., Simmonds, P. G., Vollmer, M. K., Reimann, S., Kim, J., Kim, K. R., Wang, H. J., Olivier, J. G. J., Dlugokencky, E. J., Dutton, G. S., Hall, B. D., and Elkins, J. W.: History of atmospheric SF_6 from 1973 to 2008, Atmospheric Chemistry and Physics, 10, 10305-10320, 10.5194/acp-10-10305-2010, 2010.

References

Rigby, M., Montzka, S. A., Prinn, R. G., White, J. W. C., Young, D., O'Doherty, S., Lunt, M. F., Ganesan, A. L., Manning, A. J., Simmonds, P. G., Salameh, P. K., Harth, C. M., Muhle, J., Weiss, R. F., Fraser, P. J., Steele, L. P., Krummel, P. B., McCulloch, A., and Park, S.: Role of atmospheric oxidation in recent methane growth, Proc Natl Acad Sci U S A, 114, 5373-5377, 10.1073/pnas.1616426114, 2017.

Rudolph, J.: The tropospheric distribution and budget of ethane, Journal of Geophysical Research: Atmospheres, 100, 11369-11381, 10.1029/95JD00693, 1995.

Santee, M. L., Livesey, N. J., Manney, G. L., Lambert, A., and Read, W. G.: Methyl chloride from the Aura Microwave Limb Sounder: First global climatology and assessment of variability in the upper troposphere and stratosphere, Journal of Geophysical Research: Atmospheres, 118, 13,532-513,560, 10.1002/2013jd020235, 2013.

Sawa, Y., Machida, T., and Matsueda, H.: Seasonal variations of CO2 near the tropopause observed by commercial aircraft, Journal of Geophysical Research: Atmospheres, 113, 10.1029/2008JD010568, 2008.

Schuck, T. J., Brenninkmeijer, C. A. M., Slemr, F., Xueref-Remy, I., and Zahn, A.: Greenhouse gas analysis of air samples collected onboard the CARIBIC passenger aircraft, Atmos. Meas. Tech., 2, 449-464, 10.5194/amt-2-449-2009, 2009.

Schuck, T. J., Ishijima, K., Patra, P. K., Baker, A. K., Machida, T., Matsueda, H., Sawa, Y., Umezawa, T., Brenninkmeijer, C. A. M., and Lelieveld, J.: Distribution of methane in the tropical upper troposphere measured by CARIBIC and CONTRAIL aircraft, Journal of Geophysical Research: Atmospheres, 117, 10.1029/2012JD018199, 2012.

Simpson, I. J., Sulbaek Andersen, M. P., Meinardi, S., Bruhwiler, L., Blake, N. J., Helmig, D., Rowland, F. S., and Blake, D. R.: Long-term decline of global atmospheric ethane concentrations and implications for methane, Nature, 488, 490-494, 10.1038/nature11342, 2012.

Solomon, S., Rosenlof, K. H., Portmann, R. W., Daniel, J. S., Davis, S. M., Sanford, T. J., and Plattner, G.-K.: Contributions of Stratospheric Water Vapor to Decadal Changes in the Rate of Global Warming, Science, 327, 1219-1223, 10.1126/science.1182488, 2010.

Srinivasan, N. K. S., M.C.; Sutherland, J.W.; Michael, J.V.: Reflected shock tube studies of high-temperature rate constants for $OH+CH_4$ -> CH_3+H_2O and CH_3+NO_2 -> CH_3O+NO, J. Phys. Chem. A, 109, 1857 - 1863, 10.1021/jp040679j, 2005.

Stimpfle, R. M., and Anderson, J. G.: In-situ detection of OH in the lower stratosphere with a balloon borne high repetition rate laser system, J. Geophys. Res., 15, 1503–1506, 1988.

Stohl, A.: Stratosphere-troposphere exchange: A review, and what we have learned from STACCATO, Journal of Geophysical Research, 108, 10.1029/2002jd002490, 2003.

References

Stone, D., Whalley, L. K., and Heard, D. E.: Tropospheric OH and HO2 radicals: field measurements and model comparisons, Chem. Soc. Rev., 41, 6348-6404, 10.1039/C2CS35140D, 2012.

Taylor, S. J., and Letham, B.: Forecasting at scale, The American Statistician, 72, 37-45, 2018.

Thorenz, U. R., Baker, A. K., Leedham Elvidge, E. C., Sauvage, C., Riede, H., van Velthoven, P. F. J., Hermann, M., Weigelt, A., Oram, D. E., Brenninkmeijer, C. A. M., Zahn, A., and Williams, J.: Investigating African trace gas sources, vertical transport, and oxidation using IAGOS-CARIBIC measurements between Germany and South Africa between 2009 and 2011, Atmospheric Environment, 158, 11-26, 10.1016/j.atmosenv.2017.03.021, 2017.

Turner, A. J., Frankenberg, C., Wennberg, P. O., and Jacob, D. J.: Ambiguity in the causes for decadal trends in atmospheric methane and hydroxyl, Proc Natl Acad Sci USA, 114, 5367-5372, 10.1073/pnas.1616020114, 2017.

Umezawa, T., Baker, A. K., Oram, D., Sauvage, C., O'Sullivan, D., Rauthe-Schöch, A., Montzka, S. A., Zahn, A., and Brenninkmeijer, C. A. M.: Methyl chloride in the upper troposphere observed by the CARIBIC passenger aircraft observatory: Large-scale distributions and Asian summer monsoon outflow, Journal of Geophysical Research: Atmospheres, 119, 5542-5558, 10.1002/2013jd021396, 2014.

Umezawa, T., Baker, A. K., Brenninkmeijer, C. A. M., Zahn, A., Oram, D. E., and van Velthoven, P. F. J.: Methyl chloride as a tracer of tropical tropospheric air in the lowermost stratosphere inferred from IAGOS-CARIBIC passenger aircraft measurements, Journal of Geophysical Research: Atmospheres, 120, 12,313-312,326, 10.1002/2015jd023729, 2015.

Volk, C. M., Elkins, J. W., Fahey, D. W., Dutton, G. S., Gilligan, J. M., Loewenstein, M., Podolske, J. R., Chan, K. R., and Gunson, M. R.: Evaluation of source gas lifetimes from stratospheric observations, Journal of Geophysical Research: Atmospheres, 102, 25543-25564, 10.1029/97jd02215, 1997.

Waugh, D.: Age of stratospheric air: Theory, observations, and models, Reviews of Geophysics, 40, 10.1029/2000rg000101, 2002.

Wennberg, P. O., Cohen, R. C., Hazen, N. L., Lapson, L. B., Allen, N. T., Hanisco, T. F., Oliver, J. F., Lanham, N. W., Demusz, J. N., and Anderson, J. G.: Aircraft-borne, laser-induced fluorescence instrument for the in situ detection of hydroxyl and hydroperoxyl radicals, Review of Scientific Instruments, 65, 1858-1876, 1994.

Williams, J., Fischer, H., Harris, G. W., Crutzen, P. J., Hoor, P., Hansel, A., Holzinger, R., Warneke, C., Lindinger, W., Scheeren, B., and Lelieveld, J.: Variability-lifetime relationship for organic trace gases: A novel aid to compound identification and estimation of HO concentrations, Journal of Geophysical Research: Atmospheres, 105, 20473--20486, 10.1029/2000JD900203, 2000.

References

Williams, J., Gros, V., Bonsang, B., and Kazan, V.: HO cycle in 1997 and 1998 over the southern Indian Ocean derived from CO, radon, and hydrocarbon measurements made at Amsterdam Island, Journal of Geophysical Research: Atmospheres, 106, 12719--12725, 10.1029/2001JD900116, 2001.

Wirth, V.: Diabatic heating in an axisymmetric cut‐off cyclone and related stratosphere‐troposphere exchange, Quarterly Journal of the Royal Meteorological Society, 121, 127-147, 1995.

WMO: Definition of the tropopause, World Meteorol. Org. Bull., 6, 136pp, 1957.

WMO: Scientific Assessment of Ozone Depletion: 2010, Global Ozone Research and Monitoring Project-Report No. 52, Geneva, Switzerland, 516, 2011.

Xiao, Y., Logan, J. A., Jacob, D. J., Hudman, R. C., Yantosca, R., and Blake, D. R.: Global budget of ethane and regional constraints on U.S. sources, Journal of Geophysical Research: Atmospheres, 113, 10.1029/2007JD009415, 2008.

Yokouchi, Y., Ikeda, M., Inuzuka, Y., and Yukawa, T.: Strong emission of methyl chloride from tropical plants, Nature, 416, 163-165, 10.1038/416163a, 2002.

Zahn, A., and Brenninkmeijer, C. A.: New directions: A chemical tropopause defined, Atmospheric Environment, 3, 439-440, 2003.

G. APPENDICES

Appendix 1 Karu et al. (2020b)

Atomic emission detector with gas chromatographic separation and cryogenic pre-concentration (CryoTrap-GC-AED) for atmospheric trace gas measurements

Authors: Einar Karu, Mengze Li, Lisa Ernle, Carl AM Brenninkmeijer, Jos Lelieveld, Jonathan Williams

Publication date: 2020/6/16

Journal: Atmospheric Measurement Techniques Discussions

https://doi.org/10.5194/amt-2020-199
Preprint. Discussion started: 16 June 2020

Atmospheric Measurement Techniques Discussions

Atomic emission detector with gas chromatographic separation and cryogenic pre-concentration (CryoTrap-GC-AED) for atmospheric trace gas measurements

Einar Karu[1], Mengze Li[1], Lisa Ernle[1], Carl A.M. Brenninkmeijer[1], Jos Lelieveld[1], Jonathan Williams[1]

[1]Atmospheric Chemistry Department, Max Planck Institute for Chemistry, 55128 Mainz, Germany

Correspondence to: Jonathan Williams (jonathan.williams@mpic.de)

Abstract. A gas detection system has been developed, characterized and deployed for pressurized gas phase sample analyses and near real-time online measurements. It consists of a cryogenic pre-concentrator (CryoTrap), a gas chromatograph (GC), and a new high-resolution atomic emission detector (AED III). Here the CryoTrap–GC–AED instrumental setup is presented and the performance for iodine (1635 ± 135 counts I-atom^{-1} pptv^{-1}), sulfur (409 ± 57 counts S-atom^{-1} pptv^{-1}), carbon (636 ± 69 counts C-atom^{-1} pptv^{-1}), bromine (9.1 ± 1.8 counts Br-atom^{-1} pptv^{-1}) and nitrogen (28 ± 2 counts N-atom^{-1} pptv^{-1}) emission lines is reported and discussed. The limits of detection (LODs) are in the low pptv range (0.5 – 9.7 pptv) and the signal is linear to at least 4 orders of magnitude, which makes it a suitable method for diverse volatile organic compound (VOC) measurements in the atmosphere, even in remote, unpolluted regions. The new system was utilized in a field study in a boreal forest at Hyytiälä, Finland in late summer 2016 which made monoterpene measurements possible among the other VOCs. Furthermore, pressurized global whole-air sample measurement collected onboard the Lufthansa Airbus A340-600 IAGOS-CARIBIC aircraft in the upper troposphere and lower stratosphere region was carried out with the new setup, providing the observational data of many VOCs, including the long-lived organosulfur compound carbonyl sulfide.

1 Introduction

Atomic spectrometric analysis provides highly sensitive, equimolar, linear response at least over 5 orders of magnitude (> 10^5) and accurate elemental composition data of samples. If detection is preceded by analyte separation using gas chromatography (GC), compound specific data is obtainable. The first atomic emission detector (AED) with a plasma as an excitation source coupled with a GC was introduced in 1965 (McCormack et al., 1965). This group was the first to recognize the analytic potential of combining a GC separation with microwave induced plasma excitation and an electronic emission spectra detector. Early AEDs, using microwave induced plasmas, were operated at reduced pressures (Risby et al., 1983), until an atmospheric pressure version was developed in 1977 (Beenaker, 1977). The first commercial AED based on a microwave induced plasma and photodiode array detector coupled to a GC was released by Hewlett Packard in 1990 (Quimby and Sullivan, 1990). These systems provided speciated element specific chromatograms and were used in a variety of applications including the analysis of oils for sulfur containing compounds (Link et al., 2002). In contrast with the alternative analytical approach of gas

https://doi.org/10.5194/amt-2020-199
Preprint. Discussion started: 16 June 2020

Atmospheric Measurement Techniques Discussions

chromatography coupled to mass spectrometry (GC–MS), the AED has the advantage of being equimolar and linear in detector response. That said it is important to keep in mind that a detector is often the last step in the whole analytical instrumental setup, therefore the response factor (RF) reflects the entire analyte pathway from the sample inlet up to the detector signal recording. This means that analyte losses by adsorption and absorption effects taking place in the transfer lines, pre-concentration stages, GC column and in the detector flow paths etc. contribute to the final RF. In this study, great care was taken to minimize the loss factors. Hence, the RF for a particular compound group can be derived for one element (e.g. carbon) from the similar single compound specific RFs and then applied to all carbon containing compounds within the group in the chromatogram. This greatly simplifies the calibration and allows quantification of compounds not present in a calibration standard. For this reason, the AED has been used for the quantification of species that have been identified by GC-MS (Apel et al., 1998; Greenberg et al., 1999). Recently, further technical developments in the AED have led to improvements in sensitivity that allow trace gases in air to be quantified directly, making such systems of interest to atmospheric scientists. The simultaneous high-resolution wavelength recording capability of the detector (161 – 211 nm) in the CryoTrap–GC–AED system allows for reliable screening for elements present in the speciated compounds, thus simplifying the identification of unknown compounds. Furthermore, the newly developed system in principle allows for unknown compound quantification in a chromatogram within the uncertainty range when a broad range of compound specific RFs are used for the determination of the single element RF.

In this study, the instrumental setup and performance of the CryoTrap–GC–AED system are examined. The performance for iodine, sulfur, carbon, bromine and nitrogen emission lines is examined. The calibration linearities, limits of detection and compound specific response factors are reported for 64 compounds.

2 Experimental

The CryoTrap–GC–AED system consists of three stages: a liquid nitrogen based pre-concentration system (Entech model 7200, USA); a gas chromatographic separation (Agilent GC 7890B, USA); and a helium plasma based third generation atomic emission detector (Joint Analytical Systems AED III High Resolution, Germany). The schematic of the instrumental setup is shown in Fig. 1. Ultra-high purity helium (UHP, purity 99.9999%, Westfalen, Germany) flowing through a heated purifying catalyst (Valco Instruments VICI, USA) is used throughout the system as the carrier and purging gas.

2.1 Cryogenic pre-concentration (CryoTrap)

The sample is introduced to the pre-concentration unit (CryoTrap) via an eight port multi position valve, consisting of the helium supply gas, four sample introduction inlets, an internal standard, a calibration standard and a blind port (Fig. 1, upper panel). The four sample introduction lines are each 2.0 m long (Restek Corp. Silcosteel, USA) with outer diameter 1/16″ (1.59 mm), inner diameter 0.040″ (1.02 mm). The sample is drawn onto the two enrichment traps via an evacuated volumetric reservoir, where the sample introduction volume is accurately determined by measuring the pressure at given temperature. All

https://doi.org/10.5194/amt-2020-199
Preprint. Discussion started: 16 June 2020

Atmospheric Measurement Techniques Discussions

the CryoTrap internal flow path surfaces are coated with a thin high density ceramic Silonite-D layer to provide extremely inert surfaces, which nearly eliminates the adsorption of the analytes to the surfaces.

The CryoTrap internal flow path is flushed with the sample gas before each pre-concentration step. After that the sample air is drawn through the first stage of pre-concentration, called the dehydration module (Fig. 1, middle panel), where H_2O is selectively removed on an empty Silonite-D coated stainless-steel trap (outer diameter 1/8″ (3.18 mm), 31 cm long) held at -50°C. After collecting the required volume of sample, the trap is flushed with 75.0 mL of helium to remove any remaining air. Then module 1 is heated to 10°C and forward purged with 50.0 mL (10 mL min^{-1}) helium flow onto the main Tenax packed and Silonite-D coated volatile organic compound (VOC) enrichment trap (module 2, the second step of pre-concentration; outer diameter 1/8″ (1.02 mm), 31 cm long) held at -60°C. The forward helium purge helps to successfully transfer heavy, polar and semi-volatile organic compounds (SVOCs) onto the main module 2 VOC trap. The last pre-concentration step is pre-cooling of the cryo-focusing trap (module 3, ~4 cm long part of Silonite-D coated 1/32″ (0.79 mm) transfer line) to -180°C and thereafter kept at -160°C during module 2 back flushing at 230°C for 2.5 min, which will refocus the volatiles to a much smaller dead volume for splitless injection onto a GC column. The module 3 1/32″ (0.79 mm) transfer line is rapidly heated to 60°C for 2 min inside a sheathing 1/8″ (3.18 mm) perfluoroalkoxy alkane (PFA) tube with hot air supplied through the rotary plate kept at 100°C. This ensures rapid and splitless injection of analyte molecules to the GC column through a transfer line heated to 110°C. The pre-concentration unit is equipped with two bulkhead heaters in between the heated rotary plate and the traps for better water condensation management.

2.2 Gas chromatograph (GC)

Gas chromatography is a common choice for analytical separation of VOCs for measurement with various detectors (Bourtsoukidis et al., 2017; Apel et al., 1998). We use an Agilent 7890B GC for the compound separation. The GC was fitted with a Supelco SPB-624 capillary column (length × inner diameter: 60 m × 250 µm; film thickness 1.40 µm), which is an intermediate polar, proprietary phase bonded fused silica GC column. The SPB-624 type columns are widely used for volatile non-halogenated, halogenated, and aromatic compounds analysis.

Helium is used as the column carrier gas, of which the flow rate is controlled over the GC electronic pneumatic control (EPC) valve number 3. First, helium flows from the GC EPC valve into a 1/16″ (1.59 mm) stainless steel line connected to the CryoTrap rotary valve number 2 (Fig. 1). After the pre-concentration procedure the helium flow with the remobilized analytes is guided back to the GC oven through a heated (110°C) Silonite-D coated 1/32″ (0.79 mm) transferline. Then, in the GC oven a Swagelok T-split union guides the flow to the analytical column for splitless injection. The other end of the GC capillary column was led directly to the AED cavity through a heated transferline (250°C).

https://doi.org/10.5194/amt-2020-199
Preprint. Discussion started: 16 June 2020

Atmospheric Measurement Techniques Discussions

2.3 Atomic emission detector, third generation (AED III)

AED measures the energy emitted at characteristic wavelengths by sample atoms present in the helium plasma cavity to quantify their number in a chromatographic peak. Combining this data with GC analyte separation, the amount of the substance can be quantitatively determined.

The helium carrier gas (3.5 mL min^{-1}) eluting from the GC is led to the AED cavity through the capillary column that is housed in the heated transfer line (250°C). The helium plasma discharge cavity is also kept at constant 250°C temperature. The mixture of the carrier (helium) and reagent gases (hydrogen and oxygen) flow through a fused silica discharge tube where the gases are ionized into a plasma state by microwave energy. In the high-energy plasma the eluted sample compounds from the GC are broken down into free radicals, ions and atoms. As they return from their excited state to ground state configuration, light radiation is emitted in their element specific characteristic wavelengths. The emitted ultraviolet radiation passes through a fused silica lens and a narrow slit, and then is reflected onto a reflective holographic grating by a fixed mirror. The grating disperses the light into discrete vertical bandwidths along a plane-concave polychromatic grating. Thereafter, the grating reflects and focuses the light in the wavelength range 161 – 211 nm in a horizontal plane onto two back-thinned charge-coupled devices (CCDs). The CCDs convert light intensities across the given spectrum into electrical currents which are recorded by the "AED III Instrument Control Software". The software calibrates the received light intensity signal from the CCD diodes into wavelengths intensity data according to a calibration table. This process (element installation) takes place automatically before every sample measurement. After each measurement, all the wavelength dependent emission data are stored with 0.01 nm resolution. An example of a 5 element simultaneously recorded chromatogram of the 84 component Apel-Riemer-2015 gas calibration standard is shown in Fig. 2.

2.4 Characterization experiments

All the characterization experiments started with a zero-air (hydrocarbon free synthetic air with 20.5% oxygen and nitrogen rest (Westfalen, Germany), which flows through an extra catalyst kept at 500°C to remove the trace amounts of hydrocarbons) measurement for determining the instrumental background. Furthermore, at the beginning of the experimental design the highest calibration standard levels' carryover and retention potentials of all the compounds of interest were tested with the zero-air measurement directly after as the following sample. The trap back-flushing and bakeout times were adapted accordingly.

Three independent gas calibration standards were used for the characterization experiments: the 84 component (each nominally at 50 ppbv mixing ratio (MR) in UHP nitrogen rest) Apel-Riemer-2015 gas calibration standard (Table S1) and the 30 component (each nominally at 4 ppbv MR in UHP nitrogen rest) non-methane hydrocarbon (NMHC) ozone precursor National Physical Laboratory 2017 (NPL-2017) primary calibration standard gas cylinders (Table S2).

The Apel-Riemer-2015 standard used for the characterization measurements was diluted with the same zero-air as described above with two mass flow controllers (MFC). The MFC for the calibration gas had a range up to 20 mL min^{-1} and the MFC

https://doi.org/10.5194/amt-2020-199
Preprint. Discussion started: 16 June 2020

Atmospheric Measurement Techniques Discussions

for zero-air a range up to 5 L min^{-1}. For these experiments a constant 1 L min^{-1} zero-air flow was used and five steps (1, 5, 10, 15, 20 mL min^{-1}) of calibration gas were used, to produce nominal MRs of 50, 250, 500, 750 and 1000 pptv. This MR range is relevant for many ambient VOC measurements. With each sample pre-concentration a 1400 ml aliquot of the diluted sample flow was trapped and the rest of the flow was led to lab exhaust. Calibration level measurements were repeated four times. No dilution for the NPL primary calibration standard was used and thus trapped directly in the amounts of 40, 60, 80 and 250 mL (producing MR in the range of 114, 171, 229 and 714 pptv for 1.4 L unknown sample relevance). The NPL calibration step measurements were also repeated four times.

With separate tests the maximum linearity range of the CryoTrap-GC-AED was tested with the undiluted Apel-Riemer-2015 calibration gas measurement (~ 50 ppbv per compound). For higher MR samples also a smaller sample volume can be trapped, making it possible to measure even higher MR samples. The system was tested to be linear to at least 4 orders of magnitude.

3 Instrument performance

The AED system was always recalibrated immediately prior to and during the measurement of the samples with unknown MRs, using the independent gas calibration standards: the Apel-Riemer-2015 and the NPL-2017 gas cylinders. In addition, during the regular automated IAGOS-CARIBIC pressurized sample measurement procedure, the National Oceanic and Atmospheric Administration (NOAA) ambient air calibration standard and the NMHC NPL standards were periodically measured after every five samples. From the calibration standard measurements, the linearities (R-squared), limits of detection (LOD), response factors per atom and measurement uncertainty were determined for all quantifiable compounds in the standard and listed in Table 1 and 2.

The LODs were calculated from the average height of the lowest calibration levels and the average height of the noise signals corresponding to the same chromatogram for each separable and measurable compound of the calibration standards. Three times signal-to-noise ratio (by peak height) was maintained to define the LOD, representing the ~99.7% confidence interval. The LOD calculation is represented by Eq. (1):

$$LOD = 3 \times \frac{\overline{noise} \times \overline{MR}}{\overline{peak\ height}}, \quad (1)$$

where $\overline{noise}$ is the average height of the noise signal, $\overline{MR}$ is the average mixing ratio of the lowest level calibration level and $\overline{peak\ height}$ is the average peak height of that calibration level of the corresponding compound.

The average per carbon atom RFs were calculated separately for each species using the average area under the peak curve ($\overline{AUC}$), the corresponding average MRs ($\overline{MR}$) and the number of carbon atoms (NOC) present in the compound of interest as show by Eq. (2):

$$\overline{RF} = \frac{\overline{AUC}}{\overline{MR} \times \mathrm{NOC}}. \quad (2)$$

https://doi.org/10.5194/amt-2020-199
Preprint. Discussion started: 16 June 2020

Atmospheric Measurement Techniques Discussions

The RFs were calculated separately for all compounds and their individual calibration MR levels and thereafter all the individual RFs over the whole calibration range were averaged to a single RF per compound.

3.1 Carbon emission line performance

The performance of the carbon emission line (193 nm) derived from measurements of three calibration standard gases is listed in Table 1. For Apel-Riemer-2015, the derived LODs are in the range 0.8 – 9.7 pptv. Each compound's RF is the average of 18 independent data points in the whole 50 – 1000 pptv calibration range. The RFs for these compounds lie between 343 ± 147 counts C-atom^{-1} pptv^{-1} (benzyl chloride) to 800 ± 291 counts C-atom^{-1} pptv^{-1} (isobutyl nitrate) and on average 587 ± 91 counts C-atom^{-1} pptv^{-1} (47 compound mean). For NPL-2017, the LODs are in a smaller range of 0.5 – 1.1 pptv (more similar compounds) and the RFs per carbon atom range from 581 ± 23 counts C-atom^{-1} pptv^{-1} (1,2,4-trimethylbenzene) to 913 ± 77 counts C-atom^{-1} pptv^{-1} (toluene). The measured 22 compound NPL-2017 gas standard average RF was 684 ± 46 counts C-atom^{-1} pptv^{-1} (about 17% higher compared to Apel-Riemer-2015 measurements and with about half the standard deviation). The both experiment average per carbon atom RF was determined 636 ± 69 counts C-atom^{-1} pptv^{-1}.

The CryoTrap-GC-AED system sensitivity and precision are also dependent on the discharge tube, as the two experiments were conducted with different discharge tubes (as the old one broke). Nevertheless, unknown samples were always directly determined against calibration standards with the same discharge tube. If a discharge tube breakage took place, a complete new calibration was carried out. The same 10 compounds (isobutene, 1,3-butadiene, pentane, isoprene, hexane, benzene, toluene, ethylbenzene, 1,3,5-trimethylbenzene and 1,2,4-trimethylbenzene) which were measured from both calibration standards are compared in Fig. 3. Three compounds: pentane, ethylbenzene and especially toluene do not adhere to the 1σ confidence interval on the one to one RF comparison between these two experiments. The reason remains unknown as there are other similar compounds to these in the comparison which stick to the correlation.

Like the RFs, also the compound specific LODs depend on the CryoTrap pre-concentration efficiency, compound transmission efficiency through the gas transfer lines, GC separation and carry through efficiency and AED helium plasma atomization and excitation efficiency. Throughout the whole instrument development process, best efforts were undertaken to use suitable transfer lines and gas union (Swagelok, USA) materials like Silcosteel (fused silica coated stainless steel), stainless steel, PFA and Teflon for minimizing analyte flow path losses, i.e. through wall losses (absorption and adsorption effects), condensation etc. Furthermore, high purity stainless steel pressure regulators were used for calibration standard gas bottles with analyte free degassing O-rings.

The compound specific per carbon atom RFs from the NPL-2017 NMHC calibration standard are summarized in Fig. 4. The AED detector should have an equimolar response but nevertheless a spread for the carbon 193 nm emission line intensity between around 550 to 900 counts pptv^{-1} C-atom^{-1} was observed depending on the compound. Thus, the CryoTrap-GC-AED detected response must be considered as a whole for the entire instrument where the trapping and transmission efficiency is compound specific and directly influence the final detected signal. The same applies also to the other elements measured. The average of the compound specific median RFs is 663 ± 66 counts pptv^{-1} C-atom^{-1}. Therefore, within the uncertainty range the

https://doi.org/10.5194/amt-2020-199
Preprint. Discussion started: 16 June 2020

Atmospheric Measurement Techniques Discussions

compound independent calibration could be applied, lowering the uncertainty is possible if similar compound group's RF is used for the target species. Nevertheless, for higher accuracy a direct calibration method is recommended. Within this study a direct calibration method was used.

3.2 Iodine, sulfur, bromine and nitrogen emission line performances

The Apel-Riemer-2015 gas phase calibration standard was used to evaluate the performance of other available and relevant atomic emission lines for atmospheric chemistry (Table 2).

Methyl iodide (iodine wavelength measured at 178 nm) has LOD of 0.7 pptv, and RF of 1635 ± 135 counts I-atom^{-1} pptv^{-1}. The LOD of methyl iodide on iodine emission line was 9.6 times more sensitive compared to carbon emission line. Carbonyl sulfide (OCS) and carbon disulfide (CS_2) had LODs of 1.9 and 1.8 pptv, respectively. OCS had RF of 342 ± 34 counts S-atom^{-1} pptv^{-1}, and CS_2 had RF of 476 ± 79 counts S-atom^{-1} pptv^{-1}. The sulfur emission line at 181 nm was determined to be on average 3.1 times more sensitive compared to the carbon 193 nm emission line, calculated from OCS and CS_2 LOD values. The average sulfur response factor determined from the two latter compounds is 409 ± 57 counts S-atom^{-1} pptv^{-1}. Bromodichloromethane (9.9 ± 1.5 counts Br-atom^{-1} pptv^{-1}), 1,2-dibromoethane (9.0 ± 1.8 counts Br-atom^{-1} pptv^{-1}) and bromoform (8.3 ± 2.0 counts Br-atom^{-1} pptv^{-1}) at bromine emission line at 163 nm had significantly higher LODs of 115.7, 61.9 and 64.2 pptv, respectively compared to iodine, sulfur and carbon emission lines. The average per bromine atom response factor was determined 9.1 ± 1.8 counts Br-atom^{-1} pptv^{-1}. Nitrogen at 174 nm proved to be the least sensitive element for AED III detector. Nitrogen containing compounds: acetonitrile, acrylonitrile, isopropyl nitrate, propyl nitrate and isobutyl nitrate varied significantly with their LODs (see Table 2), despite all containing a single nitrogen atom. The different transmission efficiency of each of the five nitrogen compounds through the system's flow paths could cause such differences. The average per nitrogen atom response factor determined from the five nitrogen compounds was 28 ± 2 counts N-atom^{-1} pptv^{-1}. The different element count scales are non-related to each other.

3.3 Advantages and disadvantages of the CryoTrap-GC-AED

Considering all the species measured with the CryoTrap-GC-AED, the system proved to be very sensitive detecting iodine, sulfur and carbon elements with RFs 1635 ± 135 counts pptv^{-1} I-atom^{-1}, 409 ± 57 counts pptv^{-1} S-atom^{-1} and 636 ± 69 counts C-atom^{-1} pptv^{-1}, respectively. The different elemental emission wavelength intensity count scales are not directly comparable due to different elemental background noise levels. From these three elements the lowest background noise level was measured for iodine, followed by sulfur and then by carbon. The element background noise level determines the LODs for these elements in the same increasing order, also seen in the Table 1 and 2.

The great advantage of the AED system is that compounds which are insensitive to the flame ionization detector (FID) and other detectors, e.g. carbonyl sulfide, can be measured by exploiting other emission lines such as sulfur. Generally, the CryoTrap-GC-AED system is in the same sensitivity range as an FID detector (Baker et al., 2010). The electron capture detector (ECD) remains more sensitive and sometimes no pre-concentration of the air sample is necessary (e.g. Schuck et al.,

https://doi.org/10.5194/amt-2020-199
Preprint. Discussion started: 16 June 2020

Atmospheric Measurement Techniques Discussions

2009) however, an ECD is limited only to the electron capturing compounds. The GC-MS systems generally have high sensitivity and good selectivity but require separate calibration gases for all species to be quantified since response factors vary considerably. Modern online mass spectrometry (MS) detectors, especially the proton transfer reaction time-of-flight mass spectrometry (PTR-TOF-MS) provide high sensitivity (sub pptv) and highly time resolved (< 1 s) measurement techniques without the need for pre-concentration, e.g. the new Tofwerk / Aerodyne Research Vocus PTR-TOF (Krechmer et al. 2018). However, without pre-separation with gas chromatography the chemical identity of signals can be ambiguous.

The specific emission wavelength range of the high-resolution AED III enables measurement capability to accurately detect at least 11 elements: antimony, arsenic, carbon, germanium, iodine, nitrogen, oxygen (requires 5% methane in 95% nitrogen reactant gas), phosphorus, selenium, silicon and sulfur, of which a maximum of 8 can be simultaneously recorded from the raw data (JAS product description on their webpage, 2020). This makes the first screening of an unknown gas phase sample for compounds with various elements much easier and faster compared to more complex mass spectra.

Some disadvantages of the current AED III detector are the short lifetime of the fused silica tube where the plasma is being maintained and the early software / electronic issues inhibiting the proper acquisition of the data. The helium plasma is sustained in a small quartz tube (47 mm long, 1.0 mm inner diameter, 1.25 mm outer diameter) with a polyimide coating (27 mm long) in the middle part of the outer surface. The tube is positioned in a water-cooled cavity, maintained at 80°C. The lifetime of the discharge tube was around 5 to 30 days, sometimes up to 3-4 months, depending on the sample throughput and quality of the replacement of the fragile discharge tube. The discharge tube could break at any moment without a warning during a measurement sequence, leading to the loss of a sample.

Furthermore, the large consumption of liquid nitrogen (around 2-3 L sample^{-1}) for the sample cryogenic pre-concentration makes it demanding on operator time, logistical field support, and somewhat expensive to operate. The use of liquid nitrogen makes it difficult to operate this instrument at remote areas. Nevertheless, the CryoTrap-GC-AED instrument was taken to a field measurement campaign at Finnish boreal forest in 2016 where among the other species it contributed to the quantification of monoterpene compounds, when accounting for the directly measured NO_3 radical reactivity in the boreal forest (Liebman et al., 2018).

4 CryoTrap-GC-AED case studies

The newly developed instrument has been deployed in near real-time field measurements and in lab based pressurized canister measurements. In the following we demonstrate two case studies, one based in the forest in Hyytiala, Finland and the other in the home laboratory in Mainz, Germany.

4.1 Finnish boreal forest field measurements at Hyytiälä site

Boreal forest (taiga) makes up around 33% of Earth's forest cover, making it the largest terrestrial biome in the world. Even in the epoch of the Anthropocene about ¾ of the boreal forest remains natural (Brandt et al., 2013). The field campaign took place in a boreal forest measurement site SMEAR II (Station for Measuring Forest Ecosystem-Atmosphere Relations II) at

https://doi.org/10.5194/amt-2020-199
Preprint. Discussion started: 16 June 2020

Atmospheric Measurement Techniques Discussions

Hyytiälä, Finland in September 2016 (Hari and Kulmala, 2005). The site is situated approximately 50 km away from the first more densely populated location, thus anthropogenic influence is relatively low, particularly when the wind masses originate from the north with low human activity and pollution.

The instrumentation was installed in an air-conditioned measurement container maintained at 25°C temperature. The CryoTrap-GC-AED system measured ambient air which was pulled from the center of a shared 8.5 m tall high-flow inlet (15 cm diameter, flowrate ~ 10 m^3 min^{-1}). From the 8.5 m inlet the air was drawn to the container through a 15 m long ½″ (1.27 cm diameter) PFA tubing at a flowrate of ~ 20 L min^{-1} (transmission time 3.3 s). The inlet line was insulated and heated (10°C above ambient) to avoid sunlight interactions and condensation. Membrane filters (polytetrafluoroethylene with pore size 5.0 µm, 47 mm diameter by Sartorius AG, Germany) were used to avoid particles entering the tubing at the connection from the high-flow inlet and replaced every 5 days. From the 15 m long sampling line inside the container the cryogenic sample trapping phase took place with a flowrate of 200 mL min^{-1} and a total of 1 400 mL air was trapped for each sample. After the injection of a pre-concentrated sample from the last focusing trap to the GC, the traps were baked out and the pre-concentration of a next sample started in parallel with the previous GC run. This enabled mean sample throughput time intervals of 1 h 22 min. The average liquid nitrogen consumption rate was 2.5 L h^{-1}. The CryoTrap and AED parameters presented in Section 2 and GC program listed in Table 3a were used.

The diel cycles of isoprene and 5 monoterpene species (α-pinene, Δ-3-carene, β-pinene, camphene, d-limonene and isoprene) are presented in Fig. 5. All monoterpene species show daytime minima and night-time maxima. This is unexpected as the emissions of monoterpenes are primarily temperature dependent and ambient temperatures were higher by day (Tarvainen et al., 2005). Here the recurring night-time MR maxima can be explained with the shallow, nocturnal boundary layer, typically accompanied by a temperature inversion in the lower troposphere, effectively trapping the ground-level emissions (Liebmann et al., 2018). The measured monoterpene species and isoprene on average accounted for about 70% of the directly measured NO_3 reactivity at night-time and about 40% during daytime, published in a separate research article (Liebmann et al., 2018).

The diel cycles of carbonyl sulfide and carbon disulfide are shown in Fig. 6. OCS showed daytime maxima between 9:00 and 15:00 UTC (12:00 and 18:00 local time), which is unexpected as daytime uptake by vegetation is generally regarded as the dominant sink for OCS (Sandoval-Soto et al., 2005). Again, the previously discussed shallow nocturnal boundary layer plays a role, as much less in-mixing of higher concentration OCS from the free troposphere takes place during night-time. Furthermore, it confirms the recently published finding at the same measurement location that OCS uptake is light independent and controlled by stomatal opening, and therefore stomatal conductance and OCS uptake can continue during night-time under these conditions (Kooijmans et al., 2017). The night-time uptake of OCS by vegetation should be further characterized and parameterized for 3D global chemistry-transport model applications. CS_2 did not show any significant diel cycle and MRs significantly varied between 0.5 and 5 pptv.

https://doi.org/10.5194/amt-2020-199
Preprint. Discussion started: 16 June 2020

Atmospheric Measurement Techniques Discussions

4.2 IAGOS-CARIBIC whole-air sample measurement with CryoTrap-GC-AED

The IAGOS-CARIBIC (In-service Aircraft for a Global Observing System – Civil Aircraft for the Regular Investigation of the Atmosphere Based on an Instrument Container) (Brenninkmeijer et al., 2007) is a regular observation project with scientific instruments on board commercial aircraft (Lufthansa Airbus A340-600 in cooperation with Lufthansa AG) which carries out atmospheric monitoring on a global scale, especially in the upper troposphere / lower stratosphere (UT/LS, ~ 10 – 12 km) region. Since December 2015, a new CryoTrap–GC–AED system has been applied to measure whole-air pressurized gas samples that were taken as part of this project. Many VOCs such as NMHCs (Baker et al., 2010), sulfur containing species, oxygenated and halogenated trace gases can be measured in the C3 – C14 range. These species are important to tropospheric ozone production, stratospheric ozone depletion and radiative forcing.

The whole-air samples (WAS) were pressurized at about 4 bar absolute pressure with two triggered retrospective air collectors (TRACs) each consisting of 14 specially manufactured glass vessels (2.74 L), and a high-resolution sampler (HIRES) which consists of 88 stainless steel canisters (1.0 L). Every time after the flights took place and the samplers were delivered to the lab, the measurement procedure began with the initial pressure measurement of all the 116 individual samples.

CryoTrap-GC-AED was applied to measure the IAGOS-CARIBIC TRAC and HIRES whole-air samples. At the beginning of each measurement sequence, a 2.0 m long sample line was connected to a TRAC or HIRES sampler port, and a leak check is conducted by evacuating the connected sample line to ~3.0 psi (0.21 bar) absolute pressure with the CryoTrap instrument pump. After the pressure stabilization in the line, a leak check was carried out for 3 min. If the pressure reading was less than ±0.5 psi (0.03 bar) different, which is within the precision range of the pressure gauge, the line is considered leak tight. The CryoTrap traps Module 1 and Module 2 (Fig. 1) are heated at 150ºC and 220ºC, respectively for 20 min for conditioning. The GC oven program is summarized in the Table 3 below. Again, the three independent gas phase calibration standards (Apel-Riemer-2015, NPL-2017, NOAA-2017) were used for calibrating the system (Table S1 and S2). A 1400 mL aliquot of an IAGOS-CARIBIC air sample was pre-concentrated. Exactly the same conditions were used for the calibration standards (except NPL standard where 50 mL were pre-concentrated) in order to have the same conditions and to thereby minimize the instrumental uncertainty. The IAGOS-CARIBIC WAS measurement sequence with the CryoTrap-GC-AED starts with a calibration. The measurement of zero-air (produced the same way as described in Section 2) is followed by the certified ambient air standard (NOAA-2017) measurement. The latter is followed by diluted Apel-Riemer-2015 gas phase standard measurement (as described in Section 2). After that the continuous measurement of the WAS samples started. The NOAA-2017 certified ambient air reference calibration standard and the NPL 30 component ozone precursor NMHC reference calibration standard were measured after every five WAS sample measurement to compensate for instrumental sensitivity drift throughout the analysis.

An example dataset of OCS MRs measured in the UT/LS region from two flights (Munich to Los Angeles and Munich to Shanghai in February 2019) are depicted in Fig. 7. The OCS data combined with the other VOC species from the same samples was used to determine the global atmospheric and lower stratospheric lifetime, troposphere to stratosphere flux of OCS and

https://doi.org/10.5194/amt-2020-199
Preprint. Discussion started: 16 June 2020

Atmospheric Measurement Techniques Discussions

the stratospheric sink using the linear relationship between the long-lived species MRs (and their variability) to their known atmospheric lifetimes. This will be discussed in detail in a separate research article (article under review).

5 Conclusions

The newly developed CryoTrap-GC-AED analytical instrument enables the measurement of gas phase samples in minute concentrations (low pptv level) suitable for ambient air VOC species measurements in the troposphere and lower stratosphere. With this instrument it is possible to measure samples from canisters (e.g. IAGOS-CARIBIC whole-air samples) and also directly with circa 1-hour sampling frequency at a measurement station (e.g. Hyytiälä Finnish boreal forest measurement campaign in 2016) (Karu, 2019; Liebmann et al., 2018). The instrument proved to be sensitive and linear over more than 4 orders of magnitude ($> 10^5$), however, the application of the equimolarity feature of the detector is limited by pre-concentration and transmission losses. Nevertheless, known compounds present in a chromatogram and not present in the calibration standard can be still quantified with an accuracy of around 30-40%. For more accurate results direct calibration against certified gas phase calibration standards with exactly the same measurement conditions and volumes is recommended. The possibility to measure 11 elements and 8 of them simultaneously might allow discovery of new atmospheric species of interest, e.g. containing selenium or silicon atoms, particularly in marine of volcanically influence environments. The instrument would become significantly more reliable if longer lasting helium discharge tubes were developed and the commercial software and electronics were improved. For further developments of the detector the possibility to measure a wider spectral range would allow detection of even more elements simultaneously.

Competing interests. The authors declare that they have no conflict of interest.

Author contribution: EK and JW developed the idea. EK established the new measurement technique. EK, ML and LE carried out the experiments. CAMB developed the CARIBIC air sampling systems. EK wrote the manuscript with support from ML and JW. All authors discussed the results, commented and helped to improve the manuscript.

Acknowledgements. We are very grateful to Claus Koeppel (Max-Planck-Institute for Chemistry, Mainz) for IAGOS-CARIBIC TRACs / HIRES WAS sampling and for conducting all the pre and after flight ground tests for accurate sample collection. We would also like to thank Florian Obersteiner (Karlsruhe Institute of Technology, Karlsruhe) for providing the very helpful IAU_Chrom data analysis software.

Financial support. EK was supported by the Max Planck Graduate Center with the Johannes Gutenberg-Universität Mainz (MPGC).

The article processing charges for this open-access publication were covered by the Max Planck Society.

Appendices

https://doi.org/10.5194/amt-2020-199
Preprint. Discussion started: 16 June 2020

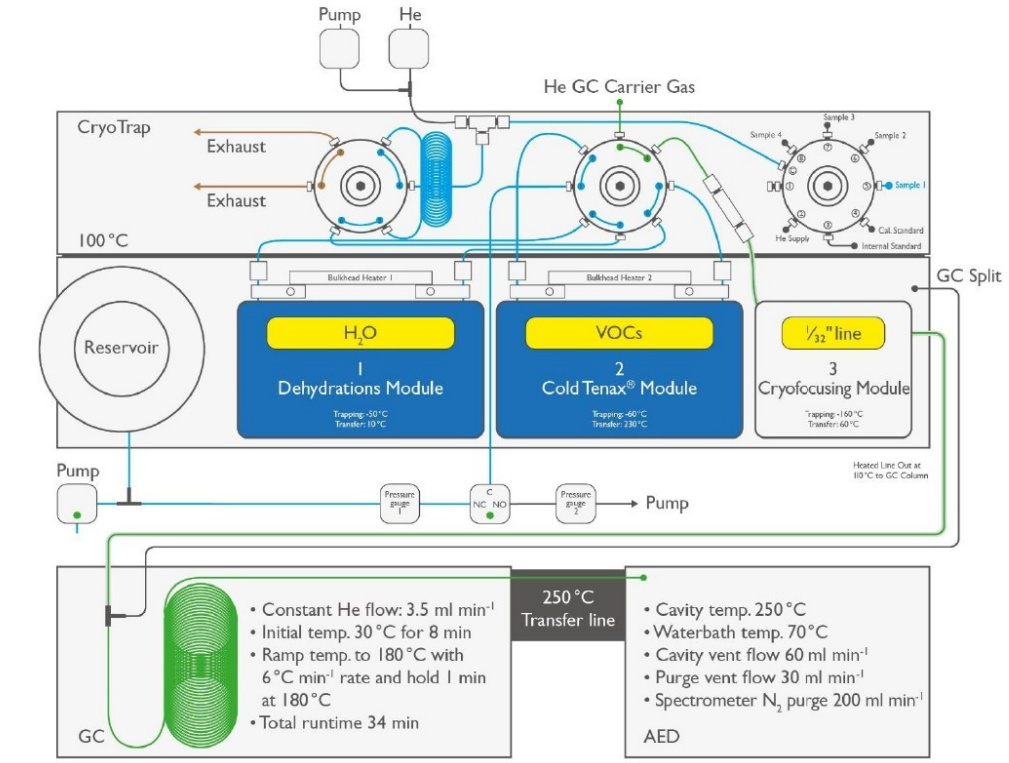

Figure 1: Schematic overview of instrumental setup, CryoTrap–GC–AED.

Appendices

https://doi.org/10.5194/amt-2020-199
Preprint. Discussion started: 16 June 2020

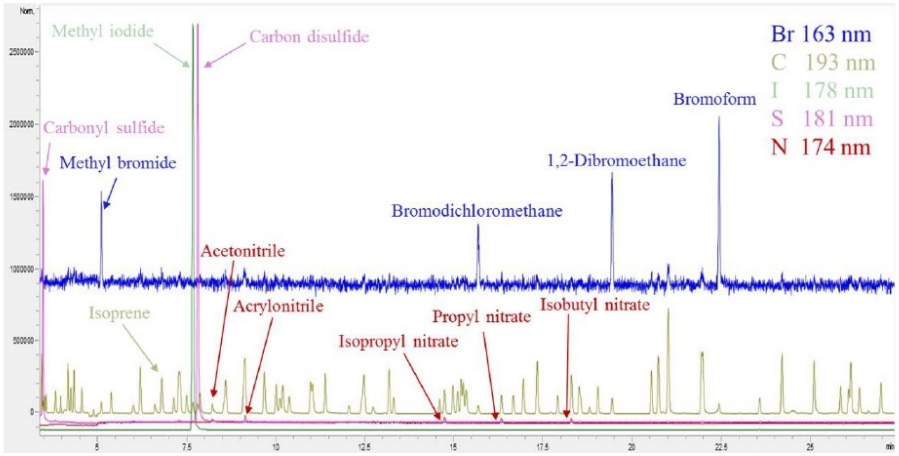

Figure 2: Example CryoTrap-GC-AED normalized multi-element overlay chromatogram of ~250 pptv 84 component Apel-Riemer-2015 gas calibration standard.

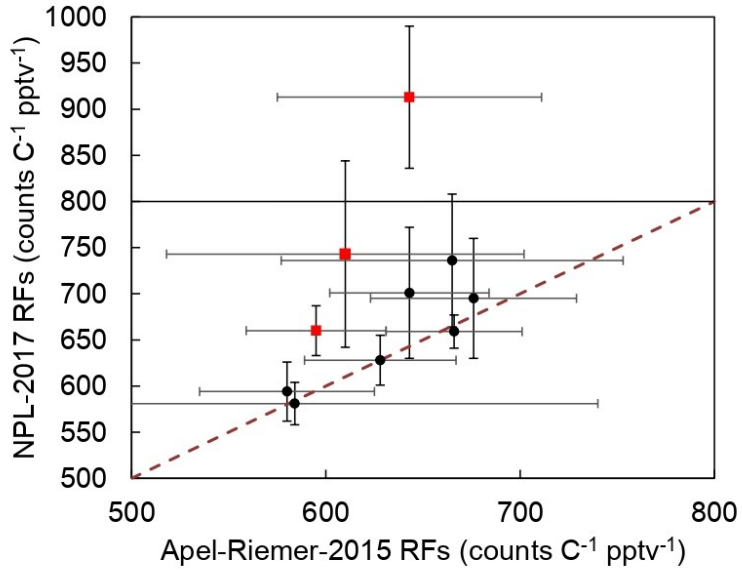

Figure 3: Response factor comparison between the 10 common compounds measured from both Apel-Riemer-2015 and NPL-2017 gas calibration standards. The black circles show the average of all the calibration level data points for the according compounds measured in the Apel-Riemer-2015 and NPL-2017 gas calibration standards. The x and y-axis whiskers represent the standard

https://doi.org/10.5194/amt-2020-199
Preprint. Discussion started: 16 June 2020

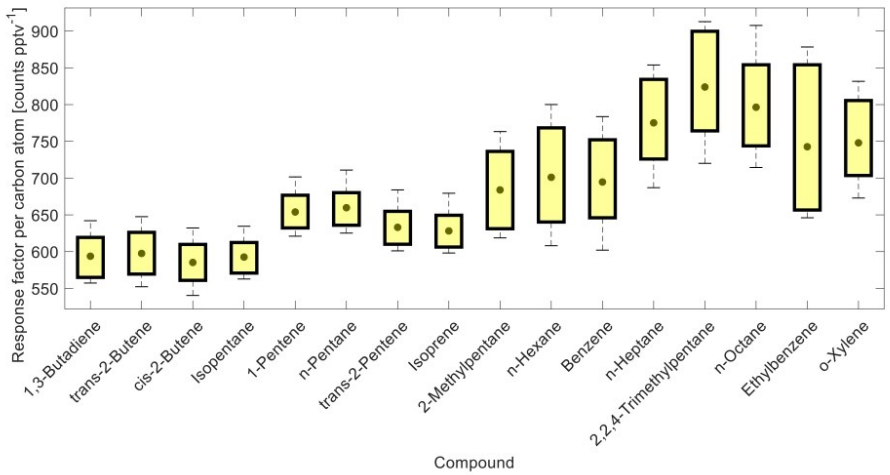

deviation of all the measured data points for the according compound in the Apel-Riemer-2015 and NPL-2017 standards, respectively. The brown dashed line shows the one to one RF correlation between the two measurement experiments. The red squares with black whiskers show the pentane, ethylbenzene and toluene 1σ outliers (from bottom of the graph to top, respectively).

Figure 4: Boxplot graph from a selection of compound-specific per carbon atom RFs determined from the NPL-2017 NMHC primary calibration gas standard. The compound carbon emission line (193 nm) response factors as counts C-atom^{-1} pptv^{-1} are ordered by a growing number of carbon atoms on the x-axis. Central gray circles indicate the means, top and bottom edges of the box represent the 75th and 25th percentiles respectively, the whiskers show the single highest and lowest data point spread, N=176.

Appendices

https://doi.org/10.5194/amt-2020-199
Preprint. Discussion started: 16 June 2020

Atmospheric Measurement Techniques Discussions

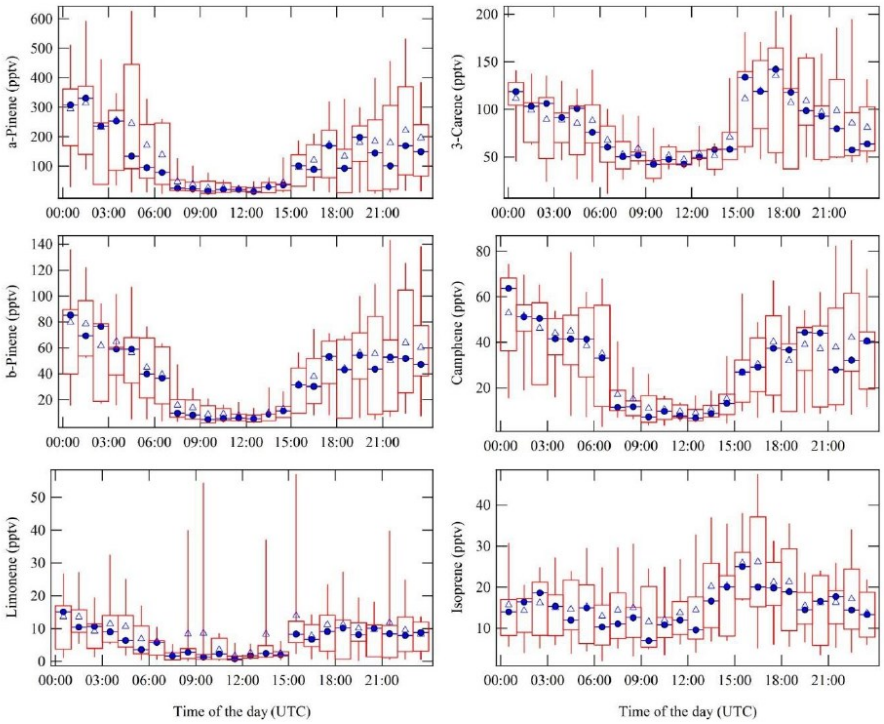

Figure 5: Complete measurement period average diel cycles of α-pinene, Δ-3-carene, β-pinene, camphene, d-limonene and isoprene. For excluding the nearby sawmill (5 km in southeast direction) monoterpene emission transport event, the data from September 9 until 11 6:30 UTC were not included in the diel cycles. Blue triangles resemble the campaign overall hourly average and blue circles represent the hourly median values. The red rectangles with the whiskers show the data spread, where 50% of the data falls into the rectangles. The upper whiskers signify the upper 75-percentile data spread and the lower whiskers indicate the lower 25-percentile of the data variation. Substantially higher MRs were observed at night-time compared to day.

https://doi.org/10.5194/amt-2020-199
Preprint. Discussion started: 16 June 2020

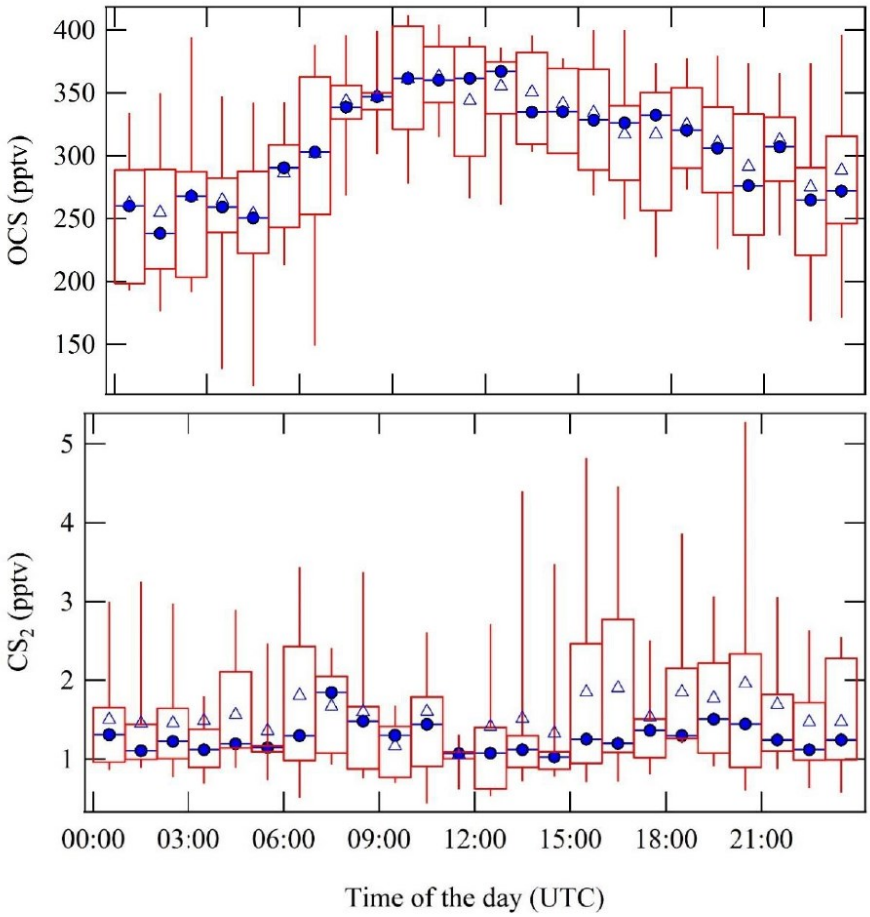

370 **Figure 6: Diel cycles of OCS MRs (upper) and CS_2 MRs (bottom) based on all AED measured data points throughout the measurement campaign. Blue triangles show the overall hourly mean and blue circles show the hourly median values. The red rectangles with the whiskers show the data spread, where 50% of the data falls into the rectangles. The upper whiskers represent the upper 75-percentile data spread and the lower whiskers denote the lower 25-percentile data variation.**

Appendices

https://doi.org/10.5194/amt-2020-199
Preprint. Discussion started: 16 June 2020

Atmospheric Measurement Techniques Discussions

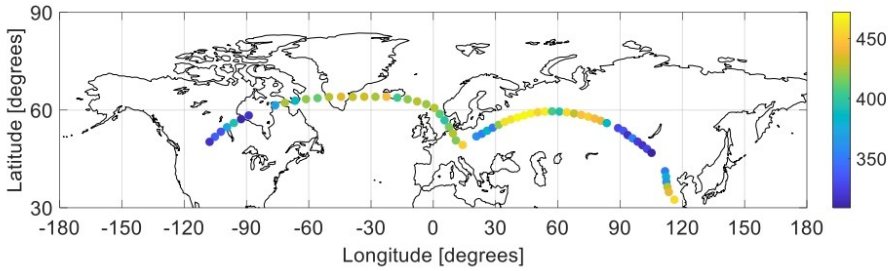

375 **Figure 7: Two IAGOS-CARIBIC example flights from Munich to Los Angeles and from Munich to Shanghai (in February 2019) with OCS MRs according to the color scale [pptv].**

380 **Table 1: CryoTrap-GC-AED system limits of detection (LODs) on 3σ level, R^2 linearity and average response factors (RFs) per carbon atom values derived from (a) Apel-Riemer-2015 and (b) NPL-2017 gas calibration standard measurements.**

(a) Apel-Riemer-2015

Compound	LOD (pptv)	R^2	No. of C atoms	Average RF per C atom ± standard deviation (counts C-atom^{-1} pptv^{-1})
Carbonyl sulfide	6.1	0.99832	1	637 ± 37
Dichlorodifluoromethane (R-12)	2.7	0.99189	1	589 ± 39
Chlorodifluoromethane (HCFC-22)	2.4	0.99589	1	745 ± 32
Chloromethane	2.9	0.99581	1	661 ± 43
Methanol	3.7	0.92247	1	529 ± 172
Methyl bromide	5.1	0.99429	1	553 ± 64
Trichlorofluoromethane	5.6	0.99431	1	652 ± 34
Methyl iodide	6.7	0.99668	1	552 ± 68
Carbon disulfide	5.4	0.99015	1	696 ± 109
Chloroform	5.7	0.99474	1	652 ± 55
Tetrachloromethane	7.0	0.99447	1	637 ± 69
Bromoform	5.8	0.99384	1	737 ± 57
Vinyl chloride	2.0	0.99492	2	549 ± 46
Acetaldehyde	1.8	0.99402	2	636 ± 35
Chloroethane	2.6	0.99469	2	550 ± 46
Acetonitrile	4.8	0.96653	2	523 ± 133
1,1-Dichloroethane	3.9	0.97800	2	430 ± 35

https://doi.org/10.5194/amt-2020-199
Preprint. Discussion started: 16 June 2020

Atmospheric Measurement Techniques Discussions

1,2-Dichloroethane	3.3	0.99494	2	563 ± 46
Trichloroethylene	9.7	0.95093	2	457 ± 280
1,1,2-Trichloroethane	3.3	0.99287	2	715 ± 99
1,2-Dibromoethane	3.4	0.99489	2	638 ± 98
1,1,2,2-Tetrachloroethane	3.2	0.99468	2	654 ± 100
Propene	0.8	0.99478	3	620 ± 33
2-Propanol	1.7	0.99457	3	698 ± 37
Isopropyl nitrate	2.2	0.99886	3	742 ± 137
Propyl nitrate	9.6	0.99813	3	439 ± 232
cis-1,3-Dichloropropene	2.8	0.99452	3	512 ± 84
Isobutene	0.9	0.99532	4	666 ± 35
1,3-Butadiene	1.0	0.99492	4	580 ± 45
Methacrolein	1.5	0.99458	4	728 ± 79
Butanol	2.5	0.99537	4	384 ± 42
Isobutyl nitrate	2.0	0.99878	4	800 ± 291
Pentane	1.1	0.98933	5	595 ± 36
Isoprene	1.2	0.99494	5	628 ± 39
Hexane	1.0	0.99496	6	643 ± 41
Benzene	0.9	0.99451	6	676 ± 53
4-Methyl-2-pentanone (MIBK)	1.9	0.99513	6	566 ± 150
2-Hexanone	2.7	0.99284	6	357 ± 129
Hexanal	6.1	0.98819	6	386 ± 182
Chlorobenzene	1.4	0.99540	6	573 ± 107
1,3-Dichlorobenzene	2.8	0.98789	6	399 ± 133
Benzyl chloride	4.7	0.97921	6	343 ± 147
1,2-Dichlorobenzene	2.6	0.99017	6	412 ± 125
Toluene	0.9	0.99502	7	643 ± 68
Ethylbenzene	0.9	0.99536	8	610 ± 92
1,3,5-Trimethylbenzene	0.9	0.99470	9	665 ± 88
1,2,4-Trimethylbenzene	1.1	0.99135	9	584 ± 156

(b) NPL-2017

Appendices

https://doi.org/10.5194/amt-2020-199
Preprint. Discussion started: 16 June 2020

Atmospheric Measurement Techniques Discussions

Compound	LOD (pptv)	R^2	No. of C atoms	Average RF per C atom ± standard deviation (counts C-atom^{-1} pptv^{-1})
Propene & Propane	0.8	0.99444	3	627 ± 18
Isobutane	0.8	0.99164	4	659 ± 18
1,3-Butadiene	0.8	0.99432	4	594 ± 32
trans-2-Butene	0.8	0.99083	4	598 ± 33
cis-2-Butene	1.0	0.99129	4	585 ± 30
Isopentane	1.1	0.99598	5	593 ± 26
1-Pentene	0.9	0.99263	5	654 ± 26
n-Pentane	0.9	0.99263	5	660 ± 27
trans-2-Pentene	0.9	0.99026	5	633 ± 27
Isoprene	1.0	0.99181	5	628 ± 27
2-Methylpentane	0.9	0.97498	6	684 ± 54
n-Hexane	0.8	0.96687	6	701 ± 71
Benzene	0.7	0.96992	6	695 ± 65
n-Heptane	0.6	0.99386	7	775 ± 62
Toluene	0.5	0.99127	7	913 ± 77
2,2,4-Trimethylpentane	0.6	0.99205	8	824 ± 76
n-Octane	0.5	0.98977	8	796 ± 68
Ethylbenzene	0.5	0.92709	8	743 ± 101
o-Xylene	0.5	0.99552	8	748 ± 60
1,3,5-Trimethylbenzene	0.5	0.96353	9	736 ± 72
1,2,4-Trimethylbenzene	0.6	0.99727	9	581 ± 23
1,2,3-Trimethylbenzene	0.6	0.99681	9	619 ± 26

385 **Table 2: CryoTrap-GC-AED system limits of detection (LODs) on 3σ level, R^2 linearity and response factors (RFs) per iodine, sulfur, bromine and nitrogen atom values derived from Apel-Riemer-2015 calibration standard measurements.**

Compound	LOD (pptv)	R^2	Element	Average RF per atom ± standard deviation (counts atom^{-1} pptv^{-1})
Methyl iodide (iodine)	0.7	0.99668	I	1635 ± 135
Carbonyl sulfide (sulfur)	1.9	0.99964	S	342 ± 34

Appendices

https://doi.org/10.5194/amt-2020-199
Preprint. Discussion started: 16 June 2020

Carbon disulfide (sulfur)	1.8	0.99966	S	476 ± 79
Bromodichloromethane (bromine)	115.7	0.98930	Br	9.9 ± 1.5
1,2-Dibromoethane (bromine)	61.9	0.99226	Br	9.0 ± 1.8
Bromoform (bromine)	64.2	0.99082	Br	8.3 ± 2.0
Acetonitrile (nitrogen)	265.1	0.98281	N	19.8 ± 2.7
Acrylonitrile (nitrogen)	139.4	0.99657	N	28.2 ± 0.8
Isopropyl nitrate (nitrogen)	64.6	0.98954	N	35.8 ± 2.9
Propyl nitrate (nitrogen)	82.0	0.99180	N	25.8 ± 2.2
Isobutyl nitrate (nitrogen)	57.1	0.99060	N	28.2 ± 2.1

Table 3: The GC oven programs for (a) Finish boreal forest and (b) IAGOS-CARIBIC measurements.

(a) Finnish boreal forest

Rate (°C min^{-1})	**Temperature (°C)**	**Hold time (min)**
	35	5
6	180	5
Total runtime: 34.0 min		
Pressure (psi)	**Average velocity (cm sec^{-1})**	**Holdup time (min)**
44.25 (3.05 bar)	44.02	2.27

390

(b) IAGOS-CARIBIC

Rate (°C min^{-1})	**Temperature (°C)**	**Hold time (min)**
	30	8
6	180	1
Total runtime: 34.2 min		
Pressure (psi)	**Average velocity (cm sec^{-1})**	**Holdup time (min)**
45.02 (3.10 bar)	44.23	2.26

https://doi.org/10.5194/amt-2020-199
Preprint. Discussion started: 16 June 2020

Atmospheric Measurement Techniques Discussions

References

Apel, E.C., Calvert, J.G., Greenberg, J.P., Riemer, D., Zika, R., Kleindienst, T.E., Lonneman, W.A., Fung, K., and Fujita, E.: Generation and validation of oxygenated volatile organic carbon standards for the 1995 Southern Oxidants Study Nashville Intensive. Journal of Geophysical Research: Atmospheres, 103, 22281-22294, 1998.

Baker, A. K., Slemr, F., and Brenninkmeijer, C. A. M.: Analysis of non-methane hydrocarbons in air samples collected aboard the CARIBIC passenger aircraft. Atmospheric Measurement Techniques, 3, 311-321, 2010.

Barkley, M. P., Palmer, P. I., Boone, C. D., Bernath, P. F., and Suntharalingam, P.: Global distributions of carbonyl sulfide in the upper troposphere and stratosphere. Geophysical Research Letters, 35, 2008.

Beenaker, C.: Evaluation of a microwave-induced plasma in helium at atmospheric pressure as an element-selective detector for gas chromatography. Spectrochimica Acta Part B: Atomic Spectroscopy, 32, 173-187, 1977.

Bourtsoukidis, E., Helleis, F., Tomsche L., Fischer, H., Hofmann, R., Lelieveld, J., and Williams, J.: An aircraft gas chromatograph–mass spectrometer System for Organic Fast Identification Analysis (SOFIA): design, performance and a case study of Asian monsoon pollution outflow. Atmospheric Measurement Techniques, 10, 5089-5105, 2017.

Brandt, J.P., Flannigan, M., Maynard, D.G., Thompson, I., and Volney, W.J.A: An introduction to Canada's boreal zone: Ecosystem processes, health, sustainability, and environmental issues. Environmental Reviews, 21, 207-226, 2013.

Brenninkmeijer, C. A. M., Crutzen, P., Boumard, F., Dauer, T., Dix, B., Ebinghaus, R., Filippi, D., Fischer, H., Franke, H., Frieβ, U., Heintzenberg, J., Helleis, F., Hermann, M., Kock, H. H., Koeppel, C., Lelieveld, J., Leuenberger, M., Martinsson, B. G., Miemczyk, S., Moret, H. P., Nguyen, H. N., Nyfeler, P., Oram, D., O'Sullivan, D., Penkett, S., Platt, U., Pupek, M., Ramonet, M., Randa, B., Reichelt, M., Rhee, T. S., Rohwer, J., Rosenfeld, K., Scharffe, D., Schlager, H., Schumann, U., Slemr, F., Sprung, D., Stock, P., Thaler, R., Valentino, F., van Velthoven, P., Waibel, A., Wandel, A., Waschitschek, K., Wiedensohler, A., Xueref-Remy, I., Zahn, A., Zech, U., and Ziereis, H.: Civil Aircraft for the regular investigation of the atmosphere based on an instrumented container: The new CARIBIC system. Atmospheric Chemistry and Physics, 7, 4953-4976, 2007.

Brühl, C., Lelieveld, J., Crutzen, P. J., and Tost, H.: The role of carbonyl sulphide as a source of stratospheric sulphate aerosol and its impact on climate. Atmospheric Chemistry and Physics, 12, 1239-1253, 2012.

Crutzen, P. J.: The possible importance of CSO for the sulfate layer of the stratosphere. Geophysical Research Letters, 3, 73-76, 1976.

Hari, P., and Kulmala, M.: Station for measuring ecosystem-atmosphere relations (SMEAR II). Boreal Environment Research, 10, 315-322, 2005.

Greenberg, J.P., Guenther, A., Zimmerman, P., Baugh, W., Geron, C., Davis, K., Helmig, D., and Klinger, L.F.: Tethered balloon measurements of biogenic VOCs in the atmospheric boundary layer. Atmospheric Environment, 33, 855-867, 1999.

JAS product description: https://www.jas.de/en/products/jas/aed/AED%20III%20High%20Resolution%20(HR)/, last access: 26 May 2020.

Appendices

https://doi.org/10.5194/amt-2020-199
Preprint. Discussion started: 16 June 2020

Atmospheric Measurement Techniques Discussions

Jobson, B. T., Parrish, D. D., Goldan, P., Kuster, W., Fehsenfeld, F. C., Blake, D. R., Blake, N. J., and Niki, H.: Spatial and temporal variability of nonmethane hydrocarbon mixing ratios and their relation to photochemical lifetime. Journal of Geophysical Research: Atmospheres, 103, 13557-13567, 1998.

Junge, C. E.: Residence time and variability of tropospheric trace gases. Tellus, 26, 477-488, 1974.

Karu, E.: Atmospheric sulfur compounds in the troposphere and stratosphere measured with an atomic emission detector. PhD Dissertation, Max Plank Institute for Chemistry & Johannes Gutenberg University Mainz, 1-164, 2019.

Kjellström, E.: A Three-Dimensional Global Model Study of Carbonyl Sulfide in the Troposphere and the Lower Stratosphere. Journal of Atmospheric Chemistry, 29, 151-177, 1998.

Kooijmans, L.M.J., Maseyk, K., Seibt, U., Sun, W., Vesala, T., Mammarella, I., Kolari, P., Aalto, J., Franchin, A., Vecchi, R., Valli, G., and Chen, H.: Canopy uptake dominates nighttime carbonyl sulfide fluxes in a boreal forest, Atmospheric Chemistry and Physics, 17, 11453–11465, 2017.

Krechmer, J., Lopez-Hilfiker, F., Koss, A., Hutterli, M., Stoermer, C., Deming, B., Kimmel J., Warneke C., Holzinger, R., Jayne J., Worsnop, D., Fuhrer K., Gonin M., and de Gouw, J.: Evaluation of a New Reagent-Ion Source and Focusing Ion–Molecule Reactor for Use in Proton-Transfer-Reaction Mass Spectrometry. Analytical Chemistry, 90, 12011-12018, 2018.

Liebmann, J., Karu, E., Sobanski, N., Schuladen J., Ehn, M.3, Schallhart, S., Quéléver L., Hellen H., Hakola H., Hoffmann T., Williams J., Fischer H., Lelieveld J., and Crowley, J.N.: Direct measurement of NO_3 radical reactivity in a boreal forest. Atmospheric Chemistry and Physics, 18, 3799–3815, 2018.

Link, D.D., Baltrus, J.P., Rothenberger, K.S., Zandhuis, P., Minus, D., and Striebich, R.C.: Rapid Determination of Total Sulfur in Fuels Using Gas Chromatography with Atomic Emission Detection. Journal of Chromatographic Science, 40, 500-504, 2002.

McCormack, A., Tong, S., and Cooke, W.: Sensitive Selective Gas Chromatography Detector Based on Emission Spectrometry of Organic Compounds. Analytical Chemistry, 37, 1470-1476, 1965.

Montzka, S., Calvert, P., Hall, B., Elkins, J., Conway, T., Tans, P., and Sweeney, C.: On the global distribution, seasonality, and budget of atmospheric carbonyl sulfide (COS) and some similarities to CO_2. Journal of Geophysical Research: Atmospheres, 112, 2007.

Murphy, D. and Fahey, D.: An estimate of the flux of stratospheric reactive nitrogen and ozone into the troposphere. Journal of Geophysical Research: Atmospheres, 99, 5325-5332, 1994.

Plumb, R. A. and Ko, M. K.: Interrelationships between mixing ratios of long-lived stratospheric constituents. Journal of Geophysical Research: Atmospheres, 97, 10145-10156, 1992.

Risby, T. H., Talmi, Y., and Uden, P. C.: Microwave induced electrical discharge detectors for gas chromatography. Critical Reviews in Analytical Chemistry, 14, 231-265, 1983.

https://doi.org/10.5194/amt-2020-199
Preprint. Discussion started: 16 June 2020

Atmospheric Measurement Techniques Discussions

Sandoval-Soto, L., Stanimirov, M., von Hobe, M., Schmitt, V., Valdes, J., Wild, A, and Kesselmeier, J.: Global uptake of carbonyl sulfide (COS) by terrestrial vegetation: Estimates corrected by deposition velocities normalized to the uptake of carbon dioxide (CO2). Biogeosciences Discussions, 2, 125-132, 2005.

Schuck, T. J., Brenninkmeijer, C. A. M., Slemr, F., Xueref-Remy, I., and Zahn, A.: Greenhouse gas analysis of air samples collected onboard the CARIBIC passenger aircraft. Atmospheric Measurement Techniques, 2, 449–464, 2009.

Williams, J., Gros, V., Bonsang, B., and Kazan, V.: HO cycle in 1997 and 1998 over the southern Indian Ocean derived from CO, radon, and hydrocarbon measurements made at Amsterdam Island. Journal of Geophysical Research: Atmospheres, 106, 12719-12725, 2001.

Quimby, B.D., and Sullivan, J.J.: Evaluation of a microwave cavity, discharge tube, and gas flow system for combined gas chromatography-atomic emission detection. Analytical Chemistry, 62, 1027-1034, 1990.

Prather, M.J., Hsu, J., DeLuca, N.M., Jackman, C.H., Oman, L.D., Douglass, A.R., Fleming, E.L., Strahan, S.E., Steenrod, S.D., Søvde, O.A., Isaksen, I.S.A., Froidevaux, L., and Funke, B.: Measuring and modeling the lifetime of nitrous oxide including its variability. Journal of Geophysical Research: Atmospheres, 120, 5693-5705, 2015.

Plumb, R.A., and Ko, M.K.W.: Interrelationships between mixing ratios of long-lived stratospheric constituents. Journal of Geophysical Research: Atmospheres, 97, 10145-10156, 1992.

Cantrell, C.A.: Technical Note: Review of methods for linear least-squares fitting of data and application to atmospheric chemistry problems. Atmospheric Chemistry and Physics Discussions, 8, 6409-6436, 2008.

Barkley, M.P., Palmer, P.I., Boone, C.D., Bernath, P.F., and Suntharalingam, P.: Global distributions of carbonyl sulfide in the upper troposphere and stratosphere. Geophysical Research Letters, 35, 2008.

Krysztofiak, G., Té, Y.V., Catoire, V., Berthet, G., Toon, G.C., Jégou, F., Jeseck, P., and Robert, C.: Carbonyl Sulphide (OCS) Variability with Latitude in the Atmosphere. Atmosphere-Ocean, 53, 89-101, 2015.

Trenberth, K.E., and Smith, L., The mass of the atmosphere: A constraint on global analyses. Journal of Climate, 18, 864-875, 2005.

Tarvainen, V., Hakola, H., Hellén, H., Bäck, J., Hari, P., and Kulmala, M.: Temperature and light dependence of the VOC emissions of Scots pine, Atmospheric Chemistry and Physics, 5, 989–998, 2005.

Thomason, L., and Peter, T.: Assessment of stratospheric aerosol properties (ASAP), Report on the SPARC Assessment Kick-Off Workshop, Paris, France, 4-6 November 2001. Stratospheric Processes and Their Role in Climate Newsletter, 18, 2002.

Kremser, S., Thomason, L.W., von Hobe, M., Hermann, M., Deshler, T., Timmreck, C., Toohey, M., Stenke, A., Schwarz, J.P., Weigel, R., Fueglistaler, S., Prata, F.J., Vernier, J., Schlager, H., Barnes, J.E., Antuña-Marrero, J., Fairlie, D., Palm, M., Mahieu, E., Notholt, J, Rex, M., Bingen, C., Vanhellemont, F., Bourassa, A., Plane, J.M.C., Klocke, D., Carn, S.A., Clarisse, L., Trickl, T., Neely, R., James, A.D., Rieger, L., Wilson, J.C., and Meland, B.: Stratospheric aerosol—Observations, processes, and impact on climate. Reviews of Geophysics, 54, 278-335, 2016.

Atomic emission detector with gas chromatographic separation and cryogenic pre-concentration (CryoTrap-GC-AED) for atmospheric trace gas measurements

Einar Karu[1], Mengze Li[1], Lisa Ernle[1], Carl A.M. Brenninkmeijer[1], Jos Lelieveld[1], Jonathan Williams[1]

[1]Atmospheric Chemistry Department, Max Planck Institute for Chemistry, 55128 Mainz, Germany

Correspondence to: Jonathan Williams (jonathan.williams@mpic.de)

Supplementary

Apel-Riemer-2015, 84 multi-component gas calibration standard

Table S1: Retention times of Apel-Riemer-2015, Apel-Riemer Environmental, Inc. 84 multi-component gas phase calibration mix in UHP nitrogen balance. Stated uncertainty better than ±5% for all components. MR certificate analysis date: June 9, 2015.

IAGOS-CARIBIC-2018 RT 30°C (min)	Compound	CAS #	Concentration (ppb)
3.46	Propene	115-07-1	51.8
3.50	Carbonyl Sulfide (OCS)	463-58-1	51.2
3.55	Dichlorodifluoromethane (R-12)	75-71-8	49.6
3.61	Chlorodifluoromethane (HCFC-22)	75-45-6	50.8
3.91	1,2-Dichlorotetrafluoroethane (R-114)	76-14-2	55.5
4.06	Chloromethane	74-87-3	52.5
4.31	Isobutene	115-11-7	51.3
4.39	Vinyl Chloride	75-01-4	52.3
4.50	1,3-Butadiene	106-99-0	51.7
4.77	Acetaldehyde	75-07-0	58.2
5.20	Methanol	67-56-1	51.7
5.38	Bromomethane	74-83-9	55.0
5.72	Chloroethane	75-00-3	54.8
6.50	Trichlorofluoromethane (F-11)	75-69-4	51.8
6.77	Pentane	109-66-0	61.8
	Ethanol	64-17-5	45.3

7.61	Isoprene	78-79-5	52.4
8.24	Acrolein	107-02-8	46.1
	Propanal	123-38-6	43.2
8.38	1,1-Dichloroethene	75-35-4	75.4
	1,1,2-Trichloro-1,2,2-Trifluoroethane (CFC-113)	76-13-1	70.6
	Acetone	67-64-1	43.2
8.85	Methyl Iodide	74-88-4	69.4
9.00	Carbon Disulfide (CS_2)	75-15-0	47.0
9.44	2-Propanol	67-63-0	50.7
9.95	Acetonitrile	75-05-8	50.0
	Dichloromethane	75-09-2	52.2
10.22	Cyclopentane	287-92-3	52.8
11.14	Acrylonitrile	107-13-1	64.3
11.03	trans-1,2-Dichloroethene	156-60-5	62.3
	Methyl Tertiary Butyl Ether (MTBE)	1634-04-4	61.0
11.82	Hexane	110-54-3	52.1
12.25	Methacrolein	78-85-3	48.9
12.36	1,1-Dichloroethane	75-34-3	57.8
12.58	Vinyl Acetate	108-05-4	56.4
12.93	1-Propanol	71-23-8	51.4
13.57	Butanal	123-72-8	59.6
13.66	Methyl Vinyl Ketone	78-94-4	74.4
14.05	cis-1,2-Dichloroethene	156-59-2	52.3
14.10	Methyl Ethyl Ketone	78-93-3	51.1
14.90	Chloroform	67-66-3	51.9
15.32	1,1,1-Trichloroethane	71-55-6	52.4
	Cyclohexane	110-82-7	53.4
15.65	Tetrachloromethane	56-23-5	51.4
16.18	Benzene	71-43-2	48.1
16.36	1,2-Dichloroethane	107-06-2	58.5
17.83	Trichloroethylene	79-01-6	54.8
	1-Butanol	71-36-3	40.5
18.04	Isopropyl nitrate	1712-64-7	44.7

18.31	Hydroxyacetone	116-09-6	53.1
	2-Pentanone	107-87-9	50.2
18.40	1,2-Dichloropropane	78-87-5	50.5
18.56	Pentanal	110-62-3	59.9
18.64	3-Pentanone	96-22-0	52.5
18.69	1,4-Dioxane	123-91-1	50.7
19.07	Bromodichloromethane	75-27-4	49.2
19.81	Propyl nitrate	627-13-4	47.4
20.14	cis-1,3-Dichloropropene	10061-01-5	49.6
20.47	4-Methyl-2-Pentanone	108-10-1	51.7
20.85	Toluene	108-88-3	51.6
21.33	trans-1,3-Dichloropropene	10061-02-6	51.3
21.49	1,1,2-Trichloroethane	79-00-5	52.9
21.90	Isobutyl nitrate	543-29-3	45.0
22.14	3-Hexanone	598-38-8	50.9
	Tetrachloroethylene	127-18-4	55.5
22.44	2-Hexanone	591-78-6	52.0
22.68	Hexanal	66-25-1	55.8
23.06	1,2-Dibromoethane	106-93-4	50.2
24.21	Chlorobenzene	108-90-7	53.3
24.42	Ethyl Benzene	100-41-4	50.8
24.71	m-Xylene	108-38-3	50.8
	p-Xylene	106-42-3	51.5
25.66	o-Xylene	95-47-6	50.6
25.70	Styrene	100-42-5	52.5
26.16	Bromoform	75-25-2	52.4
27.34	1,1,2,2-Tetrachloroethane	79-34-5	50.7
27.96	1,3,5-Trimethylbenzene	108-67-8	51.2
28.88	1,2,4-Trimethylbenzene	95-63-6	50.7
29.61	(m-)1,3-Dichlorobenzene	541-73-1	52.9
29.84	(p-)1,4-Dichlorobenzene	106-46-7	55.6
29.91	1,2,3-Trimethylbenzene	526-73-8	46.2
30.15	Benzyl Chloride	100-44-7	61.7

30.75	(o-)1,2-Dichlorobenzene	95-50-1	61.8
	1,2,4-Trichlorobenzene	120-82-1	52.7

NPL-2017, National Physical Laboratory (NPL) 30 component NMHC primary calibration standard

Table S2: Retention times of NPL-2017 30 ozone precursor NMHC gas phase primary calibration reference material in UHP nitrogen balance. Stated uncertainties are based on 2σ, providing a coverage probability of ~95%. Calibration date 7 May – 21 June 2017.

IAGOS-CARIBIC-2018		NPL-2017 (Bottle: D51 7546)	
RT 30°C (min)	**Compound**	**MR (pmol mol^{-1})**	**Uncertainty (pmol mol^{-1})**
	Ethene	3930	80
	Ethyne	4140	210
3.15	Ethane	4010	80
3.46	Propene	3930	80
	Propane	3950	80
3.93	Isobutane	4030	110
4.31	1-Butene	3980	80
4.36	n-Butane	3990	80
4.50	1,3-Butadiene	4040	80
4.60	trans-2-Butene	4000	80
4.88	cis-2-Butene	3990	80
5.90	Isopentane	3940	80
6.58	1-Pentene	4040	80
6.76	n-Pentane	3960	80
7.28	trans-2-Pentene	3980	80
7.61	Isoprene	4140	90
10.11	2-Methylpentane	4150	80
11.81	n-Hexane	4150	80
16.17	Benzene	4140	80
16.33	2,2,4-Trimethylpentane	3900	80
16.84	n-Heptane	4160	80
20.84	Toluene	4020	110
21.08	n-Octane	3910	80

24.41	Ethylbenzene	4350	110
24.70	m-Xylene p-Xylene	8460	220
25.64	o-Xylene	4160	110
27.95	1,3,5-Trimethylbenzene	3940	100
28.86	1,4,4-Trimethylbenzene	4060	110
29.90	1,2,3-Trimethylbenzene	3890	100

5

Appendix 2 Karu et al. (2020a)

Carbonyl sulfide (COS) in the UTLS region: estimates of lifetimes and fluxes

Authors: Einar Karu, Mengze Li, Lisa Ernle, Carl A.M. Brenninkmeijer, Jos Lelieveld, Jonathan Williams

Status: in review

Journal: Geophysical Research Letters

Carbonyl sulfide (OCS) in the UT/LS region: estimates of lifetimes and fluxes

Einar Karu[1], Mengze Li[1], Lisa Ernle[1], Carl A.M. Brenninkmeijer[1], Jos Lelieveld[1], Jonathan Williams[1]

[1]Atmospheric Chemistry Department, Max Planck Institute for Chemistry, 55128 Mainz, Germany

Correspondence to: Jonathan Williams (jonathan.williams@mpic.de)

ORCID:
Einar Karu: 0000-0002-1610-0132
Mengze Li: 0000-0003-0620-6301
Jos Lelieveld: 0000-0001-6307-3846
Jonathan Williams: 0000-0001-9421-1703

Key Points:

- OCS atmospheric lifetime of 2.1 ± 1.3 years and lower stratospheric lifetime of 47 ± 16 years were determined.
- Total flux of OCS into the stratosphere estimated as 118 ± 39 Gg (S) yr^{-1}, of which 52% is transported back into the troposphere.
- The lower back transport estimate helps to explain the currently unexplained stratospheric sulfate aerosol burden.

Appendices

Abstract

Carbonyl sulfide (OCS) is the most abundant sulfur compound in the atmosphere and plays a role in forming stratospheric sulfate aerosol particles, thereby influencing ozone chemistry and climate. In this study, whole-air samples containing OCS were collected onboard a passenger aircraft (IAGOS-CARIBIC) from the upper troposphere/lower stratosphere (UT/LS, 10 ~ 12 km) region and analyzed with an automated CryoTrap–GC–AED system in the laboratory. Global OCS mixing ratios are presented and by using the OCS measurements in conjunction with other trace gases, an atmospheric OCS lifetime of 2.1±1.3 years, and lower stratospheric OCS lifetime of 47±16 years were determined. A total flux of 118±39 Gg (S) yr^{-1} of OCS from the troposphere into the stratosphere was estimated, and the stratospheric OCS sink estimate yielded 57±19 Gg (S) yr^{-1}. The 52% smaller sink can be interpreted as 61 Gg (S) yr^{-1} OCS which is transported back from the stratosphere into the troposphere.

Plain Language Summary

Carbonyl sulfide (OCS) is the most abundant sulfur compound in the atmosphere. Due to its long atmospheric lifetime, OCS can be transported into the stratosphere where it forms a layer of sulfate aerosol particles at 30 km altitude. By reflecting incoming sunlight and through chemical processes this layer influences the Earth's climate and the ozone layer. In this study, we have determined OCS mixing ratios in air samples collected in the upper troposphere / lower stratosphere (UT/LS, 10-12 km) region, from 2015 to 2018. From these measurements we estimated the total atmospheric lifetime and the stratospheric lifetime of OCS as 2.1 ± 1.3 years, and 47 ± 16 years, respectively. We also estimated the total flux of OCS transported from the troposphere into the stratosphere as 118 ± 39 Gg (S) yr^{-1}, of which 52% (61 Gg (S) yr^{-1}) were transported back into the troposphere as OCS.

Appendices

1 Introduction

Carbonyl sulfide (OCS or COS) is the most abundant sulfur-containing compound in the atmosphere. Atmospheric OCS distributions are generally derived from tropospheric surface observations (Montzka et al., 2007), satellite retrievals (Glatthor et al. 2017; Glatthor et al. 2015; Barkley et al., 2008) or with models (Brühl et al., 2015; Brühl et al., 2012; Kjellström, 1998). Direct oceanic emission of OCS and oxidation of carbon disulfide (CS_2) and dimethyl sulfide (DMS) are its major sources in the atmosphere, whereas emissions from industrial production and coal burning add their anthropogenic fractions. Uptake by vegetation and soils, as well as oxidation by OH are its major sinks (Campbell et al., 2015; Brühl et al., 2012; Montzka et al., 2007; Watts, 2000). Due to its variable biogeochemical sources and sinks, a clear global scale seasonality of OCS mixing ratios and fluxes is observed and modelled, with a minimum in the boreal summer (June, July and August) and a maximum in winter (December, January and February), which is similar to the seasonality of CO_2 (Commane et al., 2015; Montzka et al., 2007, Watts, 2000).

The large spatial and temporal variations of sources and sinks makes it difficult to estimate OCS lifetime accurately, resulting in large variations in the estimateed lifetime. Johnson estimated a net lifetime for tropospheric OCS of 4 – 7 years (Johnson, 1981), and Montzka narrowed it down to 1.5 – 3.0 years (Montzka et al., 2007). With the tracer-tracer correlation method developed by (Plumb and Ko, 1992), Engel and Schmidt estimated the OCS stratospheric lifetime to be 69 ± 28 years using balloon borne measurements (Engel and Schmidt, 1994), and 64 ± 21 years was calculated from satellite observations in the middle stratosphere by (Barkley et al., 2008). By virtue of its relatively long lifetime, OCS can be transported into the stratosphere where it is oxidized or photodissociated, which leads to the formation of sulfate aerosol particles (forming the Junge layer) at circa 30 km altitude. This layer of sulfate particles can impact ozone chemistry and the climate (Brühl et al., 2012; Crutzen, 1976).

In this study, we present a global OCS dataset with samples collected onboard the IAGOS-CARIBIC (In-service Aircraft for a Global Observing System – Civil Aircraft for the Regular Investigation of the Atmosphere Based on an Instrument Container) project during December 2015 – December 2018. This data is exploited to derive: 1) OCS flux into the stratosphere (Section 3.2); 2) atmospheric OCS lifetime (Section 3.3); 3) lower stratospheric OCS lifetime (Section 3.4), and; 4) stratospheric OCS sink (Section 3.5).

2 Materials and Methods

2.1 IAGOS-CARIBIC whole-air samples

The IAGOS-CARIBIC project globally monitors atmospheric chemistry and physics parameters with long distance flights at upper troposphere / lower stratosphere (UT/LS) altitudes (10 ~ 12 km) (Brenninkmeijer et al., 2007). The whole-air samples (WAS) were collected with two triggered retrospective air collectors (TRACs) each consisting of 14 specially manufactured

glass vessels (2.74 L), and high-resolution sampler (HIRES), which consists of 88 stainless steel canisters (1.0 L). Directly after each flight the 116 whole air samples were delivered to the laboratory for chemical analysis.

2.2 Measurements

OCS measurements. Air samples have been measured with a newly developed CryoTrap–GC–AED system which consists of three stages: a liquid nitrogen pre-concentration system (Entech model 7200, USA); a gas chromatographic separation of analyte compounds (Agilent GC 7890B, USA); and a helium plasma based third generation atomic emission detector (Joint Analytical Systems AEDIII High Resolution, Germany). Details of this measurement system and its performance are discussed in the PhD dissertation of Karu (2019). In short, the sulfur emission line (181 nm) of this system was used to measure OCS (sulfur emission line is over three times more sensitive compared to carbon emission line at 193 nm), and the limit of detection (LOD, three times signal-to-noise ratio by peak height) for OCS is 1.9 pptv. Before, during (every 5 samples), and after measurement of the WAS samples from each flight, a primary ambient air calibration standard gas bottle produced and calibrated (according to the latest NOAA-2004 OCS scale) by the NOAA Earth System Research Laboratories was used to calibrate the system for the OCS measurements.

N_2O, CH_4, CH_3Cl, C_2H_6, C_3H_8, and CO measurements. These chemical compounds were measured by various instruments. Details for the greenhouse gases GC–ECD/FID system are given by Schuck et al. (2009), for the non-methane hydrocarbons GC–FID by Baker et al. (2010), and for carbon monoxide a UV resonance fluorescence instrument was used (Scharffe et al., 2012).

3 Results and Discussion

3.1 Overview of OCS observations

In total, 708 carbonyl sulfide sample data points were obtained from the HIRES and TRACs in the time frame from December 2015 until December 2018 through CryoTrap-GC-AED measurements. An overview map of the latitude and longitude of these OCS MRs is shown in Fig. 1. The container was flown eastbound from Germany to China, westbound to various locations in America and traversing into the Southern Hemisphere to Brazil and South Africa. The global coverage afforded by this measurement program allows several aspects of the atmospheric chemistry of OCS to be assessed. The observed OCS MRs are typically within the range 301 – 552 pptv. In the following sections we demonstrate how this unique dataset can be used to derive the global OCS flux into the stratosphere, the global and stratospheric atmospheric lifetimes of OCS, and estimate the stratospheric sink of OCS.

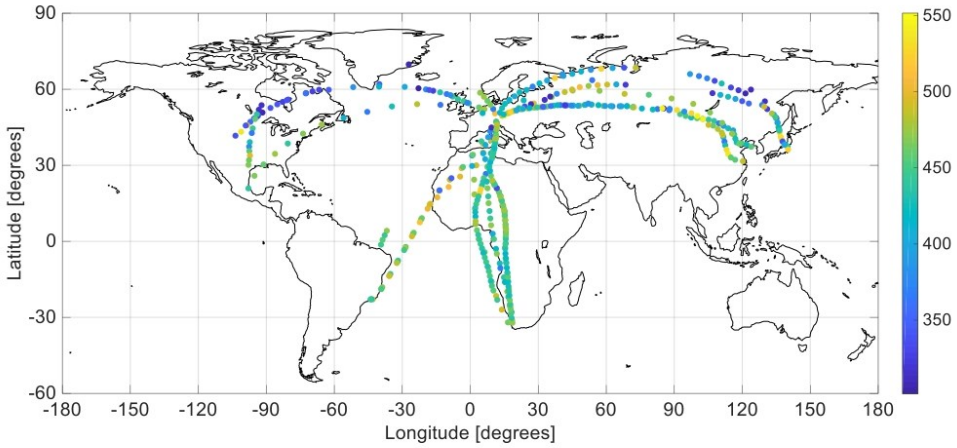

Figure 1: Global overview of OCS measurement data in the UT/LS. Color coded circles represent OCS MRs [pptv].

3.2 OCS flux into the stratosphere

Plumb and Ko (1992) presented a theoretical concept showing that pairs of long-lived atmospheric species consistently display simple linear relationships in the lower stratosphere. Therefore, the measured mixing ratios of one species can be used to predict the other if the stratospheric lifetimes of both species are known (Plumb and Ko, 1992). Murphy and Fahey (1994) used observed correlations of N_2O and NO_y/O_3 to calculate the globally averaged net downward transport of reactive nitrogen (NO_y) and ozone from the stratosphere to the troposphere through the tropopause (Murphy and Fahey, 1994). In this study, we used the same method to derive the OCS flux to the stratosphere as shown in Eq. (1):

$$\phi_{OCS} = \mathrm{m} \times S_{N2O} \times \frac{M_S}{M_{N2}}, \quad (1)$$

where ϕ_{OCS} is the OCS flux, m is the slope of observed OCS vs N_2O correlation, S_{N2O} is the annual global average stratospheric sink of N_2O. The M_S and M_{N2} are the molar masses of sulfur and two nitrogen atoms, respectively. A filter to select for stratospheric air samples was applied with potential vorticity (PV) of PV > 2 PVU (potential vorticity units) and an orthogonal fit of the observed OCS vs N_2O was made. An example correlation plot with samples originating from the flight from Munich to Seoul in December 2017 is shown in Fig. 2. Using all measurement flight data, an average slope of 6.44 ± 2.13 was determined. This corresponds to a total flux of 118 ± 39 Gg (S) yr^{-1} of OCS from the troposphere into the stratosphere, which supports the 150 Gg (S) yr^{-1} earlier estimate made by the EMAC 3D global chemistry model simulation (Brühl et al., 2012).

Appendices

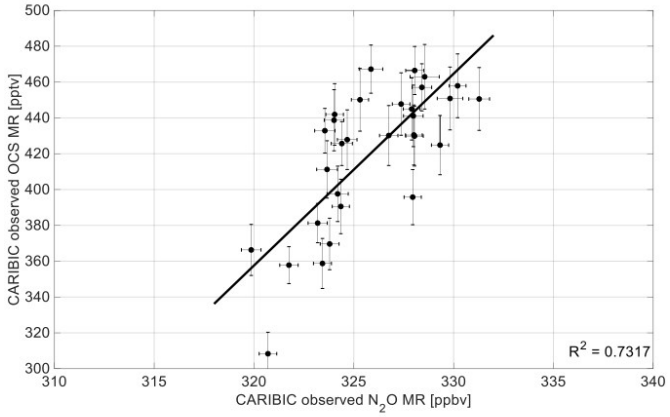

Figure 2: Orthogonal fit of N_2O vs OCS with 1σ uncertainty error bars from flight 537 Munich to Seoul (December 2017).

3.3 OCS atmospheric lifetime

Junge first reported the inverse relationship between the variation in concentration of atmospheric trace gases and their lifetime (Junge, 1974). This dependency has been later examined with various observations in the troposphere and stratosphere (Williams et al., 2001; Jobson et al., 1999; Jobson et al., 1998; Colman et al., 1998): The relationship is represented in Eq. (2) (from Jobson et al 1999):

$$S_{\ln X} = A\tau^{-b}, \quad (2)$$

where S_{lnX} is the standard deviation of the natural logarithm of the mixing ratios of the trace gases, τ is the corresponding lifetime of the trace gases. The A and b are the fitting parameters.

In this study, we have used six observed species to determine the OCS atmospheric lifetime using this relationship. The compounds used were propane (C_3H_8), ethane (C_2H_6), carbon monoxide (CO), methyl chloride (CH_3Cl), methane (CH_4) and nitrous oxide (N_2O). Their corresponding atmospheric lifetimes were taken from the 2011 WMO report (WMO, 2011) and are 0.03, 0.15, 0.17, 1.5, 12 years, respectively and 116 years for N_2O (Prather et al., 2015). Only the flights where the R^2 correlation between the 6 species was > 0.5 were used for the OCS atmospheric lifetime calculations.

The average atmospheric OCS lifetime was calculated to be 2.1 ± 1.3 years with the method, represented in Fig. 3. The variability lifetime plot is defined by all species except OCS, then the variability of OCS is calculated and applied to the line of best fit to derive a lifetime. The values obtained for OCS agree with the range of 1.5 – 3.0 years OCS lifetime reported by (Montzka et al., 2007).

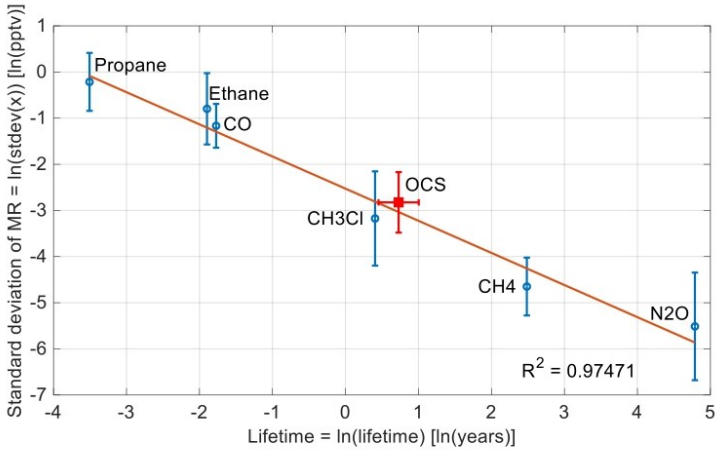

Figure 3: Standard deviation correlation of IAGOS-CARIBIC observational MR dataset (natural logarithm taken) of 6 atmospheric trace gas species with various atmospheric lifetimes for determining the corresponding global atmospheric lifetime of carbonyl sulfide. Data obtained from 4 IAGOS-CARIBIC measurement instruments. Red square with red error bars indicates the average atmospheric lifetime of OCS derived from this linear regression model.

3.4 Stratospheric OCS lifetime

Due to the low concentrations of ethane and propane in the stratosphere, we estimated stratospheric OCS lifetime with the following method. A tracer-tracer correlation between two long lived atmospheric constituents allows for the estimation of the stratospheric lifetime of a species if the stratospheric lifetime of the other is known, as described by (Plumb and Ko, 1992) and later applied by (Barkley et al., 2008) and (Krysztofiak et al., 2015). To derive the stratospheric OCS lifetime, the correlation between OCS and N_2O has been used. The lifetime of N_2O in the stratosphere is relatively well known and is globally estimated as 116 ± 9 years (τ_{N2O}) (Prather, et al. 2015), allowing calculation of the OCS stratospheric lifetime (τ_{OCS}) by the following (Eq. 3):

$$\tau_{OCS} = \frac{\overline{MR_{OCS}}}{\overline{MR_{N2O}}} \times \bar{m} \times \tau_y \,. \quad (3)$$

Potential vorticity was the selection criterion (PV > 2 PVU) used to distinguish stratospheric air samples. An orthogonal fit (total least squares) method was used for the OCS and N_2O correlation for slope (m) determination, as the fit considers the uncertainty of both species (Cantrell, 2008).

An average OCS MR of 0.415 ± 0.032 ppbv (MR_{OCS}) and a mean N_2O MR of 324.0 ± 0.2 ppbv (MR_{N2O}) were determined for the stratospheric samples. A mean slope of 265.0 ± 82.3 ($\bar{m}$) was calculated. An average stratospheric OCS lifetime (τ_{OCS}) of 39 ± 15 years was determined, where the uncertainty accounts for the geometric mean of 1σ of the slope determined lifetime and the N_2O atmospheric lifetime.

The same approach was also applied with the thermal tropopause, $H_{tp} > 0$ km filter. An average OCS MR of 0.416 ± 0.035 ppbv, and a mean N_2O MR of 323.7 ± 0.2 ppbv was calculated. An average slope of 367.6 ± 107.2 was computed, which translates to a mean stratospheric OCS lifetime of 55 ± 18 years.

A significant difference of the estimated OCS stratospheric lifetime was observed between PV and H_{tp} filter methods, where the latter leads to a 41% longer lifetime. In this case, the modelled thermal tropopause height, $H_{tp} > 0$ km, based on the ECMWF metrological analysis, was limited to 43 samples and the PV > 2 PVU data to 65 samples. Acquiring more frequent samples in this region in future, will lead to a better estimate. The mean of these two estimates with a weighted average uncertainty leads to an average stratospheric OCS lifetime of 47 ± 16 years. This lifetime is shorter than reported by the ACE satellite and balloon-borne study by Barkley et al. (2008) (64 ± 21 years) at altitudes 6 – 30 km and Krysztofiak et al. (2015) (68 ± 20 years at polar latitudes and 58 ± 14 years at tropical latitudes) with measurements up to 34 km.

The shorter stratospheric lifetime derived in this study is dependant on the air samples collected at a lower altitude of 10 – 12 km, which represents UT/LS region. Some in-mixing from the upper troposphere into lowermost stratosphere is common (e.g. Hintsa et al., 1998), which will reduce the stratospheric lifetime and explain the differences. This also explains why the thermal tropopause filter leads to a longer OCS lifetime compared to the dynamical tropopause filter, as the former was often higher up in the stratosphere. The age of air in this region (~1 year) is shorter than in the middle stratosphere where Barkley et al. (2008); and Krysztofiak et al. (2015) measured. As the major sinks of OCS are in the troposphere, we may expect a shorter lifetime in the UT/LS region compared to the stratosphere at higher altitudes. Also, the shorter stratospheric OCS lifetime of this study corresponds to a larger stratospheric sink estimate, and the consequence of this will be discussed in the following Section 3.5.

3.5 Stratospheric sink of carbonyl sulfide

A shorter stratospheric lifetime of OCS will lead to a larger stratospheric sink of OCS. The stratospheric sink (S) of a species equals its atmospheric burden (B) divided by the compound's stratospheric lifetime (τ), as presented in (Eq. 4):

$$S = \frac{B}{\tau}. \quad (4)$$

Assuming a total atmospheric mass of 5.148×10^{21} g (Trenberth and Smith 2005), and an average lower most stratospheric OCS MR of 415 pptv calculated from 32 flights (December 2015 to December 2018), yields a total OCS atmospheric mass of 4.43×10^{12} g (converting OCS volume mixing ratio to a mass mixing ratio with the dry air molar mass of 28.96 g mol^{-1}). Using the IAGOS-CARIBIC OCS stratospheric lifetime, leads to an OCS stratospheric sink estimate of 107 ± 36 Gg yr^{-1} (57 ± 19 Gg (S) yr^{-1}). This is consistent with the estimate of 34 – 66 Gg (S) yr^{-1} OCS stratospheric sink by (Barkley et al., 2008).

As the tropospheric transport of OCS is considered to be the only source to the stratosphere and the OCS MRs do not show a substantial trend over time, the stratospheric OCS sink should balance the net OCS flux from the troposphere. On average the stratospheric sink was 52% smaller compared to the tropospheric influx as estimated in Section 3.2, but still within the uncertainty range when considering the region specificity. As the OCS flux into the stratosphere estimate is only a one-way

flux, from the troposphere to the stratosphere, the net flux will be smaller by the fraction of the OCS which is transported back from the stratosphere to troposphere without being converted into sulfate aerosol, which was also discussed by Kremser et al. (2016) and by Thomason and Peter (2002). Sheng et al. (2015) used an aerosol-chemistry-climate model and estimated that ~90% of the total OCS flux into stratosphere returns unprocessed back to the troposphere. Unfortunately, this cannot explain the large fraction (56 – 70%) of stratospheric sulfate aerosol burden from OCS (Kremser et al., 2016; Sheng et al., 2015; Brühl et al., 2012). Whereas, the 52% (61 Gg (S) yr^{-1} of OCS) from this study matches with the sulfate aerosol burden and could serve as a first order estimate for OCS back transport from the stratosphere to the troposphere. The latter together with the smaller volcanoes, which remained undetected in the past, and are important sulfur source to the stratosphere (Solomon et al., 2011; Vernier et al., 2011) can help to explain the unexplained sulfate aerosol burden in the stratosphere.

4 Conclusions

From the IAGOS-CARIBIC carbonyl sulfide analysis an average atmospheric OCS lifetime of 2.1 ± 1.3 years has been derived through the variability analysis of 6 other co-measured trace gases with well-known lifetimes. A substantially longer stratospheric lifetime of 47 ± 16 years was determined by employing the N_2O and OCS tracer-tracer correlation in the lower stratosphere. The definition of the tropopause height by either the potential vorticity or the temperature gradient, which classifies the air samples as tropospheric or stratospheric, had a significant influence on the calculations. In addition, an OCS flux from the troposphere into the stratosphere of 118 ± 39 Gg (S) yr^{-1} was estimated. A stratospheric sink of OCS was estimated as 57 ± 19 Gg (S) yr^{-1} from the computed stratospheric lifetime. The 52% smaller sink compared to the flux could be interpreted as a 61 Gg (S) yr^{-1} estimate of the OCS fraction transported back from the stratosphere to the troposphere.
To lower the uncertainties, we recommend future measurements in this region, especially high frequency data of OCS and other sulfur containing gases like CS_2 and DMS to improve the global sulfur cycle estimates.

Data availability. Datasets for this research are available at the IAGOS-CARIBIC data repository [upon request in accordance with the IAGOS-CARIBIC Data Protocol for external data users] at http://www.caribic-atmospheric.com/Data.php.

Competing interests. The authors declare that they have no conflict of interest.

Author contribution. EK and JW developed the idea. EK established the new measurement technique. EK, ML and LE carried out the experiments. EK wrote the manuscript with support from ML and JW. All authors discussed the results, commented and helped to improve the manuscript.

Acknowledgements. We are very grateful to Claus Koeppel (Max-Planck-Institute for Chemistry, Mainz) for IAGOS-CARIBIC TRACs / HIRES WAS sampling and for conducting all the pre- and after-flight ground tests for accurate sample

collection. We would also like to thank Florian Obersteiner (Karlsruhe Institute of Technology, Karlsruhe) for providing the very helpful IAU_Chrom data analysis software. Furthermore, we thank Marc von Hobe for his insightful comments.

Financial support. EK was supported by the Max Planck Graduate Center with the Johannes Gutenberg-Universität Mainz (MPGC).

The article processing charges for this open-access publication were covered by the Max Planck Society.

References

Baker, A. K., Slemr, F., and Brenninkmeijer, C. A. M.: Analysis of non-methane hydrocarbons in air samples collected aboard the CARIBIC passenger aircraft. Atmospheric Measurement Techniques, 3, 311-321, 2010.

Barkley, M. P., Palmer, P. I., Boone, C. D., Bernath, P. F., and Suntharalingam, P.: Global distributions of carbonyl sulfide in the upper troposphere and stratosphere. Geophysical Research Letters, 35, 2008.

Brenninkmeijer, C. A. M., Crutzen, P., Boumard, F., Dauer, T., Dix, B., Ebinghaus, R., Filippi, D., Fischer, H., Franke, H., Frieß, U., Heintzenberg, J., Helleis, F., Hermann, M., Kock, H. H., Koeppel, C., Lelieveld, J., Leuenberger, M., Martinsson, B. G., Miemczyk, S., Moret, H. P., Nguyen, H. N., Nyfeler, P., Oram, D., O'Sullivan, D., Penkett, S., Platt, U., Pupek, M., Ramonet, M., Randa, B., Reichelt, M., Rhee, T. S., Rohwer, J., Rosenfeld, K., Scharffe, D., Schlager, H., Schumann, U., Slemr, F., Sprung, D., Stock, P., Thaler, R., Valentino, F., van Velthoven, P., Waibel, A., Wandel, A., Waschitschek, K., Wiedensohler, A., Xueref-Remy, I., Zahn, A., Zech, U., and Ziereis, H.: Civil Aircraft for the regular investigation of the atmosphere based on an instrumented container: The new CARIBIC system. Atmospheric Chemistry and Physics, 7, 4953-4976, 2007.

Brühl, C., Lelieveld, J., Tost, H., Höpfner, M., and Glatthor, N.: Stratospheric sulfur and its implications for radiative forcing simulated by the chemistry climate model EMAC. Journal of Geophysical Research: Atmospheres, 120, 2103-2118, 2015.

Brühl, C., Lelieveld, J., Crutzen, P. J., and Tost, H.: The role of carbonyl sulphide as a source of stratospheric sulphate aerosol and its impact on climate. Atmospheric Chemistry and Physics, 12, 1239-1253, 2012.

Campbell, J.E., Whelan, M.E., Seibt, U., Smith, S.J., Berry, J.A., and Hilton, T.W.: Atmospheric carbonyl sulfide sources from anthropogenic activity: Implications for carbon cycle constraints. Geophysical Research Letters, 42, 3004-3010, 2015.

Cantrell, C.A.: Technical Note: Review of methods for linear least-squares fitting of data and application to atmospheric chemistry problems. Atmospheric Chemistry and Physics Discussions, 8, 6409-6436, 2008.

Colman, J.J., Blake, D.R., and Rowland, F.S.: Atmospheric residence time of CH_3Br estimated from the Junge spatial variability relation. Science, 281, 392-396, 1998.

Commane, R., Meredith, L.K., Baker, I.T., Berry, J.A., Munger, J.W., Montzka, S.A., Templer, P.H., Juice, S.M., Zahniser, M.S., and Wofsy, S.C.: Seasonal fluxes of carbonyl sulfide in a midlatitude forest. Proceedings of the National Academy of Sciences of the United States of America, 112, 14162-14167, 2015.

Crutzen, P. J.: The possible importance of CSO for the sulfate layer of the stratosphere. Geophysical Research Letters, 3, 73-76, 1976.

Engel, A., and Schmidt, U.: Vertical profile measurements of carbonyl sulfide in the stratosphere. Geophysical Research Letters, 21, 2219-2222, 1994.

Glatthor, N., Höpfner, M., Leyser, A., Stiller, G.P., von Clarmann, T., Grabowski, U., Kellmann, S., Linden, A., Sinnhuber, B.-M., Krysztofiak, G., and Walker, K.A.: Global carbonyl sulfide (OCS) measured by MIPAS/Envisat during 2002–2012. Atmospheric Chemistry and Physics, 17, 2631-2652, 2017.

Glatthor, N., Höpfner, M., Baker, I.T., Berry, J., Campbell, J.E., Kawa, S.R., Krysztofiak, G., Leyser, A., Sinnhuber, B.-M., Stiller, G.P., Stinecipher, J., and von Clarmann, T.: Tropical sources and sinks of carbonyl sulfide observed from space. Geophysical Research Letters, 42, 10082-10090, 2015.

Hintsa, E.J., Boering, K.A., Weinstock, E.M., Anderson, J.G., Gary B.L., Pfister, L., Daube, B.C., Wofsy, S.C., Loewenstein, M., Podolske, J.R., Margitan, J.J., and Bui, T.P.: Troposphere-to-stratosphere transport in the lowermost stratosphere from measurements of H_2O, CO_2, N_2O and O_3. Geophysical Research Letters, 14, 2655-2658, 1998.

Jobson, B.T., McKeen, S.A., Parrish, D.D., Fehsenfeld, F.C., Blake, D.R., Goldstein, A.H., Schauffler, S.M., and Elkins, J. W.: Trace gas mixing ratio variability versus lifetime in the troposphere and stratosphere: Observations. Journal of Geophysical Research: Atmospheres, 104, 16091-16113, 1999.

Jobson, B. T., Parrish, D. D., Goldan, P., Kuster, W., Fehsenfeld, F. C., Blake, D. R., Blake, N. J., and Niki, H.: Spatial and temporal variability of nonmethane hydrocarbon mixing ratios and their relation to photochemical lifetime. Journal of Geophysical Research: Atmospheres, 103, 13557-13567, 1998.

Johnson, J.E.: The lifetime of carbonyl sulfide in the troposphere. Geophysical Research Letters, 8, 938-940, 1981.

Junge, C. E.: Residence time and variability of tropospheric trace gases. Tellus, 26, 477-488, 1974.

Karu, E.: Atmospheric sulfur compounds in the troposphere and stratosphere measured with an atomic emission detector. PhD Dissertation, Max Plank Institute for Chemistry & Johannes Gutenberg University Mainz, 24-50, 2019. (urn: nbn:de:hebis:77-diss-1000028506 , https://publications.ub.uni-mainz.de/theses/frontdoor.php?source_opus=100002850&la=en)

Kjellström, E.: A Three-Dimensional Global Model Study of Carbonyl Sulfide in the Troposphere and the Lower Stratosphere. Journal of Atmospheric Chemistry, 29, 151-177, 1998.

Kremser, S., Thomason, L.W., von Hobe, M., Hermann, M., Deshler, T., Timmreck, C., Toohey, M., Stenke, A., Schwarz, J.P., Weigel, R., Fueglistaler, S., Prata, F.J., Vernier, J., Schlager, H., Barnes, J.E., Antuña-Marrero, J., Fairlie, D., Palm, M., Mahieu, E., Notholt, J, Rex, M., Bingen, C., Vanhellemont, F., Bourassa, A., Plane, J.M.C., Klocke, D., Carn, S.A., Clarisse, L., Trickl, T., Neely, R., James, A.D., Rieger, L., Wilson, J.C., and Meland, B.: Stratospheric aerosol—Observations, processes, and impact on climate. Reviews of Geophysics, 54, 278-335, 2016.

Krysztofiak, G., Té, Y.V., Catoire, V., Berthet, G., Toon, G.C., Jégou, F., Jeseck, P., and Robert, C.: Carbonyl Sulphide (OCS) Variability with Latitude in the Atmosphere. Atmosphere-Ocean, 53, 89-101, 2015.

Montzka, S., Calvert, P., Hall, B., Elkins, J., Conway, T., Tans, P., and Sweeney, C.: On the global distribution, seasonality, and budget of atmospheric carbonyl sulfide (COS) and some similarities to CO_2. Journal of Geophysical Research: Atmospheres, 112, 2007.

Murphy, D. and Fahey, D.: An estimate of the flux of stratospheric reactive nitrogen and ozone into the troposphere. Journal of Geophysical Research: Atmospheres, 99, 5325-5332, 1994.

Prather, M.J., Hsu, J., DeLuca, N.M., Jackman, C.H., Oman, L.D., Douglass, A.R., Fleming, E.L., Strahan, S.E., Steenrod, S.D., Søvde, O.A., Isaksen, I.S.A., Froidevaux, L., and Funke, B.: Measuring and modeling the lifetime of nitrous oxide including its variability. Journal of Geophysical Research: Atmospheres, 120, 5693-5705, 2015.

Plumb, R.A., and Ko, M.K.W.: Interrelationships between mixing ratios of long-lived stratospheric constituents. Journal of Geophysical Research: Atmospheres, 97, 10145-10156, 1992.

Scharffe, D., Slemr, F., Brenninkmejer, C.A.M., and Zahn, A.: Carbon monoxide measurements onboard the CARIBIC passenger aircraft using UV resonance fluorescence. Atmospheric Measurement Techniques, 5, 1753-1760, 2012.

Schuck, T. J., Brenninkmeijer, C. A. M., Slemr, F., Xueref-Remy, I., and Zahn, A.: Greenhouse gas analysis of air samples collected onboard the CARIBIC passenger aircraft. Atmospheric Measurement Techniques, 2, 449–464, 2009.

Sheng, J.-X., Weisenstein, D.K., Luo, B.-P., Rozanov, E., Stenke, A., Anet, J., Bingemer, H., and Peter, T.: Global atmospheric sulfur budget under volcanically quiescent conditions: Aerosol-chemistry-climate model predictions and validation. Journal of Geophysical Research: Atmospheres, 120, 256–276, 2015.

Solomon, S., Daniel, J.S., Neely III, R.R., Vernier, J.-P., Dutton, E.G., and Thomason, L.W.: The Persistently Variable "Background" Stratospheric Aerosol Layer and Global Climate Change. Science, 333, 866-870, 2011.

Trenberth, K.E., and Smith, L., The mass of the atmosphere: A constraint on global analyses. Journal of Climate, 18, 864-875, 2005.

Thomason, L., and Peter, T.: Assessment of stratospheric aerosol properties (ASAP), Report on the SPARC Assessment Kick-Off Workshop, Paris, France, 4-6 November 2001. Stratospheric Processes and Their Role in Climate Newsletter, 18, 2002.

Vernier, J.-P., Thomason, L. W., Pommereau, J.-P., Bourassa, A., Pelon, J., Garnier, A., Hauchecorne, A., Blanot, L., Trepte, C., Degenstein, D., and Vargas, F.: Major influence of tropical volcanic eruptions on the stratospheric aerosol layer during the last decade. Geophysical Research Letters, 38, 1-8, 2011.

Watts, S.F.: The mass budgets of carbonyl sulfide, dimethyl sulfide, carbon disulfide and hydrogen sulfide. Atmospheric Environment, 34, 761-779, 2000.

Williams, J., Gros, V., Bonsang, B., and Kazan, V.: HO cycle in 1997 and 1998 over the southern Indian Ocean derived from CO, radon, and hydrocarbon measurements made at Amsterdam Island. Journal of Geophysical Research: Atmospheres, 106, 12719-12725, 2001.